UNIVERSIDADE DA BEIRA INTERIOR
Engenharia

Analytical Model for the Performance Curves of a Family of Propellers based on Wind Tunnel Tests

(versão corrigida após defesa)

Miguel Cabeleira dos Santos

Dissertação para obtenção do Grau de Mestre em

Engenharia Aeronáutica

(Ciclo de Estudos Integrado)

Orientador: Prof. Doutor Pedro Vieira Gamboa

Covilhã, dezembro de 2018

Acknowledgments

First and foremost, I would like to acknowledge my supervisor, Professor Pedro Vieira Gamboa, for all the patience and guidance throughout the duration of this work.

I want to acknowledge Engineer Pedro Alves for the help provided while mounting the experimental setup in the wind tunnel at University of Beira Interior, guiding me through the wind tunnel tests and sharing his knowledge and experience with me.

I would like to thank all my friends at Desertuna for all the help and support they gave me during this chapter of my life, thanks to them, I learned numerous things and surpassed many challenges.

I want to thank all my true friends, I will never forget them, for their support and friendship. A special thank you to Alexandre Nunes, Beatriz Leal, Inês Cruz, Luís Correia and Mariana Costa.

Above all, I would like to thank my parents, João and Lídia, and my sister, Joana, for all the motivation and support given to me through my whole life.

Resumo

O principal objetivo do trabalho levado a cabo nesta dissertação é a construção e validação de um modelo analítico para o desempenho de uma família de hélices com base em dados experimentais em condições de baixo número de Reynolds. Este tipo de hélices é mais utilizado em Veículos Aéreos Não Tripulados (VANTs).

O modelo foi projetado em MATLAB® utilizando vários métodos de regressão, tal como o método dos mínimos quadrados (MMQ), baseado em dados experimentais obtidos na Universidade de Illinois em Urbana-Champaign (UIUC), de dezassete hélices testadas da APC Thin Electric. Os dados experimentais passaram por um processo de redução para um tratamento de dados mais facilitado. No âmbito do desenvolvimento deste modelo, foram feitos testes no Departamento de Ciências Aerospaciais (DCA), na Universidade da Beira Interior (UBI) a mais dez hélices da APC Thin Electric.

O modelo analítico permite calcular os valores para o coeficiente de potência e para a eficiência propulsiva para hélices com dimensões próximas ou iguais das que foram utilizadas para a sua construção. Este modelo será útil para proporcionar uma melhor fase de projeto, providenciando uma mais rápida e eficiente seleção de hélice. Os dados dos testes ao desempenho das hélices obtidos durante o processo experimental foram catalogados para aumentar a documentação existente sobre hélices testadas em condições de baixo número de Reynolds.

Palavras-chave

Hélice de Baixo Número de Reynolds, Teste de Hélices em Túnel de Vento, Modelo de Hélices.

Abstract

The main objective of the work done in this dissertation is the construction and validation of an analytical model for the performance curves of a family of propellers tested at low Reynolds numbers. This kind of propellers is more commonly used in Unmanned Aerial Vehicles (UAVs).

The model was designed in MATLAB® using a variety of regression techniques, such as the Least Squares Method (LSQ), via experimental data acquired at University of Illinois at Urbana-Champaign (UIUC), of measurements of seventeen APC Thin Electric propellers. The experimental data went through a reduction process for easier analysis. In order to further develop this model, tests were run at the Department of Aerospace Sciences (DCA) of University of Beira Interior (UBI) for ten more APC Thin Electric propellers.

The analytical model will predict power coefficient and propeller efficiency accurately for the propellers with dimensions close to those that were used for its development. This model will be useful to achieve optimal design, providing a faster and more efficient propeller selection phase. The propeller performance obtained during the experimental tests will also be catalogued to further increase the documentation on propellers tested at LRN.

Keywords

Low Reynolds Propeller Performance, Propeller Tests at Wind Tunnels, Propeller Model.

Contents

Introduction 1

1.1 Motivation 1

1.2 Objectives 2

1.3 Document Structure 2

State of the Art 3

2.1 Propeller's Characteristics 3

2.3 Analysis programs 5

2.3.1 PropSelector 5

2.3.2 JBLADE 5

2.3.3 QPROP Propeller/Windmill analysis and design 6

2.3.4 XROTOR 6

2.4 Experimental Studies 6

2.4.1 UIUC Propeller Database 7

2.4.2 Department of Aerospace Sciences at UBI 7

2.2 Surrogate Models 8

2.4.3 Curve fitting methods 8

Methodology 11

3.1 Experimental procedure 11

3.2 Data reduction 13

3.3 Least Squares Method 17

3.4 "Goodness" of fits 19

3.4.1 Statistical Error 19

3.4.2 Standard Deviation 19

3.4.3 Coefficient of Determination 20

Results and discussion 21

4.1 Experimental data 21

4.2 Curve fitting 22

4.2.1 Power Coefficient 22

4.2.2 Propeller Efficiency 31

4.2.3 Additional Parameters 34

4.3 Validation 37
4.3.1 Comparison with UIUC Propeller Database 38
4.3.2 Application of the model to the data acquired at UBI 45
4.4 New Analytical Model 50
4.4.1 Power Coefficient 50
4.4.2 Propeller Efficiency 55
4.4.3 Additional Parameters 58
4.5 Verification of the new model 62
Conclusion 73
5.1 Future Work 73
References 75

List of Figures

Figure 1 - Typical representation of propeller efficiency curves (McCormick, 1979). 4
Figure 2 - Typical representation of propeller thrust coefficient curves (McCormick, 1979). ...4
Figure 3 - Typical representation of propeller power coefficient curves (McCormick, 1979). ...5
Figure 4 - Schematic of the Wind Tunnel at UBI. 8
Figure 5 - Divided Difference table [19]. 10
Figure 6 - Experimental Setup designed by Alves [16]. 11
Figure 7 - Data acquisition program interface. 13
Figure 8 - Example of data points of C_P and C_{Pr}. 15
Figure 9 - Example of data points of η and η_r. 16
Figure 10 - Dispersion for propellers with $\frac{p}{D}$ ratio of 0.5 (a and b) and the results of *lsqlin* function in MATLAB® (c). 22
Figure 11 - 1 of 2 different behaviors of data for propellers with $\frac{p}{D}$ ratio not equal to 0.5 (a, b, c, and d) and the results of *lsqlin* function in MATLAB® (e). 23
Figure 12 - 2 of 2 different behaviors of data for propeller with $\frac{p}{D}$ not equal to 0.5 (a, b, c) and the results of *lsqlin* function in MATLAB® (d). 24
Figure 13 - 3D plot of C_{P1} 27
Figure 14 - 3D plot of $C_{\mathrm{P2,3}}$. 30
Figure 15 - 1 of 2 behaviors of propeller efficiency when $\frac{p}{D} > 0.9$ 31
Figure 16 - 2 of 2 behaviors of propeller efficiency when $\frac{p}{D} < 0.9$. 31
Figure 17 - 3D plot of η_1. 33
Figure 18 - $J_{max}(D,p)$ 34
Figure 19 - $C_{Pr0}(D,p)$. 35
Figure 20 - $\eta_{rmax}(D,p)$ 36
Figure 21 - Propeller Performance comparison with UIUC data for propeller 8x4. 39
Figure 22 - Propeller Performance comparison with UIUC data for propeller 8x6. 39
Figure 23 - Propeller Performance comparison with UIUC data for propeller 8x8. 39
Figure 24 - Propeller Performance comparison with UIUC data for propeller 9x4.5. 40
Figure 25 - Propeller Performance comparison with UIUC data for propeller 9x6. 40
Figure 26 - Propeller Performance comparison with UIUC data for propeller 9x7.5. 40
Figure 27 - Propeller Performance comparison with UIUC data for propeller 9x9. 41
Figure 28 - Propeller Performance comparison with UIUC data for propeller 10x5. 41
Figure 29 - Propeller Performance comparison with UIUC data for propeller 10x7. 41
Figure 30 - Propeller Performance comparison with UIUC data for propeller 11x5.5. 42
Figure 31 - Propeller Performance comparison with UIUC data for propeller 11x7. 42

Figure 32 - Propeller Performance comparison with UIUC data for propeller 11x8. 42
Figure 33 - Propeller Performance comparison with UIUC data for propeller 11x8.5. 43
Figure 34 - Propeller Performance comparison with UIUC data for propeller 11x10. 43
Figure 35 - Propeller Performance comparison with UIUC data for propeller 14x12. 43
Figure 36 - Propeller Performance comparison with UIUC data for propeller 17x12. 44
Figure 37 - Propeller Performance comparison with UIUC data for propeller 19x12. 44
Figure 38 - Testing of the first model with data from propeller 7x4. 45
Figure 39 - Testing of the first model with data from propeller 13x4. 46
Figure 40 - Testing of the first model with data from propeller 13x10. 46
Figure 41 - Testing of the first model with data from propeller 14x10. 46
Figure 42 - Testing of the first model with data from propeller 15x6. 47
Figure 43 - Testing of the first model with data from propeller 15x10. 47
Figure 44 - Testing of the first model with data from propeller 16x10. 47
Figure 45 - Testing of the first model with data from propeller 18x8. 48
Figure 46 - Testing of the first model with data from propeller 20x8. 48
Figure 47 - Testing of the first model with data from propeller 20x15. 48
Figure 48 - Representation of the propellers used to create (data acquired from UIUC, circles) and validate (data acquired at UBI, triangles) the analytical model. 49
Figure 49 - Dispersion for propellers with $\frac{p}{D}$ ratio lower than 0.6 (a, b and c) and the results of *lsqlin* function in MATLAB® (d). 50
Figure 50 - Dispersion for propellers with $\frac{p}{D}$ ratio between 0.6 and 0.8 (a, b, c and d) and the results of *lsqlin* function in MATLAB® (e). 51
Figure 51 - Dispersion for propellers with $\frac{p}{D}$ ratio higher than 0.8 (a, b) and the results of *lsqlin* function in MATLAB® (c). 52
Figure 52 - 3D plot of $\frac{C_{Pr}}{C_{Pr0}}\left(\frac{J}{J_{max}}, \frac{p}{D}\right)$. 54
Figure 53 - 1 of 3 behaviors of propeller efficiency for $\frac{p}{D} > 0.9$ 55
Figure 54 - 2 of 3 behaviors of propeller efficiency for $0.5 < \frac{p}{D} < 0.9$ 55
Figure 55 - 3 of 3 behaviors of propeller efficiency for $\frac{p}{D} < 0.5$. 56
Figure 56 - 3D plot of $\frac{\eta_r}{\eta_{rmax}}\left(\frac{J}{J_{max}}, \frac{p}{D}\right)$. 57
Figure 57 - 3D plot of $J_{max}(D, p)$. 59
Figure 58 - 3D plot of $C_{Pr0}(D, p)$ 60
Figure 59 - 3D plot of $\eta_{rmax}(D, p)$ 61
Figure 60 - Propeller Performance comparison with UBI data for propeller 7x4. 63
Figure 61 - Propeller Performance comparison with UIUC data for propeller 8x4. 63
Figure 62 - Propeller Performance comparison with UIUC data for propeller 8x6. 64
Figure 63 - Propeller Performance comparison with UIUC data for propeller 8x8. 64
Figure 64 - Propeller Performance comparison with UIUC data for propeller 9x4.5. 64
Figure 65 - Propeller Performance comparison with UIUC data for propeller 9x6. 65

Figure 66 - Propeller Performance comparison with UIUC data for propeller 9x7.5..... 65
Figure 67 - Propeller Performance comparison with UIUC data for propeller 9x9. 65
Figure 68 - Propeller Performance comparison with UIUC data for propeller 10x5..... 66
Figure 69 - Propeller Performance comparison with UIUC data for propeller 10x7..... 66
Figure 70 - Propeller Performance comparison with UIUC data for propeller 11x5.5. 66
Figure 71 - Propeller Performance comparison with UIUC data for propeller 11x7..... 67
Figure 72 - Propeller Performance comparison with UIUC data for propeller 11x8..... 67
Figure 73 - Propeller Performance comparison with UIUC data for propeller 11x8.5. 67
Figure 74 - Propeller Performance comparison with UIUC data for propeller 11x10. 68
Figure 75 - Propeller Performance comparison with UBI data for propeller 13x4..... 68
Figure 76 - Propeller Performance comparison with UBI data for propeller 13x10. 68
Figure 77 - Propeller Performance comparison with UBI data for propeller 14x10. 69
Figure 78 - Propeller Performance comparison with UIUC data for propeller 14x12. 69
Figure 79 - Propeller Performance comparison with UBI data for propeller 15x6..... 69
Figure 80 - Propeller Performance comparison with UBI data for propeller 15x10. 70
Figure 81 - Propeller Performance comparison with UBI data for propeller 16x10. 70
Figure 82 - Propeller Performance comparison with UIUC data for propeller 17x12. 70
Figure 83 - Propeller Performance comparison with UBI data for propeller 18x8..... 71
Figure 84 - Propeller Performance comparison with UIUC data for propeller 19x12. 71
Figure 85 - Propeller Performance comparison with UBI data for propeller 20x8..... 71
Figure 86 - Propeller Performance comparison with UBI data for propeller 20x15. 72

List of Tables

Table 1 - Convergence criteria to achieve wind tunnel freestream speed and propeller's RPM steady. 12
Table 2 - Values of *D*, *p*, C_{Pr0} and $\frac{D+p}{C_{Pr0}}$ for each propeller with $\frac{p}{D} \neq 0.5$: 25
Table 3 - Values of *D*, *p* and C_{Pr0} for propeller with $\frac{p}{D} = 0.5$. 25
Table 4 - Averages of propellers' $\frac{p}{D}$ ratio. 32
Table 5 - Values of D, p, J_{max}, C_{Pr0} and η_{rmax} used in the plotting of the functions above. .. 37
Table 6 - Mean relative error of the model's predictions for the first model. 38
Table 7 - Mean relative error (MRE), δmax and standard deviation of the model's prediction of the propeller's tested at UBI. 45
Table 8 - Values of D, p, J_{max} , C_{Pr0} and η_{rmax} for each propeller. 58
Table 9 - Mean relative error, Max relative error and standard deviation of the model's prediction of all the propellers and total R^2 value. 62

Lista de Acrónimos

APC	Advanced Precision Composites
BEM	Blade Element Momentum Theory
DCA	Department of Aerospace Sciences
GPL	General Public License
LRN	Low Reynolds Number
LSQ	Linear Least Squares Method
MATLAB	Matrix Laboratory
MIT	Massachusetts Institute of Technology
MRE	Mean Relative Error
NACA	National Advisory Committee for Aeronautics
RSM	Response Surface Models
UBI	Universidade da Beira Interior
UIUC	University of Illinois Urbana-Champaign

Nomenclature

c	Propeller blade chord, *m*.
C_P	Power Coefficient.
C_Q	Torque Coefficient.
C_T	Thrust coefficient.
D	Propeller diameter, *in*.
J	Advance Ratio.
n	Rotational speed, *cycles*/*s*.
N	Rotational speed, *cycles*/*min*.
p	Propeller pitch, *in*.
P	Power, *W*.
P_{atm}	Atmospheric pressure, *Pa*.
Q	Torque, *Nm*.
R	Air constant, $R = 287$ $J{\cdot}kg^{-1}{\cdot}K^{-1}$.
R^2	Coefficient of determination.
Re	Reynolds number.
T	Thrust, *N*.
T_{atm}	Atmospheric temperature, *K*.
V	Freestream velocity, *m*/*s*.

Greek parameters

δ	Relative error, %
δ_{max}	Maximum relative error, %
η	Propeller efficiency.
μ	Dynamic viscosity, *kg*/*ms*.
ρ	Air density, kg/m^3.

Chapter 1

Introduction

In the introductive chapter to this study, the motivation to develop the analytical model is explained, the objectives of the study are enumerated, and a section explaining the structure of this document is presented.

1.1 Motivation

With the Unmanned Aerial Vehicle industry becoming larger in modern times, the design of UAVs becomes more important every day. An efficient airplane requires a rigorous design, and this includes its propulsive systems. Most UAVs propulsive systems use propellers to generate the thrust they need to fly, which can be evaluated by measuring the thrust and power coefficients and propeller efficiency. Good predictions of these performance curves will be a great asset during preliminary design, or UAV optimization problems.

A study conducted by Brandt and Selig [1] shows that propeller efficiencies vary greatly depending on the propeller, thus, making an accurate prediction of propeller performance curves, can greatly improve overall UAV design productivity and optimization procedures. This selection requires many tests in wind tunnels to acquire enough data to analyze the propeller's performance. To conduct tests for propellers in a wind tunnel, the latter must be equipped with an experimental setup designed to place a propeller inside the test section, and each test takes around two hours, depending on the number of different propeller speeds one desires to test, and the number of freestream velocity points to analyze. Therewith the construction of an analytical model will enable to rapidly develop and test different propeller designs, compare them, make small changes and test again, without the complexity of wind tunnel tests, and in the end, when a reduced sample of propellers has been attained, one can study them in greater detail at a wind tunnel.

1.2 Objectives

The goal of this work is to design a mathematical model for propeller performance of a family of propellers, namely the Thin Electric Propellers of the brand APC. To achieve this, the work is divided in two phases:

- The first is to construct the model using data provided by UIUC;
- The second phase includes tests conducted at UBI in order to collect experimental propeller performance data to further develop the analytical model.

The second phase is also important, because of the lack of documentation on propellers studied at LRN conditions, for the characterization of uncatalogued propellers performance.

1.3 Document Structure

The document starts with a brief introduction explaining the motivation and the objectives of this work. Following, is the state of the art, where the propeller's characteristics are explained, the most relevant parameters for propeller performance analysis and an example of the curve behavior of such parameters. Thereafter, some examples of already existing programs that analyze the propeller's performance are displayed followed by a brief explanation on how important surrogate models based on experimental data are. This chapter will be finished with a small section that presents some of the experimental studies over the propellers tested at Low Reynolds Numbers (LRN). The third chapter includes the experimental procedure for testing these propellers at the wind tunnel at UBI, followed by the data reduction procedure, also an explanation about the most common and effective regression techniques and validation of curve fits is provided. In the fourth chapter, the results of this study are shown, the first model presented was created with the data retrieved from UIUC Propeller Database [2], and then it was used the same model to predict the propeller's performance tests at UBI, comparing the results. Finally, the updated analytical model with both data retrieved from UIUC [2] and data collected from tests conducted at UBI will be presented along with the statistical validation with error calculation and the coefficient of determination for both C_P and η. Finally, the fifth chapter will provide a conclusion about this project and some of the work that can be conducted in the future.

Chapter 2

State of the Art

In this chapter a brief explanation on which propeller's characteristics are relevant to this study is shown, followed by a list of already existing propeller performance parameter programs available online. In the end of this section, a brief sample of experimental studies conducted prior to this research are displayed.

2.1 Propeller's Characteristics

A propeller uses its blade's rotation, which acts as a rotating wing, to produce lift and drag. Propeller nomenclature is usually a set of two numbers. The first one is the total propeller diameter, and the second is the pitch of the propeller blades themselves, which refers to the angle between the propeller blade chord line and the plane of rotation of the propeller. Blade pitch is most often described in terms of units of distance that the propeller would move forward in one rotation. For instance, when naming a 10x5 propeller, it means that it has a 10-inch diameter and a 5-inch blade pitch.

The propeller's performance is evaluated by the thrust and power coefficients, C_T and C_P, respectively, which depend primarily on the advance ratio, *J*, the blade Reynolds number ***Re***, and on the propeller geometry [3].

$$C_T = C_T(J, Re, geometry) \qquad (2.1)$$

$$C_P = C_P(J, Re, geometry) \qquad (2.2)$$

$$J = \frac{V}{nD} \qquad (2.3)$$

$$Re = \frac{\rho V c}{\mu} \qquad (2.4)$$

where V is the freestream velocity, *n* is the propeller's rotational speed, in $cycle/s$, *D* is diameter, ***Re*** is the Reynolds number, ρ is the air density, *c* is propeller blade chord and μ is the dynamic viscosity of the fluid.

Once the propeller geometry is known, and the coefficients and propeller efficiency, η, have been generated by measurement or analysis, the thrust, *T*, and torque, *Q*, can be calculated for any other *V* and *n* by dimensionalizing the coefficients:

$$\eta = \frac{C_T J}{C_P} \quad (2.5)$$

$$T(n,V) = \frac{1}{2}\rho(nD)^2\pi\left(\frac{D}{2}\right)^2 C_T = \frac{1}{2}\rho V^2\pi\left(\frac{D}{2}\right)^2\left(\frac{C_T(J,Re)}{J^2}\right) \quad (2.6)$$

$$Q(n,V) = \frac{1}{2}\rho(nD)^2\pi\left(\frac{D}{2}\right)^3 C_P = \frac{1}{2}\rho V^2\pi\left(\frac{D}{2}\right)^3\left(\frac{C_P(J,Re)}{J^2}\right) \quad (2.7)$$

C_T, C_P and η are plotted against advance ratio, J, to analyze the propeller's performance. Figure 1, Figure 2 and Figure 3 show a few examples of these parameters' plots:

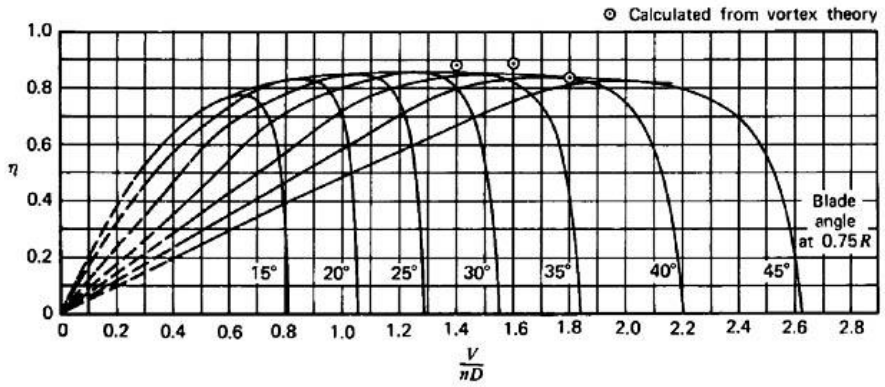

Figure 1 - Typical representation of propeller efficiency curves (McCormick, 1979).

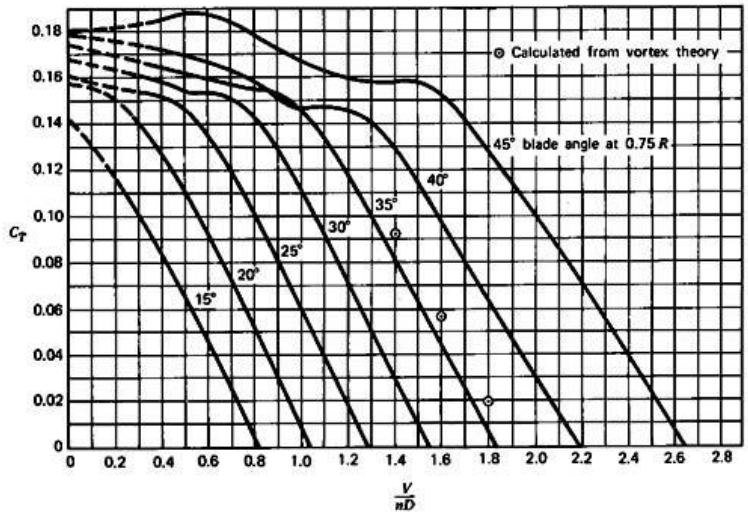

Figure 2 - Typical representation of propeller thrust coefficient curves (McCormick, 1979).

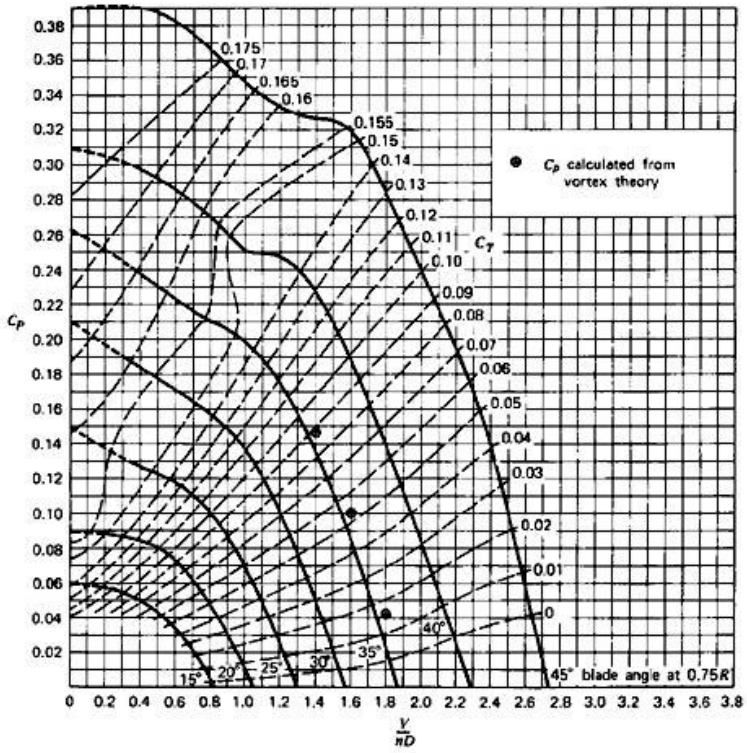

Figure 3 - Typical representation of propeller power coefficient curves (McCormick, 1979).

2.3 Analysis programs

2.3.1 PropSelector

PropSelector is a program that was designed by Brian Robert Gyles [4] which provides as output the performance of two to four blade propellers of model airplanes and is based on the mutual relations of propeller data from NACA's Technical Note No.698 [5]. There is an extended version of this program called *Extended Propselector*, which allows input of altitude and provides more output values, such as propeller thrust coefficient, tip Mach number and Pitch angle at 75% of propeller blade radius.

2.3.2 JBLADE

JBLADE is an open-source propeller design and analysis code developed in UBI, by Morgado and Silvestre [7], as part of a PhD thesis at UBI. It uses a modified BEM theory to account for the 3D flow equilibrium. It can estimate the performance curves of a given propeller, after the analysis it shows the results in a graphical interface to make it easier to build and analyze the simulations. The code used in this model is based on David Marten's QBLADE coupled with André Deperrois' XFLR5.

2.3.3 QPROP Propeller/Windmill analysis and design

QPROP is an analysis program, created by professor Mark J. Drela [8], from Massachusetts Institute of Technology (MIT), which is based on a theoretical aerodynamic formulation that uses an extension of the classical blade-element/vortex formulation, as explained in the document [9], shows as output the analysis of the performance of a propeller-motor combination.

The formulation is based on an extended version of the blade-element/vortex method. This extension, implemented by Larrabee [10], is in the correct accounting of the propeller's self-induction, making QPROP accurate for very high disk loadings [11].

2.3.4 XROTOR

XROTOR is a program that is mostly used for design and analysis of ducted and free-tip propellers. It contains some menu-driven routines that perform a variety of functions such as: designing a minimum induced loss rotor; prompted input of an arbitrary rotor geometry; the modification of a rotor's geometry; optimization of a rotor for minimum induced loss; analysis of a rotor's performance with a lot of operating parameters; incoming slipstream effects; multi-point parameter display; structural analysis and corrections for twist under load; dB noise predictions; interpolation of geometry to a radius of interest; plotting of the results of analysis.

XROTOR was developed by Drela [12], that is why the theoretical formulation of this software is almost the same as QPROP, the modification is that QPROP is more geared for doing parameter sweeps and coupling to motors while XROTOR is used for the design and analysis of ducted and free-tip propellers.

The code has been written carefully to safely protect the program from unintended crashes [13], but it is always easy to input determined values which will result in an impossible analysis problem. The mathematical model is incapable of handling flows such as the reverse far-slipstream velocity, this can happen due to the self-deforming wake algorithm being touchy if a high windmill disk loading is combined with low advance ratios. There is, however, an option to disable the self-deforming wake algorithm, but the accuracy of the results might be affected.

2.4 Experimental Studies

Compared to the vast documentation about propeller performance for full-scale airplanes, data on propellers at LRN is scarce. In this section some of the studies conducted on propellers at LRN to date, and the description of the wind tunnels used in each research are shown to better understand some variations in results due to wind tunnel design differences.

2.4.1 UIUC Propeller Database

Researchers like Brandt, Selig, Ananda and Deters conducted tests on various small propellers, to counteract this lack of documentation on propellers at LRN. Brandt [1] conducted tests on 79 propellers, where almost all of these propellers had a diameter ranging from 9 to 11 inches. These propellers were from different brands: Aeronaut, APC, Graupner, GWS, Kavon, Kyosho, Master Airscrew, Rev up and Zingali. Deters [14] conducted another study, where two types of propellers were tested, namely from the brands: APC, Crazyflie, E-Flite, GWS, KP, Micro Invent, Plantraco, Union and Vapor and ones that have been have been 3D-printed, named: DA4002, DA4022, DA4052 and NR640.

These tests were performed in the UIUC subsonic wind tunnel. The wind tunnel is an open-return type with a 7.5:1 contraction ration. The rectangular test section is nominally 0.853 x 1.219 m in cross section and 2.438 m long. Over the length of the test section, the width increases by approximately 0.0127 m to account for boundary-layer growth along the tunnel sidewalls. Test section speeds are variable up to 71.53 m/s via a 93.25 kW AC motor connected to a five-bladed fan. For the tests presented in reference [1], the maximum tunnel speed used was 24.38 m/s. To ensure good flow quality in the test section, the wind-tunnel settling chamber contains a 0.1016 m thick honeycomb in addition to four anti-turbulence screens.

2.4.2 Department of Aerospace Sciences at UBI

Some information regarding the wind tunnel at UBI [15]:

- The DCA's wind tunnel is located in the Aerodynamics and Propulsion Laboratory in the DCA at UBI, Covilhã, Castelo Branco, built by EreME;
- This tunnel works with an AC motor with variable speed, with a power rating of 15kW at 970 RPM. Connected to this motor's shaft there is an axial ventilator with 1.2 m diameter;
- The rectangular test section is 0.8 x 0.8 m in cross-section and 1.5 m long;
- The maximum speed inside the test section, in normal conditions, is about 30 m/s;
- The wind-tunnel settling chamber contains a 2 x 2 m honeycomb structure in stainless steel. The diffuser has a rectangular cross-section at the entrance and a circular exit with a diameter of 1.2 m.

Since 2014 this wind tunnel has its own Low Reynolds Number Propeller Performance Test Rig developed by PhD student Pedro Alves [16]. Prior to this setup the laboratory already had a thrust measuring mechanism developed in 2011 by Ricardo Salas [17]. The test rig was designed to collect data of propellers with a diameter between 6 to 14 inches, operating at Reynolds number between 30,000 to 300,000 (based on chord at 3/4 of the blade radius). It consists on a T-shaped pendulum, resembling the same concept implemented by UIUC. It was designed to have minimum complexity in order to ensure minimal disturbances to the flow [18].

The validation of this experimental setup included tests on different propellers such as: APC 11x5.5 Thin Electric and APC 10x4.7 Slow Flyer. Besides this validation procedure Alves also conducted tests on propellers which performance was not catalogued: 13x8 Aeronaut Carbon Electric and 12x8 Aeronaut Carbon Electric.

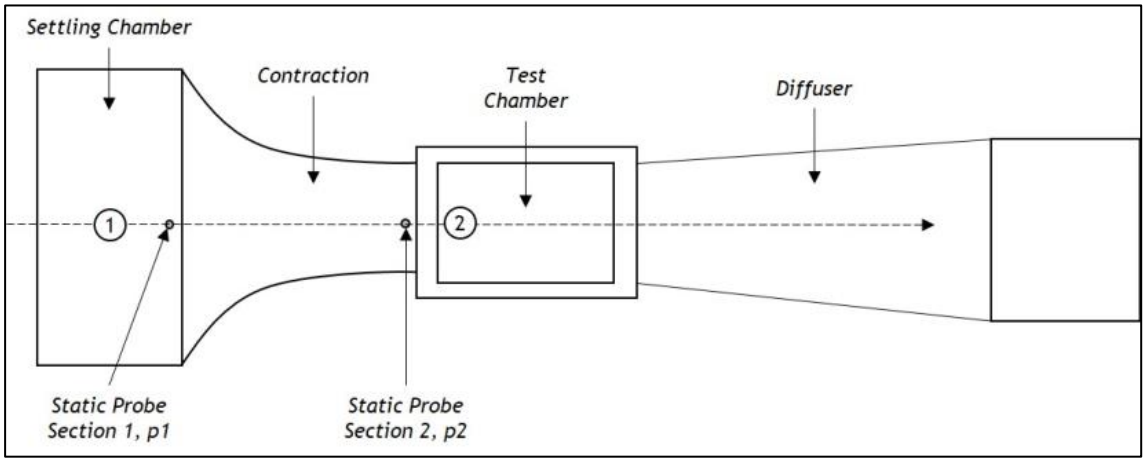

Figure 4 - Schematic of the Wind Tunnel at UBI.

2.2 Surrogate Models

Surrogate models, or metamodels, are compact scalable analytic models that estimate the results of complex tests, based on a limited set of data obtained from experimentation. These are also called response surface models (RSM), emulators, auxiliary models, repro-models, etc.

Surrogate models are a cheaper and easier solution for a test or simulation that is expensive or complex to complete because most design problems require complex experiments or simulations to evaluate certain parameters. The main goal of surrogate modeling is to achieve optimal design while reducing the number of design iterations, lowering the costs and improving overall quality. This is possible by going through a process known as curve fitting or function approximation.

2.4.3 Curve fitting methods

A curve fitting method is the process of constructing a curve that best fits a series of data points. It can be solved through interpolation, or “smoothing” which creates a mathematical function that approximately fits the data. To explain these methods in this research, references [19] and [20] were used.

2.4.3.1 Lagrange Interpolating Polynomials

This method, named after Joseph Louis Lagrange, was already used by Isaac Newton before, but it appears to have been published for the first time in 1779 by Edward Waring. Lagrange worked extensively on this subject but only published later in 1795 [20].

Let f be a function whose values are given by $n+1$ distinct numbers, $x_0, x_1, \dots, x_n$. There is a $P(x)$ polynomial with a maximum degree of n with:

$$f(x_k) = P(x_k), \text{ for each } k = 0, 1, \dots, n. \quad (2.8)$$

which is given by

$$P(x) = f(x_0)L_{n,0}(x) + \cdots + f(x_n)L_n(x) = \sum_{k=0}^{n} f(x_k)L_k(x) \quad (2.9)$$

where, for each $k = 0, 1, \dots, n$,

$$L_k(x) = \prod_{\substack{i=0 \\ i \neq k}}^{n} \frac{x - x_i}{x_k - x_i} \quad (2.10)$$

2.4.3.2 Newton Interpolation Polynomial

The Newton Interpolation Polynomial utilizes divided differences to generate a polynomial based on a given set of points.

Let f be a function defined in the interval $[a, b]$ and $x_0, x_1, \dots, x_n$ distinct points in between a and b.

$$f[x_i, x_{i+1}, \dots, x_{i+k}] = \frac{f[x_{i+1}, x_{i+2}, \dots, x_{i+k}] - f[x_i, x_{i+1}, \dots, x_{i+k-1}]}{x_{i+k} - x_i} \quad (2.11)$$

The equation set above is the definition of divided difference.

Setting as $f_{i,i+j}$ the divided difference $f[x_i, x_{i+1}, \dots, x_{i+j}]$.

x_i	$f(x_i)$	$f_{i,i+1}$	$f_{i,i+1,i+2}$	$f_{i,\dots,i+3}$	$\dots$	$f_{i,\dots,i+n}$
x_0	f_0					
		$f_{0,1}$				
x_1	f_1		$f_{0,1,2}$			
		$f_{1,2}$		$f_{0,\dots,3}$		
x_2	f_2		$f_{1,2,3}$		$\dots$	
		$f_{2,3}$		$\dots$		$f_{0,\dots,n}$
x_3	f_3		$\dots$		$\dots$	
		$\dots$		$f_{n-3,\dots,n}$		
$\dots$	$\dots$		$f_{n-2,n-1,n}$			
		$f_{n-1,n}$				
x_n	f_n					

Figure 5 - Divided Difference table [19].

From this table, the Newton's Interpolation Polynomial can be created:

$$p_n(x) = f(x_0) + f_{0,1}(x - x_0) + f_{0,1,2}(x - x_0)(x - x_1) + f_{0,\dots,3}(x - x_0)(x - x_1)(x - x_2) + \dots + f_{0,\dots,n}(x - x_0) \dots (x - x_{n-1}) \quad (2.12)$$

2.4.3.3 Least Squares Method

A popular curve fitting method is the Linear Least Squares Method (LSQ), which fits the data to minimize the sum of squared residuals:

$$r_i = y_i - p(x_i) \quad (2.13)$$

$$S = \sum_{i=1}^{n+1} r_i^2 \quad (2.14)$$

The least square method (LSQ) is probably the most popular technique in statistics. This is due to several factors. First, most common estimators can be casted within this framework. For example, the mean of a distribution is the value that minimizes the sum of squared deviations of the scores. Second, using squares makes LSQ mathematically very tractable because the Pythagorean theorem indicates that, when the error is independent of an estimated quantity, one can add the squared error and the squared estimated quantity. Third, the mathematical tools and algorithms involved in LSQ (derivatives, eigen-decomposition, singular value decomposition) have been well studied for a relatively long time [21].

Chapter 3

Methodology

3.1 Experimental procedure

The experimental setup was created by Alves [16] in 2014. It consists of three subsystems, the Propeller Balance, Signal Conditioners and the Data Acquisitions System.

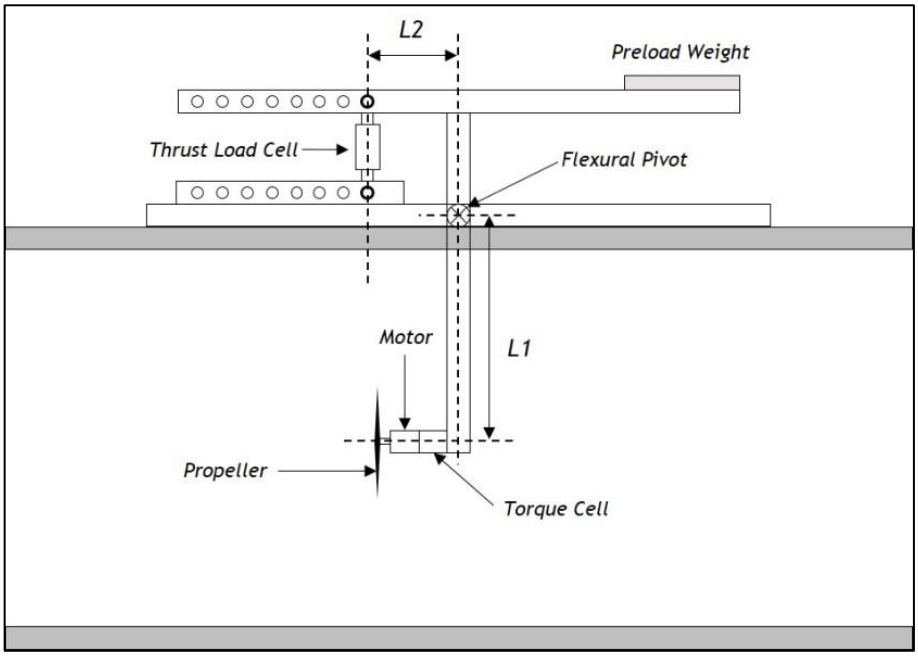

Figure 6 - Experimental Setup designed by Alves [16].

3.1.1 Thrust and Torque Measurements

The thrust load cell used is the CELTRON STC Load cell having a maximum capacity of 100N and the FN3148 manufactured by *FGP Sensors & Instrumentation* having a maximum capacity of 50N, the two cells must be changed because of the wide variety of propellers' diameters being tested, thus the error measured is smaller. To test the propellers 13x4, 13x10, 14x10, 15x6, 15x10, 16x10, 18x8, 20x8 and 20x15, all Thin Electric from APC, the 100N load cell was used. Only one propeller, the 7x4, needed to be tested with the 50N cell.

The torque produced by the propeller is measured by a RTS-200 reaction torque transducer made by Transducer Techniques according to the torque level of the propeller being tested.

Both cells (thrust and torque) are connected to a high precision strain gauge converter from *mantracourt*, model SCB-68, that converts a strain gauge sensor input to a digital serial output.

3.1.2 Propeller Speed Measurement

The propeller rotational speed is measured by a Fairchild Semiconductor QRD1114 photo-reflector, that counts the number of revolutions of the output shaft in a fixed time interval (0.75s), resulting in an accuracy of $\pm$ 0.5Rev/0.75s.

3.1.3 Freestream Velocity Measurement

The freestream velocity is measured with a differential pressure transducer, an absolute pressure transducer, and a thermocouple. This measuring mechanism uses two static pressure ports, one placed in the tunnel settling chamber and the other one at the test chamber, at the end of the contraction. The pressure outside of the tunnel is measured with an absolute pressure transducer made by Freescale Semiconductor model MPXA4115A and the local temperature is measured with a National Instruments LM335 thermocouple located at the inlet of the wind tunnel.

3.1.4 Test Methodology

For the dynamic tests, where $J > 0$, the propeller rotational speed is fixed, and the wind tunnel's freestream velocity is increased from 4 m/s to 28 m/s in 1 m/s increments, the automatic test has to be stopped once the thrust value reaches 0, because the propeller enters the windmill break state. When testing at lower rotational speeds, the increments have to be in 0.5 m/s in order to acquire more data points within these rotational speeds. At each measured freestream velocity, the thrust and torque generated by the propeller are measured, along with ambient pressure and temperature.

By executing the Labview® data acquisition and reduction software, the procedure of data collection begins. This is followed by putting the program to run test condition. The control software speeds up the motor until it reaches the predefined propeller rotational speed by the user. The test procedure is as explained in reference [16], the only difference being the convergence criteria:

Table 1 - Convergence criteria to achieve wind tunnel freestream speed and propeller's RPM steady.

Criteria
$\lvert RPM - RPM_{target} \rvert \leq 10\ RPM$
$\lvert V - V_{target} \rvert \leq 0.20\ m/s$

When both convergence criteria are met, 200 points are measured at the current freestream velocity and averaged to create a single point, it then proceeds to increase the wind tunnel rotational speed to the next velocity. After a test, all the data points acquired are written in a .txt file by clicking the “Write File” button.

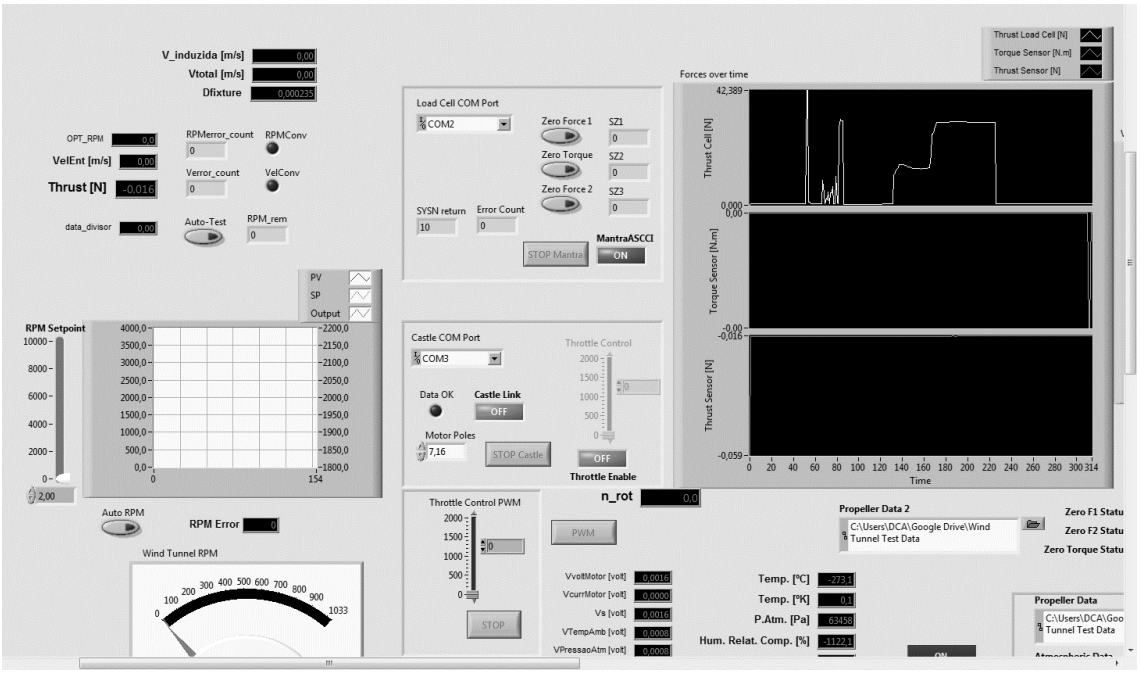

Figure 7 - Data acquisition program interface.

In Figure 7 is displayed the interface of the data acquisition program, where charts show thrust and torque readings over time, readings of propeller’s rotational speed and wind tunnel rotational speed, the thrust and torque measured by the load cells, the convergence points counter, the throttle value for propeller and wind tunnel rotational speed (automatic) and measurements of voltages, pressure and temperature.

3.2 Data reduction

The data obtained through the instruments shown in subsection 3.1 are the measured variables, of thrust, torque, freestream velocity, rotational speed, static pressure, atmospheric pressure and temperature. With the acquired measurements, the calculated variables can be obtained. Power, *P*, in *W*, is calculated with *n* and *Q*:

$$P = 2\pi nQ \quad (3.1)$$

The P_{atm}, T_{atm} and the air constant, R, 287 $J \cdot kg^{-1} \cdot K^{-1}$ are used to calculate the air density, ρ, in kg/m^3:

$$\rho = \frac{P_{atm}}{RT_{atm}} \quad (3.2)$$

Advance ratio, J, is calculated with V and n:

$$J = \frac{V}{nD} \quad (3.3)$$

Thrust coefficient, C_T and power coefficient C_P are calculated with the respective parameters T and P:

$$C_T = \frac{T}{\rho n^2 D^4} \quad (3.4)$$

$$C_P = \frac{P}{\rho n^3 D^5} \quad (3.5)$$

Finally, the propeller efficiency is calculated with the variables of C_T and C_P:

$$\eta = \frac{JC_T}{C_P} \quad (3.6)$$

After the calculation of each individual parameter, C_P and η are plotted against J. Upon observing the different behavior of all dispersions, all the power coefficient and propeller efficiency points were divided by the natural logarithm of the respective propeller rotational speed at which they were tested, therefore implicitly including the Reynolds number to the calculations since it varies with propeller RPM:

$$\frac{C_P}{\ln(N)}; \frac{\eta}{\ln(N)}$$

To simplify the terminology, from now on, these terms will be addressed as:

$$\frac{C_P}{\ln(N)} = C_{Pr} \quad (3.7)$$

$$\frac{\eta}{\ln(N)} = \eta_r \quad (3.8)$$

where the subscripted r stands for “reduced”.

The result of this reduction displayed in Figure 8 and Figure 9, where an example is shown for the APC Thin Electric 10x7 propeller, is that the data shows lesser dispersion when divided by $\ln(N)$. It should be pointed out that this effect is observable in all the tested propellers' performance curves. The data reduction is repeated for all the tested propellers.

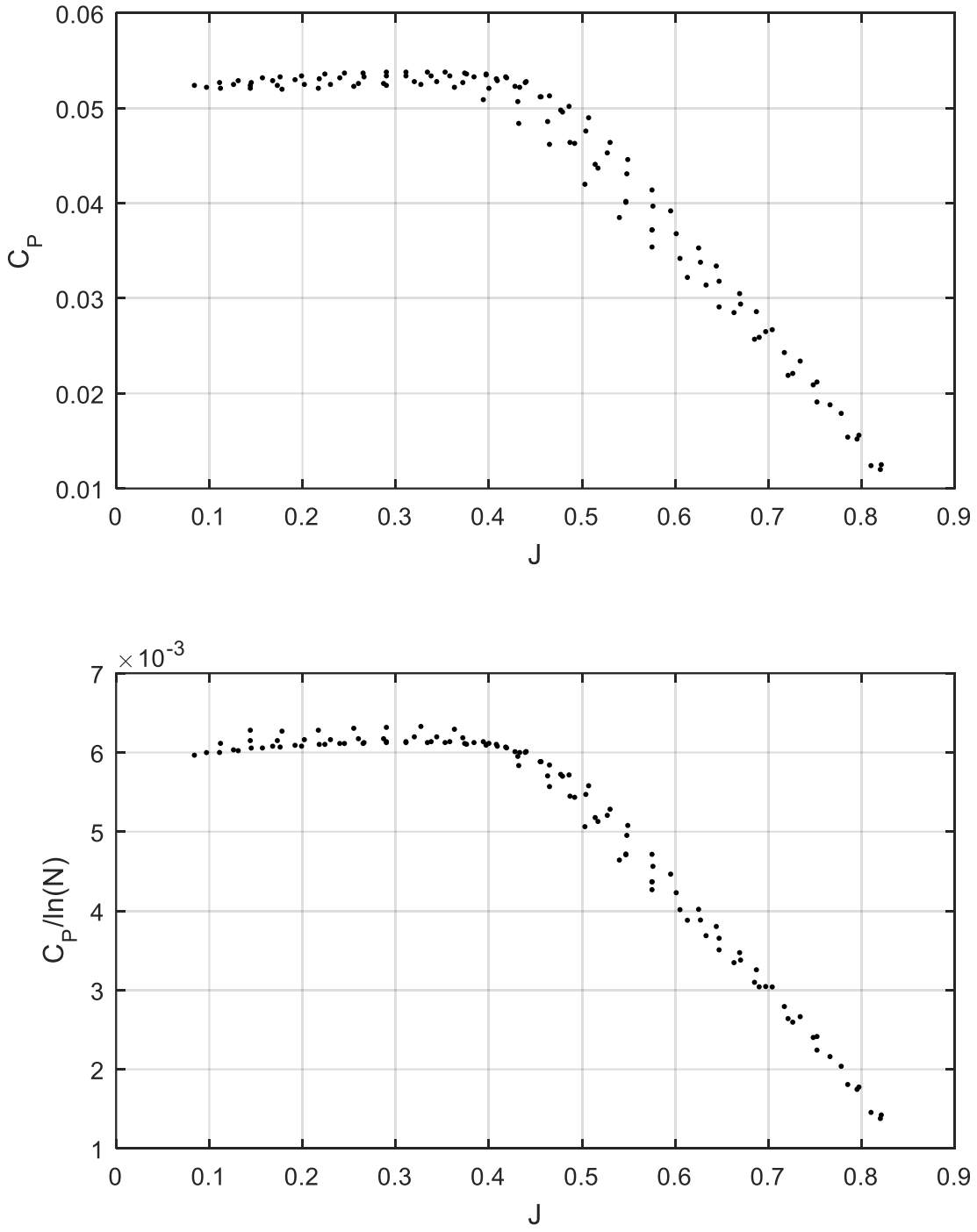

Figure 8 - Example of data points of C_P and C_{Pr}.

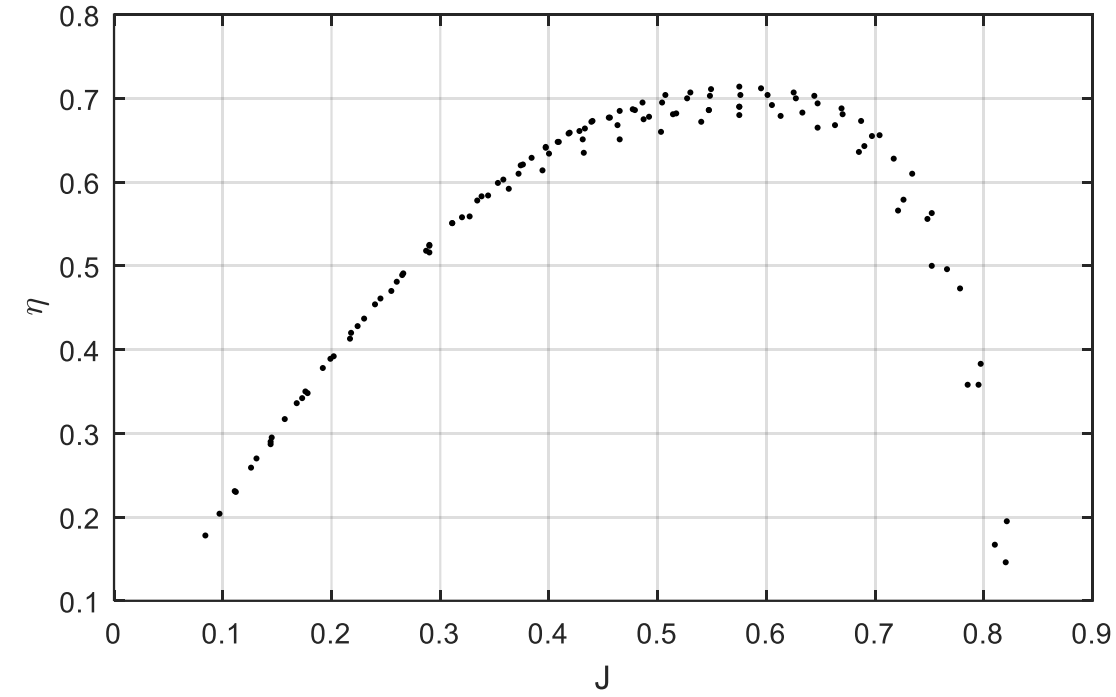

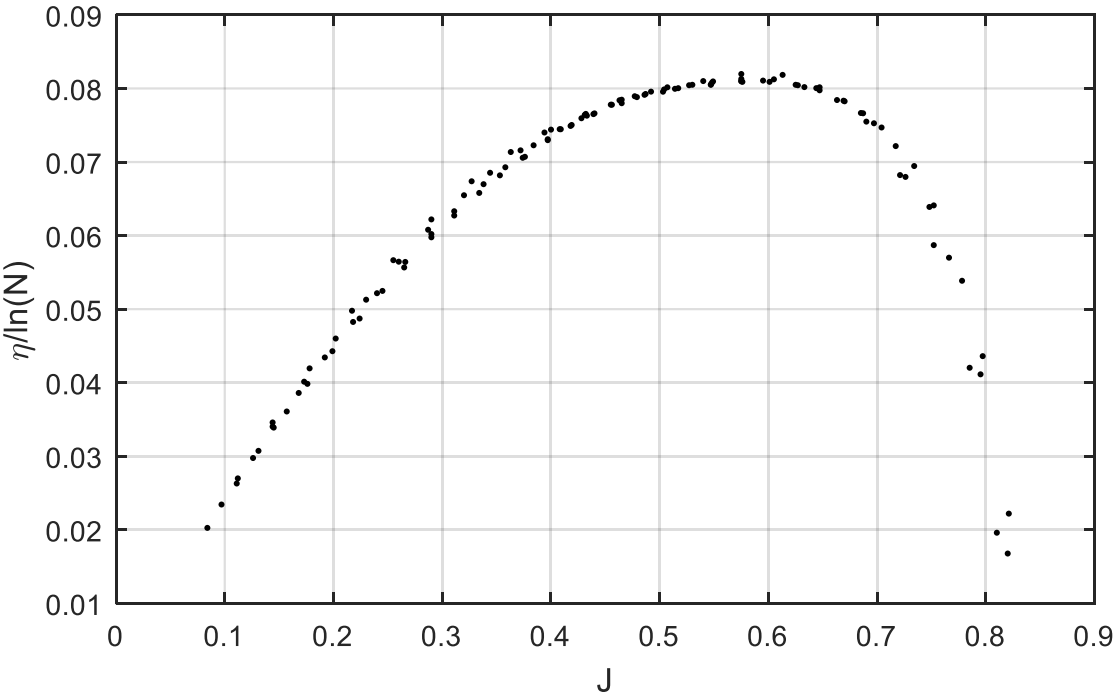

Figure 9 - Example of data points of η and η_r.

Since the curves have different sizes, but similar forms, in order to compare these curves, to come up with a model that can approximate the values of C_P and η accurately, the next step is to make these curves relative. To do this, the value of C_{Pr} must be divided by its value at $J = 0$, which will be called C_{Pr0}, and the η_r must be divided by its maximum value, η_{rmax}. This

procedure is done by using the MATLAB® "Curve Fitting Tool" to create a fitting function of C_{Pr} and η_r plotted against J, as this tool also displays the coefficients of said curve fits, it is possible to calculate the values of C_{Pr0} and η_{rmax}. The maximum value of advance ratio, J_{max}, is also retrieved from the function of η_r as propeller efficiency reaches the value of 0 before the power coefficient, and J is then divided by J_{max}.

$$\frac{C_{Pr}}{C_{Pr0}}\left(\frac{J}{J_{max}}\right) \quad (3.9)$$

$$\frac{\eta_r}{\eta_{rmax}}\left(\frac{J}{J_{max}}\right) \quad (3.10)$$

After this step, all the propeller performance curves have practically the same limits in the x-axis and the y-axis. The curve fitting procedure is the next step to construct an analytical model.

3.3 Least Squares Method

For the nth degree polynomial and a set of n+1 data points [22]:

$$p_n(x_i) = a_n x_i^n + a_{n-1} x_i^{n-1} \dots a_0 \quad (3.11)$$

For curve fit equations which are linear in the coefficients, the n+1 equations can be written in matrix form:

$$\begin{bmatrix} p_n(x_0) \\ p_n(x_1) \\ \vdots \\ p_n(x_{n+1}) \end{bmatrix} = \begin{bmatrix} x_i^n & x_i^{n-1} & \cdots & 1 \\ x_i^n & x_i^{n-1} & \cdots & 1 \\ \vdots & \vdots & \ddots & \vdots \\ x_{n+1}^n & x_{n+1}^{n-1} & \cdots & 1 \end{bmatrix} \begin{bmatrix} a_n \\ a_{n-1} \\ \vdots \\ a_0 \end{bmatrix} \quad (3.12)$$

in short matrix notation:

$$P = Xa \quad (3.13)$$

Using the least-squares approach to estimate the curve-fit coefficients, a, in matrix notation:

$$\begin{aligned} S(a) &= (P - y)^T (P - y) \\ &= a^T X^T X a - a^T X^T y - y^T X a + y^T y \end{aligned} \quad (3.14)$$

The necessary criterion for minimizing S with respect to the set of curve-fit coefficients, its derivative must be zero.

$$\frac{\delta S}{\delta a} = 0 \leftrightarrow X^T X a = X^T y \quad (3.15)$$

And the unconstrained least-squares estimates for the curve-fit coefficients can be computed from:

$$a = [X^T X]^{-1} X^T y \quad (3.16)$$

Since the ordinary LSQ fits the best line to data, it does not necessarily mean that the curve fit passes through some points that are explicit, so in this research, it was used the constrained LSQ. To do so, the method of Lagrange multipliers will be applied.
To calculate the coefficients using the constrained LSQ, suppose the curve-fit needs to pass through a certain point (x_c, y_c):

$$y_c = p(x_c) = a_n x_c^n + a_{n-1} x_c^{n-1} \dots a_0 \quad (3.17)$$

in short matrix notation:

$$b = Aa \quad (3.18)$$

Like the ordinary LSQ, it is required to minimize the augmented S function (with the Lagrangian):

$$S(a, \lambda) = a^T X^T X a - a^T X^T y - y^T X a + y^T y + \lambda^T (Aa - b) \quad (3.19)$$

Minimizing $S(a, \lambda)$ with respect to a and maximizing with respect to λ results in a system of linear equations for the optimum coefficients a^* and Lagrange multipliers λ^*:

$$\begin{bmatrix} 2X^T X & A^T \\ A & 0 \end{bmatrix} \begin{bmatrix} a^* \\ \lambda^* \end{bmatrix} = \begin{pmatrix} 2X^T y \\ b \end{pmatrix} \quad (3.20)$$

If the matrix $\begin{bmatrix} \boldsymbol{2X^T X} & \boldsymbol{A^T} \\ \boldsymbol{A} & \boldsymbol{0} \end{bmatrix}$ is invertible:

$$\begin{bmatrix} \boldsymbol{a^*} \\ \boldsymbol{\lambda^*} \end{bmatrix} = \begin{bmatrix} \boldsymbol{2X^T X} & \boldsymbol{A^T} \\ \boldsymbol{A} & \boldsymbol{0} \end{bmatrix}^{-1} \begin{pmatrix} \boldsymbol{2X^T y} \\ \boldsymbol{b} \end{pmatrix} \quad (3.21)$$

3.4 "Goodness" of fits

This subject describes how well a polynomial approximation, or a statistical model, fits the observed data. There are several ways to identify the "goodness" of the statistical model. Error calculations and the coefficient of determination are some of these methods, explained in subsections 3.4.1 and 3.4.3. To better understand the distance between the data points and the model is an explanation on standard deviation in subsection 3.4.2.

3.4.1 Statistical Error

Often used in validation of linear regressions, the absolute error is the difference between the observed value y_i at a determined x_i value, and the model's prediction, f_i at the same abscissa. The absolute error can be calculated through:

$$e_i = |y_i - f_i| \quad (3.22)$$

The relative error can be calculated with the difference between the observed value and the predicted value, divided by the observed value:

$$\delta = \frac{|y_i - f_i|}{y_i}(100) = \frac{e_i}{y_i}(100) \quad (3.23)$$

The mean relative error (MRE) is also used to evaluate the model and can be calculated as follows (N is the total number of points in the data set):

$$MRE = \frac{\sum \delta_i}{N}$$

3.4.2 Standard Deviation

The standard deviation (σ) is used to quantify the dispersion of a set of data values. It can be calculated by:

$$\sigma = \sqrt{\frac{\sum (y_i - f_i)^2}{N}} \quad (3.24)$$

where σ, represents the standard deviation, y_i is the measured value and f_i is the estimated value.

Lower values of σ indicate that the data points tend to be close to the model's prediction, and higher values indicates that the points are farther from the model's prediction.

3.4.3 Coefficient of Determination

In regression validation the coefficient of determination is the proportion of the variance in the dependent variable that is predictable from the independent variables. It is calculated with the division of the residual sum of squares with the total sum of squares:

$$R^2 = 1 - \frac{\sum(y_i - f_i)^2}{\sum(y_i - \bar{y})^2} \quad (3.25)$$

Its value can range from 0 to 1, with a value of 0 meaning the statistical model is not well defined at all, and a value of 1 meaning the statistical model perfectly fits the data.

Typically, anything above $R^2 > 0.7$ is considered a very good fit, but it all depends on the researcher's criteria.

Chapter 4

Results and discussion

In this section, the experimental data will be analyzed in order to separate the different C_P and η plots into groups with a common variable, to create a multivariable plot, using regression methods, that describes how the performance parameters behave when plotted against *J* and a common variable. The results of this analysis will be verified with the measurements from UIUC.

A test will be conducted with the analytical model, to see if the estimated performance curves match the experimental data acquired at UBI. Afterwards, this experimental data will be used to further develop the analytical model, and the updated model will be verified with the measurements from both UIUC and UBI.

4.1 Experimental data

The first step to construct the analytical model is to acquire the data. The analytical model has been constructed with data from the UIUC Propeller Database [2], namely the APC Thin Electric Propellers with the following dimensions: 8x4, 8x6, 8x8, 9x4.5, 9x6, 9x7.5, 9x9, 10x5, 10x7, 11x5.5, 11x7, 11x8, 11x8.5, 11x10, 14x12, 17x12, 19x12. The measurements include thrust and torque coefficient data over a range of advance ratios for specific RPMs. Including some measurements that were taken in static conditions for a few specific RPMs.

The data retrieved from the database includes the measurements of power coefficient, C_P which is obtained from the measured torque coefficient and advance ratio, and the propeller efficiency, which is obtained from the calculated C_P, and the measured thrust and advance ratio.

For the validation procedure, tests at the wind tunnel at UBI were conducted, by using the experimental setup created by Alves [16]. The propellers that were tested during the execution of this work are also the same brand and type, APC Thin Electric Propellers, and the dimensions are: 7x4, 13x4, 13x10, 14x10, 15x6, 15x10, 16x10, 18x8, 20x8, 20x15.

4.2 Curve fitting

4.2.1 Power Coefficient

Through analysis of all the data points after reduction, three different behaviors were observed, so the plots were separated into three segments. The first segment (Figure 10) contains the plots of data points corresponding to one behavior that is seen when the propeller's $\frac{p}{D}$ ratio is 0.5. In Figure 11 and Figure 12 are shown the remaining two behaviors that are observed when the same ratio is not equal to 0.5.

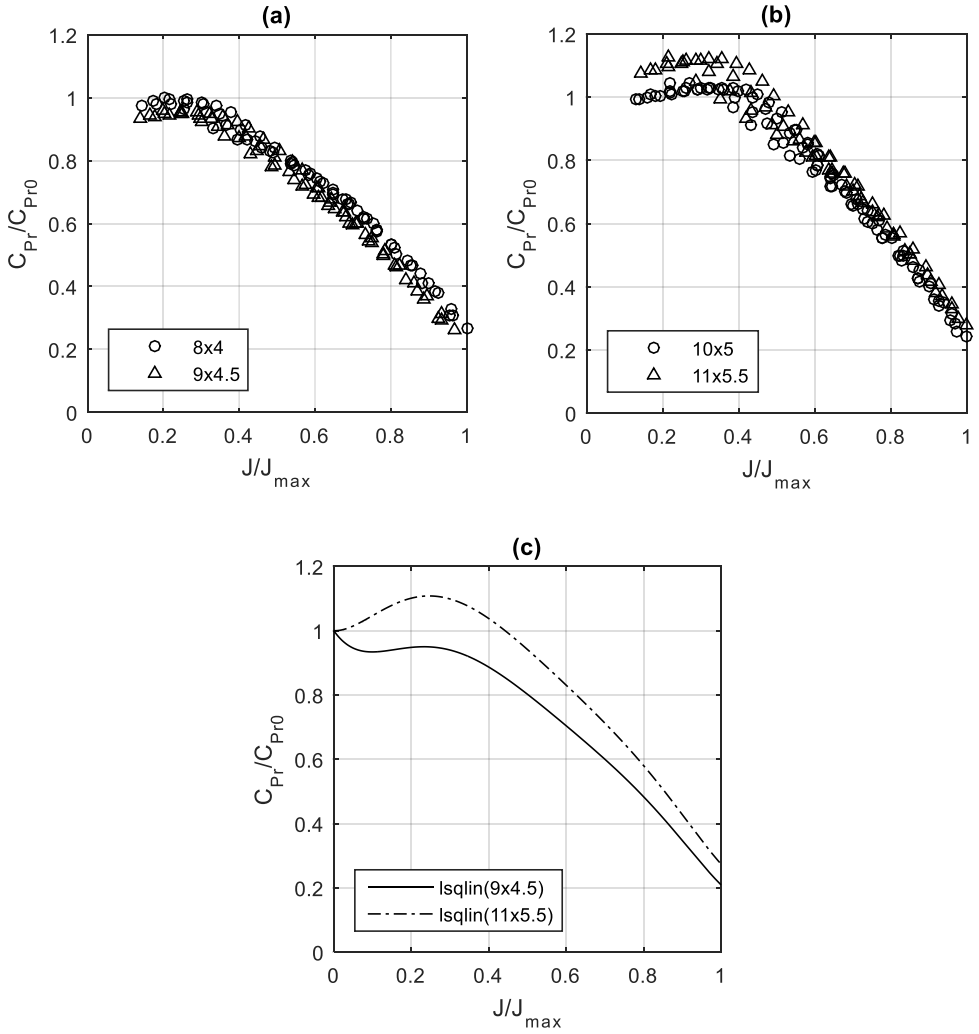

Figure 10 - Dispersion for propellers with $\frac{p}{D}$ ratio of 0.5 (a and b) and the results of *lsqlin* function in MATLAB® (c).

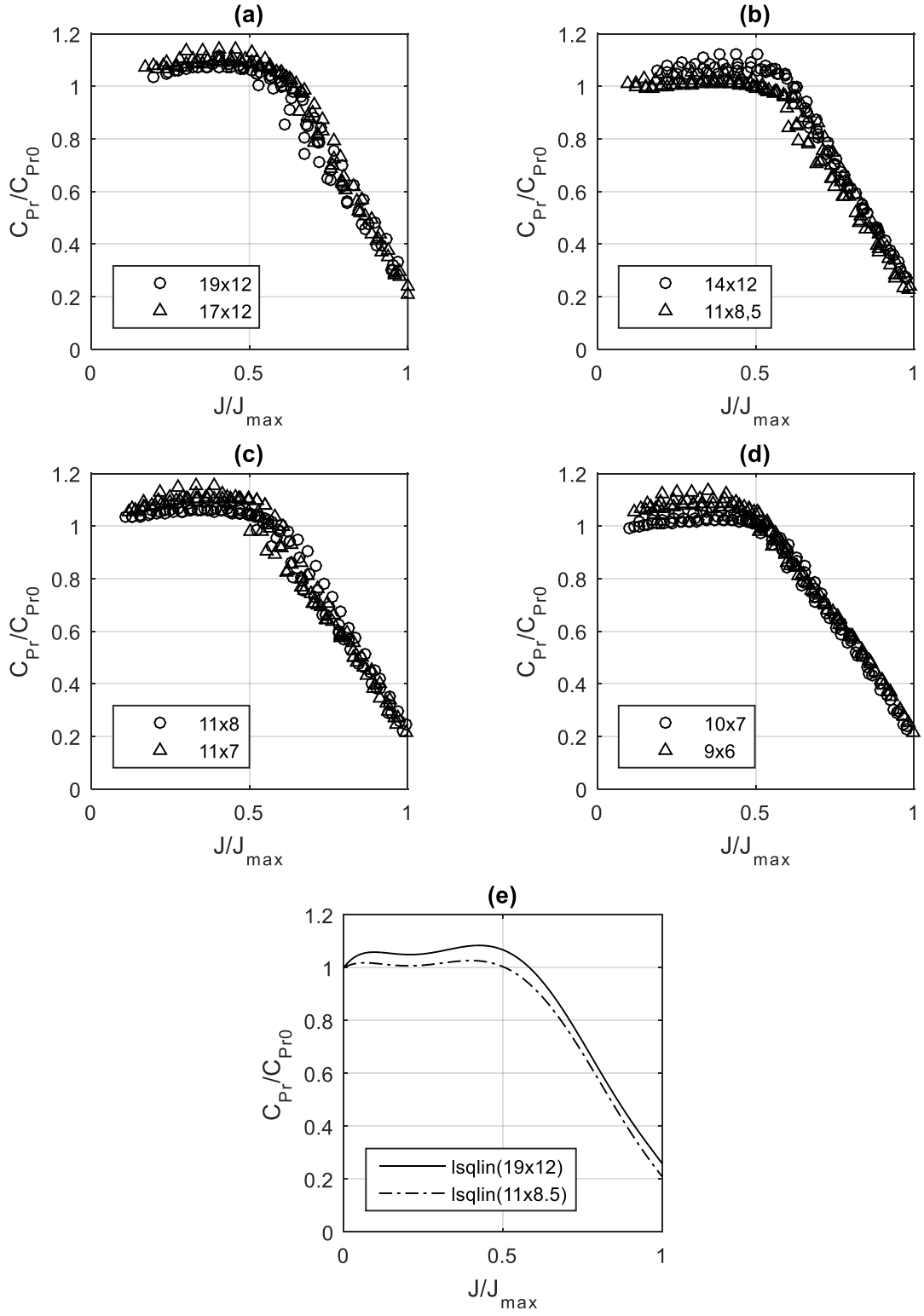

Figure 11 - 1 of 2 different behaviors of data for propellers with $\frac{p}{D}$ ratio not equal to 0.5 (a, b, c, and d) and the results of *lsqlin* function in MATLAB® (e).

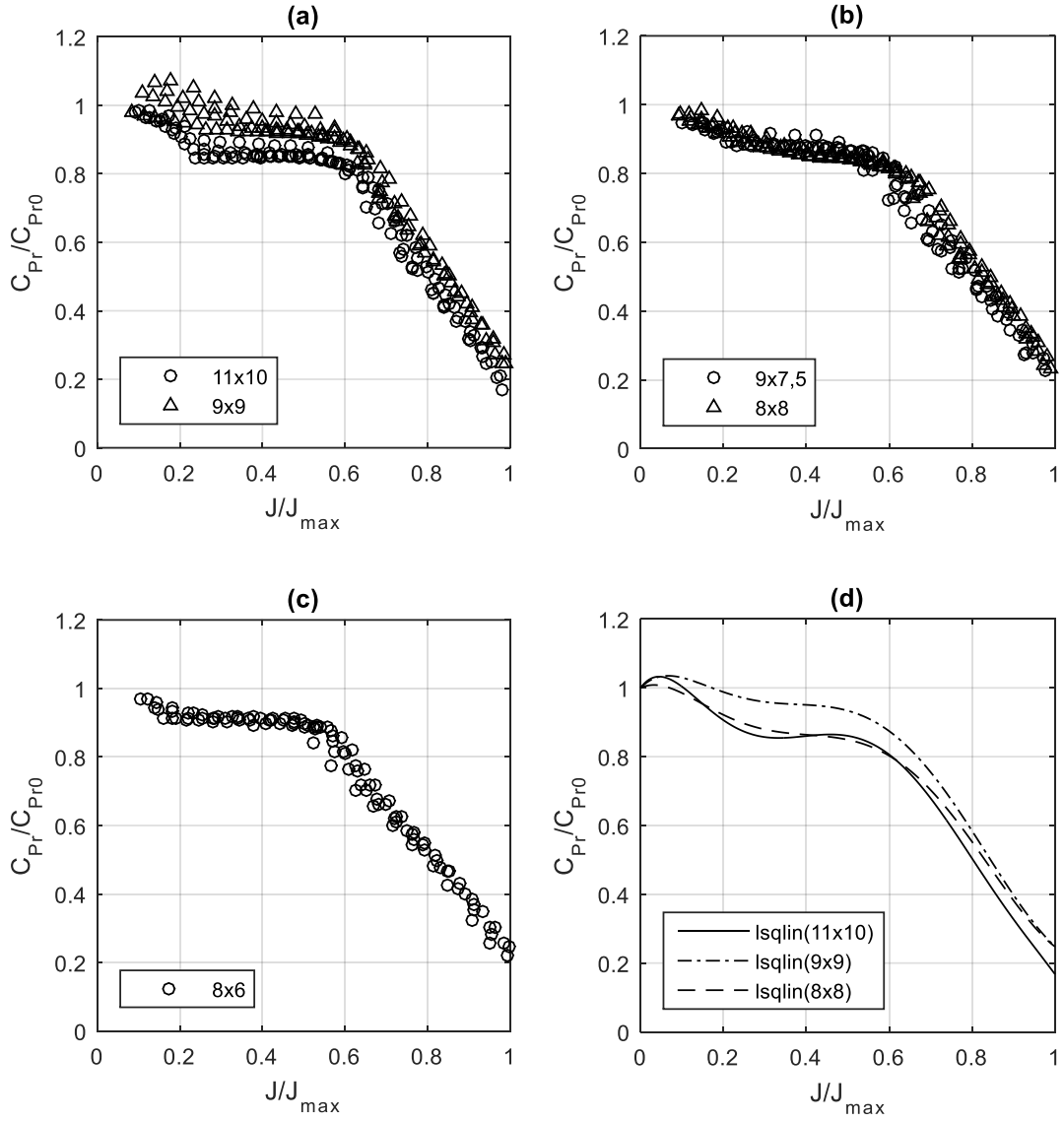

Figure 12 - 2 of 2 different behaviors of data for propeller with $\frac{p}{D}$ not equal to 0.5 (a, b, c) and the results of *lsqlin* function in MATLAB® (d).

After different attempts, the conclusion is that the graphs show different behaviors based on the $\frac{D+p}{C_{Pro}}$ ratio. Propellers with $\frac{D+p}{C_{Pro}} > 2400$ show curves like the ones in Figure 11, and propellers with $\frac{D+p}{C_{Pro}} < 2400$ tend to behave like the ones in Figure 12.

Table 2 - Values of *D*, *p*, C_{Pr0} and $\frac{D+p}{C_{Pr0}}$ for each propeller with $\frac{p}{D} \neq 0.5$:

***D* [in]**	***p* [in]**	C_{Pr0}	$\frac{D+p}{C_{Pr0}}$
8	8	0,013	1194
9	9	0,011	1556
8	6	0,008	1579
9	7,5	0,010	1650
11	10	0,009	2168
9	6	0,005	2636
10	7	0,006	2833
11	8,5	0,007	3000
11	8	0,006	3304
11	7	0,005	3600
14	12	0,007	4000
17	12	0,006	5273
19	12	0,005	6200

When $\frac{p}{D} = 0.5$ the only relationship is C_{Pr0}:

Table 3 - Values of D, p and C_{Pr0} for propeller with $\frac{p}{D} = 0.5$.

***D* [in]**	***p* [in]**	C_{Pr0}
8	4	0,004780
9	4,5	0,004888
10	5	0,004446
11	5,5	0,003555

In Figure 10, Figure 11 and Figure 12 there are various curve fits created using the *lsqlin* function in MATLAB®, which, based on constrained linear least squares theory creates plots to best fit every data point, while satisfying certain constraints, in this case, when $\frac{C_{Pr}}{C_{Pr0}}(0) = 1$. Some curves are selected to later calculate a multivariable function to best fit all the data.

The results of each curve fit shown in Figure 10, Figure 11 and Figure 12 can be found below.

$$lsqlin(9x4.5) = \frac{C_{Pr}}{C_{Pr0}}\left(\frac{J}{J_{max}}\right) = 19.6429\left(\frac{J}{J_{max}}\right)^6 - 66.5756\left(\frac{J}{J_{max}}\right)^5 + 87.1678\left(\frac{J}{J_{max}}\right)^4 + 66.1909\left(\frac{J}{J_{max}}\right)^3 - 16.0479\left(\frac{J}{J_{max}}\right)^2 + 1.6430\left(\frac{J}{J_{max}}\right) + 1 \quad (4.1)$$

$$lsqlin(11x5.5) = \frac{C_{Pr}}{C_{Pr0}}\left(\frac{J}{J_{max}}\right)$$

$$= 18.0768\left(\frac{J}{J_{max}}\right)^6 - 59.3233\left(\frac{J}{J_{max}}\right)^5 + 73.7589\left(\frac{J}{J_{max}}\right)^4 \quad (4.2)$$

$$- 41.7846\left(\frac{J}{J_{max}}\right)^3 + 8.5878\left(\frac{J}{J_{max}}\right)^2 - 0.0416\left(\frac{J}{J_{max}}\right) + 1$$

$$lsqlin(19x12) = \frac{C_{Pr}}{C_{Pr0}}\left(\frac{J}{J_{max}}\right)$$

$$= -30.2319\left(\frac{J}{J_{max}}\right)^6 + 100.8076\left(\frac{J}{J_{max}}\right)^5 - 123.1031\left(\frac{J}{J_{max}}\right)^4 \quad (4.3)$$

$$+ 66.1909\left(\frac{J}{J_{max}}\right)^3 - 16.0479\left(\frac{J}{J_{max}}\right)^2 + 1.6430\left(\frac{J}{J_{max}}\right) + 1$$

$$lsqlin(11x8.5) = \frac{C_{Pr}}{C_{Pr0}}\left(\frac{J}{J_{max}}\right)$$

$$= -17.3040\left(\frac{J}{J_{max}}\right)^6 + 59.3863\left(\frac{J}{J_{max}}\right)^5 - 72.9561\left(\frac{J}{J_{max}}\right)^4 \quad (4.4)$$

$$+ 37.7072\left(\frac{J}{J_{max}}\right)^3 - 8.3066\left(\frac{J}{J_{max}}\right)^2 + 0.6825\left(\frac{J}{J_{max}}\right) + 1$$

$$lsqlin(11x10) = \frac{C_{Pr}}{C_{Pr0}}\left(\frac{J}{J_{max}}\right)$$

$$= -37.4430\left(\frac{J}{J_{max}}\right)^6 + 128.9251\left(\frac{J}{J_{max}}\right)^5 - 165.2866\left(\frac{J}{J_{max}}\right)^4 \quad (4.5)$$

$$+ 95.2105\left(\frac{J}{J_{max}}\right)^3 - 23.8601\left(\frac{J}{J_{max}}\right)^2 + 1.6216\left(\frac{J}{J_{max}}\right) + 1$$

$$lsqlin(9x9) = \frac{C_{Pr}}{C_{Pr0}}\left(\frac{J}{J_{max}}\right)$$

$$= -14.1857\left(\frac{J}{J_{max}}\right)^6 + 55.6621\left(\frac{J}{J_{max}}\right)^5 - 78.6270\left(\frac{J}{J_{max}}\right)^4 \quad (4.6)$$

$$+ 48.6145\left(\frac{J}{J_{max}}\right)^3 - 13.4444\left(\frac{J}{J_{max}}\right)^2 + 1.2284\left(\frac{J}{J_{max}}\right) + 1$$

$$lsqlin(8x8) = \frac{C_{Pr}}{C_{Pr0}}\left(\frac{J}{J_{max}}\right)$$

$$= -9.3172\left(\frac{J}{J_{max}}\right)^6 + 40.4902\left(\frac{J}{J_{max}}\right)^5 - 60.9606\left(\frac{J}{J_{max}}\right)^4 \quad (4.7)$$

$$+ 38.8674\left(\frac{J}{J_{max}}\right)^3 - 10.3888\left(\frac{J}{J_{max}}\right)^2 + 0.5565\left(\frac{J}{J_{max}}\right) + 1$$

To minimize the number of equations when calculating the power coefficient, three functions with two variables were created, one for each behavior shown above:

1. $\frac{p}{D} = 0.5$
2. $\frac{p}{D} \neq 0.5 \; and \; \frac{D+p}{\mathrm{C_{Pr0}}} > 2400$
3. $\frac{p}{D} \neq 0.5 \; and \; \frac{D+p}{\mathrm{C_{Pr0}}} < 2400$

Using the definition of a line applied to case 1.:

$$C_{P1} = lsqlin(9x4.5) + \frac{lsqlin(11x5.5) - lsqlin(9x4.5)}{0.00355 - 0.004888}(C_{Pr0} - 0.00488)$$

$$\begin{aligned} &= 19.6429\left(\frac{J}{J_{max}}\right)^6 - 66.5756\left(\frac{J}{J_{max}}\right)^5 + 87.1678 - 54.5072\left(\frac{J}{J_{max}}\right)^3 \\ &+ 15.1975\left(\frac{j}{j_{máx}}\right)\left(\frac{J}{J_{max}}\right)^2 - 1.7161\left(\frac{J}{J_{max}}\right) \\ &- \left[(C_{Pr0} - 0.00488)\left(-1177.518797\left(\frac{J}{J_{max}}\right)^6 + 5452.857143\left(\frac{J}{J_{max}}\right)^5\right.\right. \\ &- 10081.8797\left(\frac{J}{J_{max}}\right)^4 + 9565.864662\left(\frac{J}{J_{max}}\right)^3 - 4969.699248\left(\frac{J}{J_{max}}\right)^2 \\ &\left.\left. + 1259.022556\left(\frac{J}{J_{max}}\right)\right)\right] \end{aligned} \tag{4.8}$$

Creates the following plot:

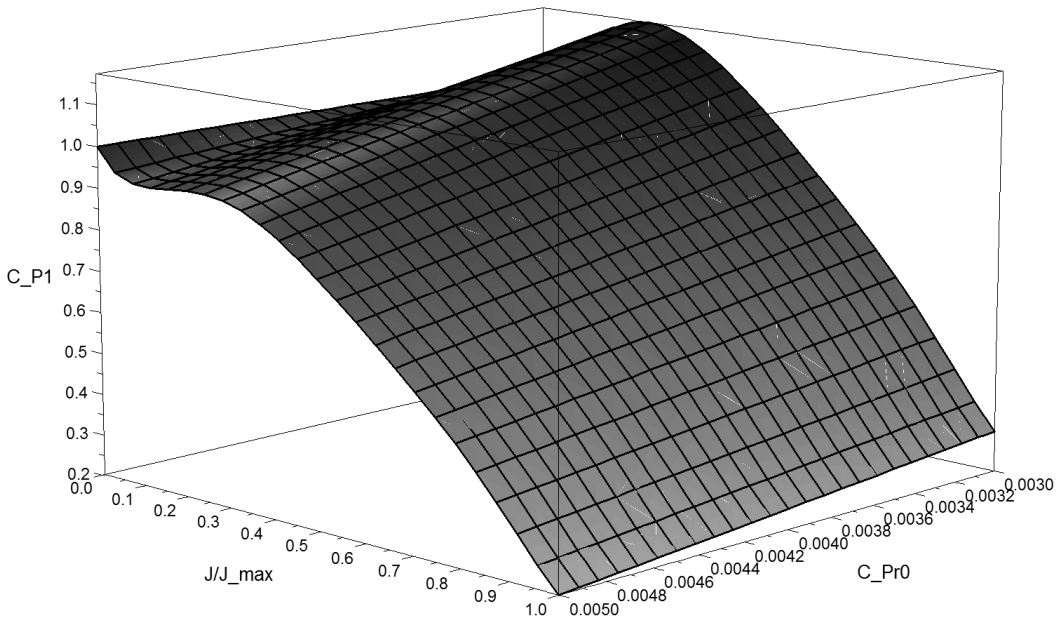

Figure 13 - 3D plot of C_{P1}.

For case 2:

$$C_{P2} = lsqlin(11x8.5) + \frac{lsqlin(19x12) - lsqlin(11x8.5)}{6200 - 3000}\left(\frac{D+p}{C_{Pr0}} - 3000\right)$$

$$\begin{aligned}
&= -17.304\left(\frac{J}{J_{max}}\right)^6 + 167.5\left(\frac{J}{J_{max}}\right)^5 - 72.9561\left(\frac{J}{J_{max}}\right)^4 + 37.7072\left(\frac{J}{J_{max}}\right)^3 \\
&- 8.3066\left(\frac{J}{J_{max}}\right)^2 + 0.6825\left(\frac{J}{J_{max}}\right) + 1 \\
&- \left[\left(\frac{D+p}{C_{Pr0}} - 3000\right)\left(-0.00403996875\left(\frac{J}{J_{max}}\right)\right.\right. \\
&+ 0.01294415625\left(\frac{J}{J_{max}}\right)^5 - 0.0156709375\left(\frac{J}{J_{max}}\right)^4 + 0.00890115625\left(\frac{J}{J_{max}}\right)^3 \\
&\left.\left. - 0.00241915625\left(\frac{J}{J_{max}}\right)^2 + 0.00030015625\left(\frac{J}{J_{max}}\right)\right)\right]
\end{aligned} \tag{4.9}$$

and for case 3, it is used the definition of a parabola:

$$C_{P3} = \frac{C_{Pr}}{C_{Pr0}}\left(\frac{J}{J_{max}}, \frac{D+p}{C_{Pr0}}\right) = A\left(\frac{D+p}{C_{Pr0}}\right)^2 + B\left(\frac{D+p}{C_{Pr0}}\right) + C \quad (4.10)$$

Solving with a system of equations:

$$\begin{cases} lsqlin(11x10) = A\left(\frac{D+p}{C_{Pr0}}\right)^2 + B\left(\frac{D+p}{C_{Pr0}}\right) + C \\ lsqlin(8x8) = A\left(\frac{D+p}{C_{Pr0}}\right)^2 + B\left(\frac{D+p}{C_{Pr0}}\right) + C \\ lsqlin(9x9) = A\left(\frac{D+p}{C_{Pr0}}\right)^2 + B\left(\frac{D+p}{C_{Pr0}}\right) + C \end{cases} \quad (4.11)$$

Solving for A, B and C results in a final equation C_{P3}:

$$\begin{aligned} C_{P3} = \frac{C_{Pr}}{C_{Pr0}}\left(\frac{J}{J_{max}}, \frac{D+p}{C_{Pr0}}\right) \\ = \Bigg(-0.00002519568556\left(\frac{J}{J_{max}}\right)^6 + 0.00007983583595\left(\frac{J}{J_{max}}\right)^5 \\ - 0.00009522857874\left(\frac{J}{J_{max}}\right)^4 + 0.00005049925633\left(\frac{J}{J_{max}}\right)^3 \\ - 0.000008799029191\left(\frac{J}{J_{max}}\right)^2\Bigg)\left(\frac{D+p}{C_{Pr0}}\right)^2 \\ + \Bigg(0.05582316189\left(\frac{J}{J_{max}}\right)^6 - 0.1775868247\left(\frac{J}{J_{max}}\right)^5 \\ + 0.213017194\left(\frac{J}{J_{max}}\right)^4 - 0.1119150618\left(\frac{J}{J_{max}}\right)^3 \\ + 0.01574791229\left(\frac{J}{J_{max}}\right)^2 + 0.005288737972\left(\frac{J}{J_{max}}\right)\Bigg)\left(\frac{D+p}{C_{Pr0}}\right) \\ + \Bigg(-40.05004857\left(\frac{J}{J_{max}}\right)^6 + 138.711635\left(\frac{J}{J_{max}}\right)^5 \\ - 179.5414078\left(\frac{J}{J_{max}}\right)^4 + 100.5001657\left(\frac{J}{J_{max}}\right)^3 \\ - 16.64743656\left(\frac{J}{J_{max}}\right)^2 - 3.979392749\left(\frac{J}{J_{max}}\right) + 1\Bigg) \end{aligned} \quad (4.12)$$

Since both C_{P2} and C_{P3} depend on the same two variables, $\frac{J}{J_{max}}$ and $\frac{D+p}{\mathrm{C_{Pr0}}}$ it is possible to plot both as a piecewise function:

$$C_{P2,3}\begin{cases} C_{P2}\left(\frac{J}{J_{max}}, \frac{p+D}{C_{Pr0}}\right), & \frac{p+D}{C_{Pr0}} < 2400 \\ C_{P3}\left(\frac{J}{J_{max}}, \frac{p+D}{C_{Pr0}}\right), & \frac{p+D}{C_{Pr0}} \geq 2400 \end{cases} \quad (4.13)$$

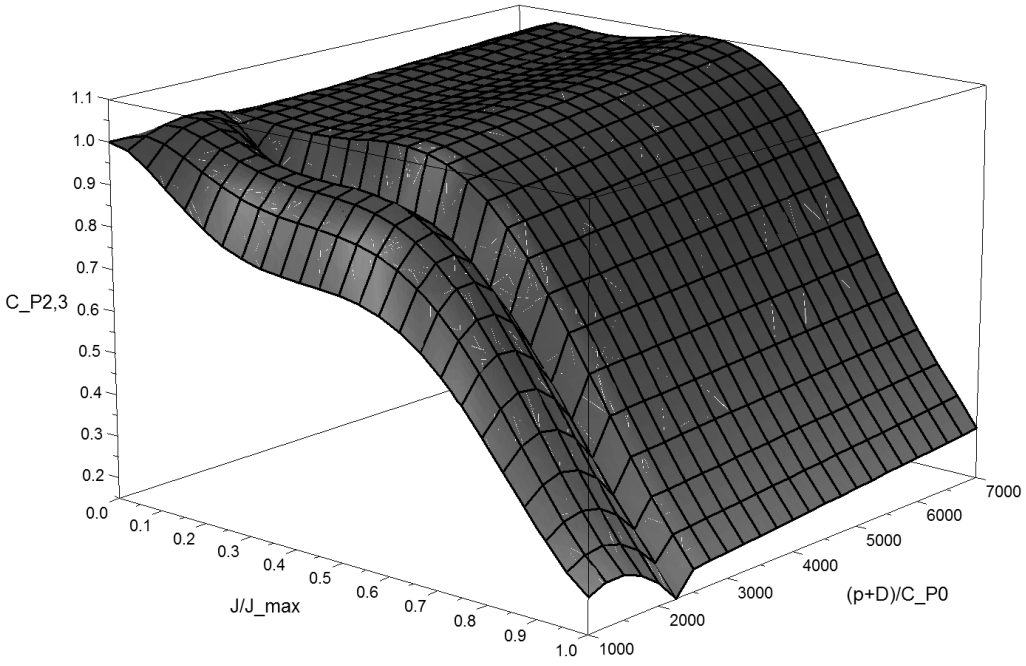

Figure 14 - 3D plot of $C_{\mathrm{P2,3}}$.

4.2.2 Propeller Efficiency

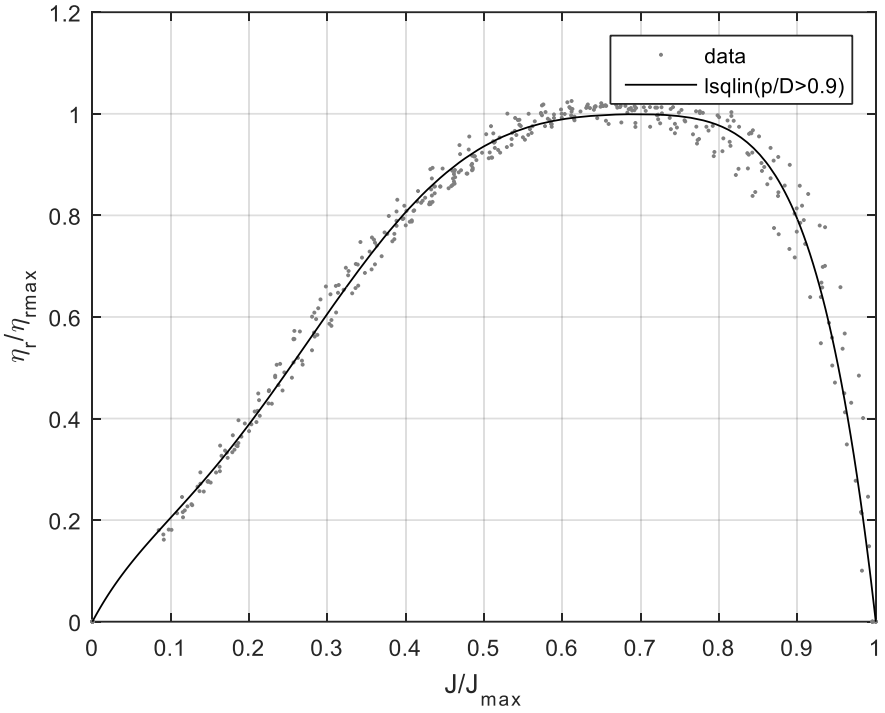

Figure 15 - 1 of 2 behaviors of propeller efficiency when $\frac{p}{D} > 0.9$.

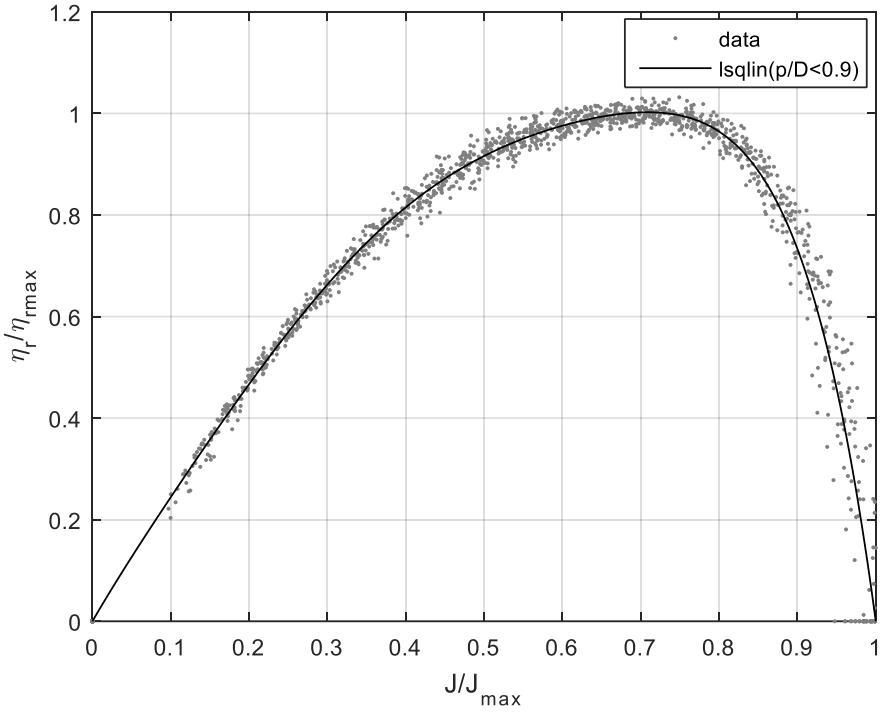

Figure 16 - 2 of 2 behaviors of propeller efficiency when $\frac{p}{D} < 0.9$.

The curve fits shown in Figure 15 and Figure 16 have also been created using the *lsqlin* function from the "Optimization Tool" in MATLAB®. The constraints used in these two cases were:

- $\frac{\eta_r}{\eta_{rmax}}(0) = 0;$
- $\frac{\eta_r}{\eta_{rmax}}(1) = 0;$
- $\frac{d\left(\frac{\eta_r}{\eta_{rmax}}\left(\left(\frac{J}{J_{max}}\right)_{\eta\_max}\right)\right)}{d\left(\frac{J}{J_{max}}\right)} = 0.$

$$lsqlin\left(\frac{p}{D} > 0.9\right) = -77.1935\left(\frac{J}{J_{max}}\right)^6 + 202.5785\left(\frac{J}{J_{max}}\right)^5 - 196.5373\left(\frac{J}{J_{max}}\right)^4 + 83.3452\left(\frac{J}{J_{max}}\right)^3 - 15.0943\left(\frac{J}{J_{max}}\right)^2 + 2.9014\left(\frac{J}{J_{max}}\right) \quad (4.14)$$

$$lsqlin\left(\frac{p}{D} < 0.9\right) = -29.4085\left(\frac{J}{J_{max}}\right)^6 + 65.2815\left(\frac{J}{J_{max}}\right)^5 - 51.8950\left(\frac{J}{J_{max}}\right)^4 + 16.7248\left(\frac{J}{J_{max}}\right)^3 - 3.3596\left(\frac{J}{J_{max}}\right)^2 + 2.6568\left(\frac{J}{J_{max}}\right) \quad (4.15)$$

To create a multivariable function that relates the two curve fits represented in Figures 14 and 15, a similar approach to the one used with the power coefficient was used, but this time the second variable introduced is $\frac{p}{D}$:

Table 4 - Averages of propellers' $\frac{p}{D}$ ratio.

Propeller	Average $\frac{p}{D}$ ratio
Propeller 8x4	0.6629263
Propeller 8x6	
Propeller 9x4.5	
Propeller 9x6	
Propeller 9x7.5	
Propeller 10x5	
Propeller 10x7	
Propeller 11x5.5	
Propeller 11x7	
Propeller 11x8	
Propeller 11x8.5	
Propeller 14x12	
Propeller 17x12	
Propeller 19x12	
Propeller 8x8	0.9696970
Propeller 9x9	
Propeller 11x10	

$$\frac{\eta_r}{\eta_{rmax}}\left(\frac{J}{J_{max}},\frac{p}{D}\right)$$
$$= lsqlin\left(\frac{p}{D} > 0.9\right) + \frac{lsqlin\left(\frac{p}{D} < 0.9\right) - lsqlin\left(\frac{p}{D} > 0.9\right)}{0.6629263 - 0.9696970}\left(\frac{p}{D} - 0.9696970\right) \quad (4.16)$$

Which resulted in:

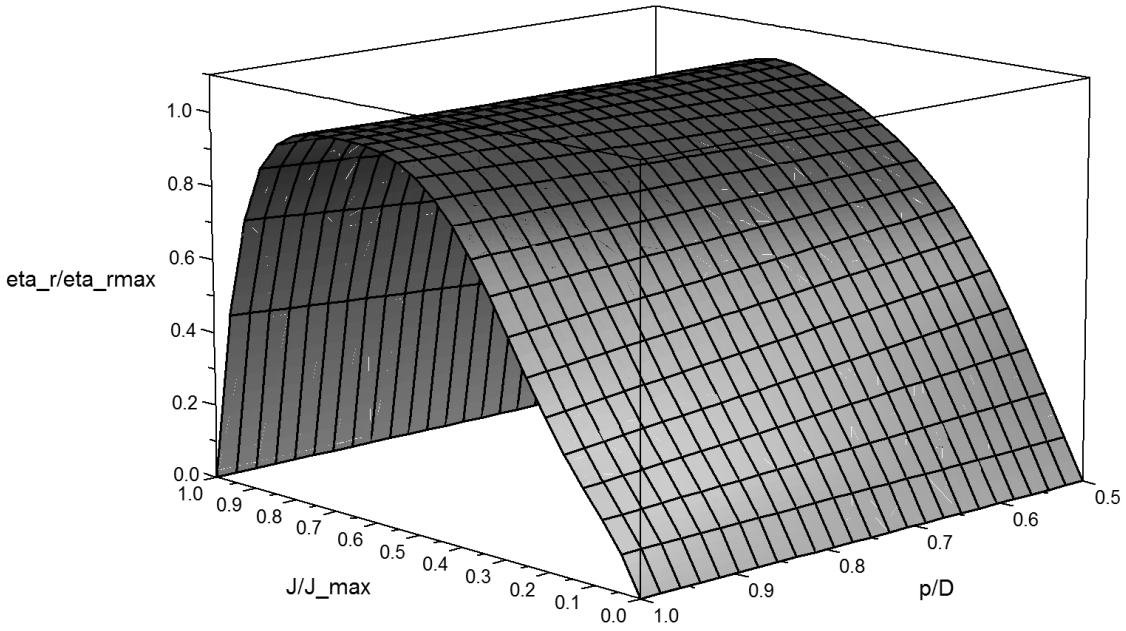

Figure 17 - 3D plot of η_1.

$$\eta_1 = \frac{\eta_r}{\eta_{rmax}}\left(\frac{J}{J_{max}},\frac{p}{D}\right)$$
$$= -77.1935\left(\frac{J}{J_{max}}\right)^6 + 202.5785\left(\frac{J}{J_{max}}\right)^5 - 196.5373\left(\frac{J}{J_{max}}\right)^4 + 83.3452\left(\frac{J}{J_{max}}\right)^3$$
$$- 15.0943\left(\frac{J}{J_{max}}\right)^2 + 2.9014\left(\frac{J}{J_{max}}\right) + \left(\frac{p}{D} - 0.969697\right)\Bigg(-155.7678096\left(\frac{J}{J_{max}}\right)^6 \quad (4.17)$$
$$+ 447.5557803\left(\frac{J}{J_{max}}\right)^5 - 471.4997228\left(\frac{J}{J_{max}}\right)^4 + 217.1667633\left(\frac{J}{J_{max}}\right)^3$$
$$- 38.25234939\left(\frac{J}{J_{max}}\right)^2 + 0.7973382073\left(\frac{J}{J_{max}}\right)\Bigg)$$

4.2.3 Additional Parameters

In order to calculate the real power coefficient and the propeller efficiency there are still some functions to create, such as: $J_{max}(D,p)$, $C_{Pr0}(D,p)$ and $\eta_{rmax}(D,p)$.
Using MATLAB® application "Curve Fitting Tool", these two variable plots were created:

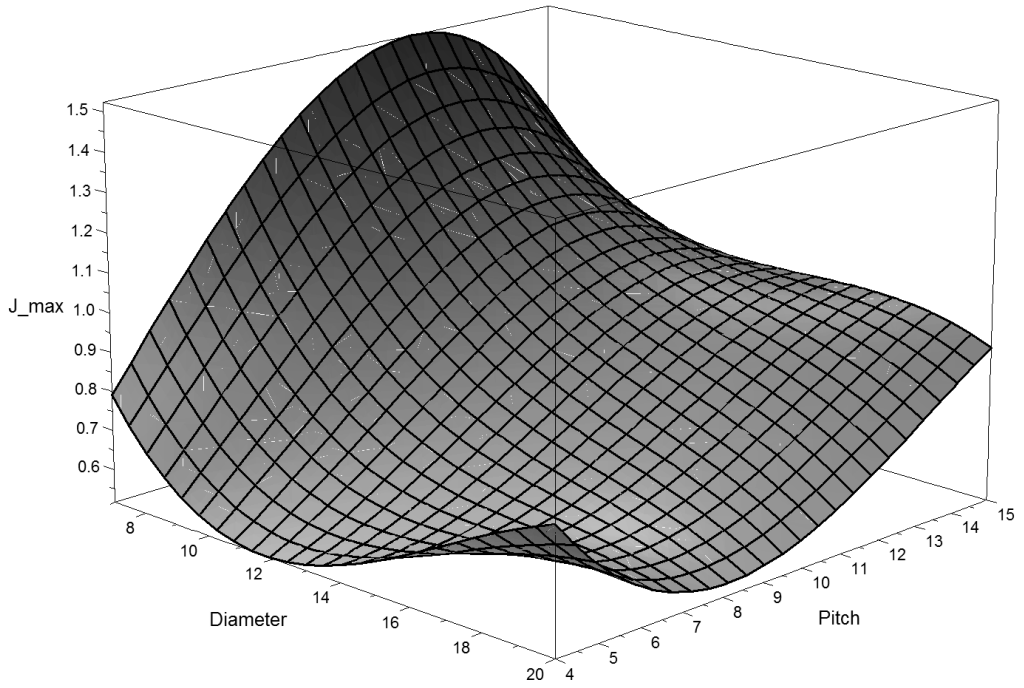

Figure 18 - $J_{max}(D,p)$.

$$J_{máx}(D,p) = 1.586 - 0.3891D + 0.3331p + 0.0323D^2 - 0.02883Dp - 0.003682p^2 - 0.0006063D^3 - 0.0003473D^2p + 0.001872Dp^2 - 0.0008377p^3 \quad (4.18)$$

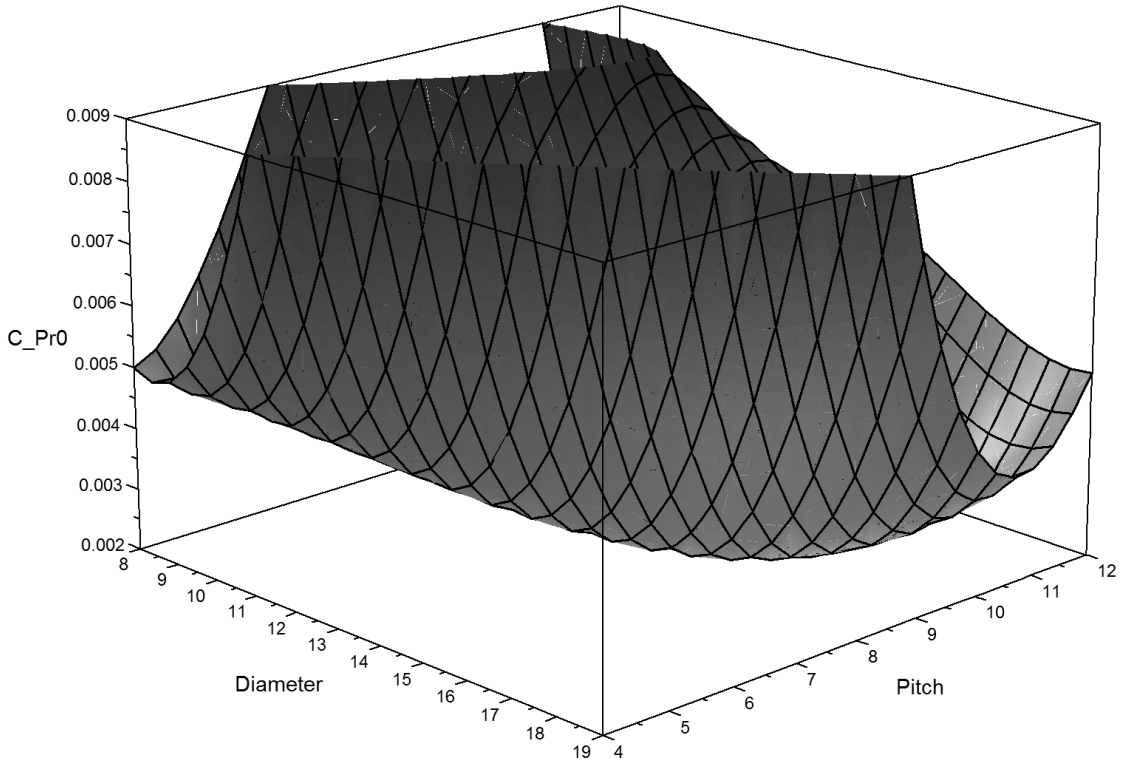

Figure 19 - $C_{Pr0}(D,p)$.

$$C_{Pr0}(D,p) = 0.006016 - 0.002697D + 0.006181p + 0.0005193D^2 - 0.001557Dp + 0.00065p^2 + 0.00002425D^3 - 0.0001404D^2p + 0.0002747Dp^2 - 0.0001503p^3 \quad (4.19)$$

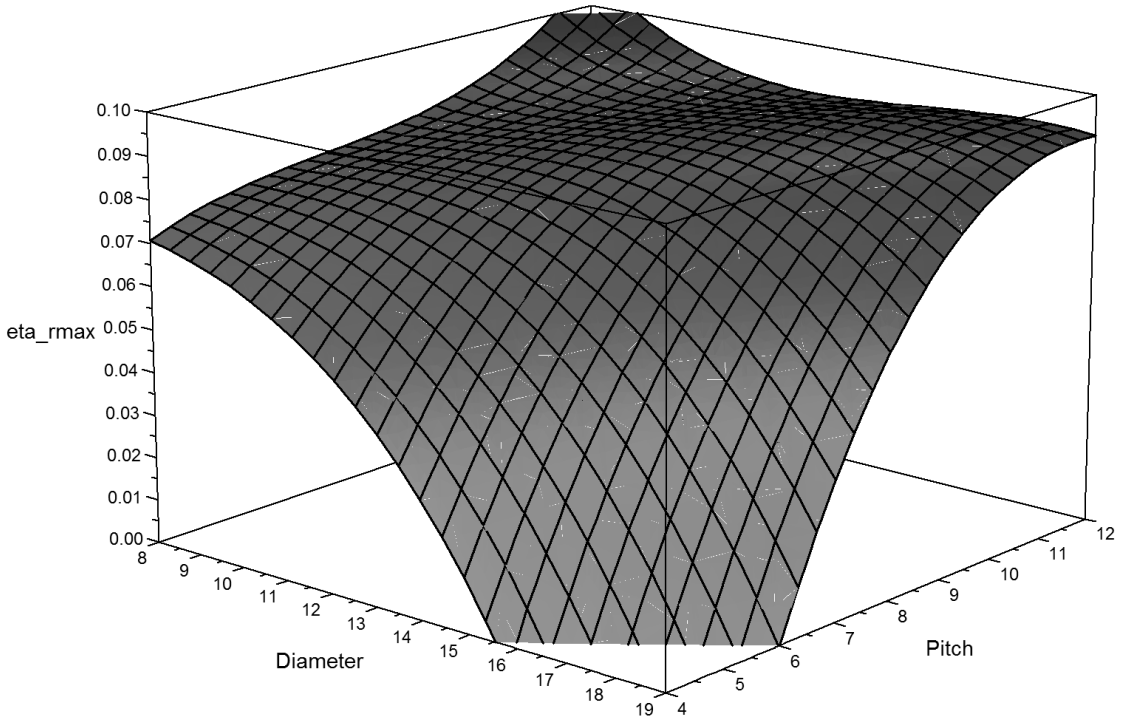

Figure 20 - $\eta_{rmax}(D,p)$.

$$\eta_{rmax}(D,p) = 0.08772 - 0.00653D + 0.0005099p + 0.0001196D^2 + 0.00136Dp - 0.0005098p^2 - 0.0000632D^3 + 0.0002344D^2p - 0.000376Dp^2 + 0.0001666p^3 \quad (4.20)$$

Table 5 - Values of D, p, J_{max}, C_{Pr0} and η_{rmax} used in the plotting of the functions above.

D [in]	p [in]	J_{max}	C_{Pr0}	η_{rmax}
8	4	0.674	0.0048	0.071
8	6	0.951	0.0089	0.078
8	8	1.170	0.0134	0.083
9	4.5	0.650	0.0049	0.071
9	6	0.801	0.0057	0.078
9	7.5	0.992	0.0100	0.083
9	9	1.110	0.0116	0.083
10	5	0.668	0.0044	0.075
10	7	0.839	0.0060	0.081
11	5.5	0.616	0.0036	0.073
11	7	0.791	0.0050	0.084
11	8	0.837	0.0057	0.086
11	8.5	0.885	0.0065	0.084
11	10	1.020	0.0097	0.087
14	12	0.935	0.0065	0.089
17	12	0.846	0.0055	0.091
19	12	0.759	0.0050	0.091

4.3 Validation

To see if the model fits the data accurately, for every propeller within the APC Thin Electric family, tested at UIUC, an estimate of the values for C_P and η, for each RPM at which they were tested, was created. This estimate is represented by the lines in the figures throughout subsection 4.3.1. Alongside these lines, the measurements made at UIUC are also represented for an easier comparison between the model's prediction, and the measured data.

In subsection 4.3.2, the analytical model will be validated by conducting tests for the APC Thin Electric Propellers with dimensions: 7x4, 13x4, 13x10, 14x10, 15x6, 15x10, 16x10, 18x8, 20x8, 20x15.

The calculated values of C_P and η, obtained with the measurements of thrust and torque coefficients at UBI, will be plotted alongside with the lines created with the analytical model, for each set RPM.

4.3.1 Comparison with UIUC Propeller Database

Demonstrated in Table 6 are the results of the mean relative error (MRE) calculations, the maximum relative error, δ_{max} and the standard deviation, σ measured for each propeller relatively to the model's predictions. The measured δ_{max} for η are somewhat higher than expected because of the sharp decline in the curve after reaching peak propeller efficiency.

Table 6 - Mean relative error of the model's predictions for the first model.

Propeller	C_P			η		
	MRE [%]	δ_{max} [%]	σ	MRE [%]	δ_{max} [%]	σ
Propeller 8x4	12.19	20.52	0.0044	7.07	164.85	0.0339
Propeller 8x6	4.64	13.29	0.0029	7.06	180.67	0.0321
Propeller 8x8	6.21	20.17	0.0061	2.65	18.01	0.0194
Propeller 9x4.5	5.51	34.6	0.0015	8.19	165.13	0.0303
Propeller 9x6	13.05	62.38	0.0045	9.63	430.11	0.0431
Propeller 9x7.5	3.88	13.15	0.0025	5.93	209.05	0.0291
Propeller 9x9	5.8	15.17	0.0052	4.89	85.86	0.0290
Propeller 10x5	14.59	24.8	0.0045	11.71	251.19	0.0712
Propeller 10x7	4.05	24.77	0.0017	2.26	38.52	0.0133
Propeller 11x5.5	4.71	14.61	0.0017	8.58	91.25	0.0437
Propeller 11x7	12.16	22.1	0.0051	14.27	485.01	0.0895
Propeller 11x8	4.91	28.29	0.0023	18.07	1254.8	0.0455
Propeller 11x8.5	4.41	16.01	0.0022	5.05	90.57	0.0388
Propeller 11x10	4.67	16.35	0.0031	12.64	434.63	0.0852
Propeller 14x12	5.79	13.46	0.0037	4.31	46.76	0.0261
Propeller 17x12	18.87	29.24	0.0077	25.53	1459.5	0.0910
Propeller 19x12	6.9	15.3	0.0028	4.94	96.46	0.0318

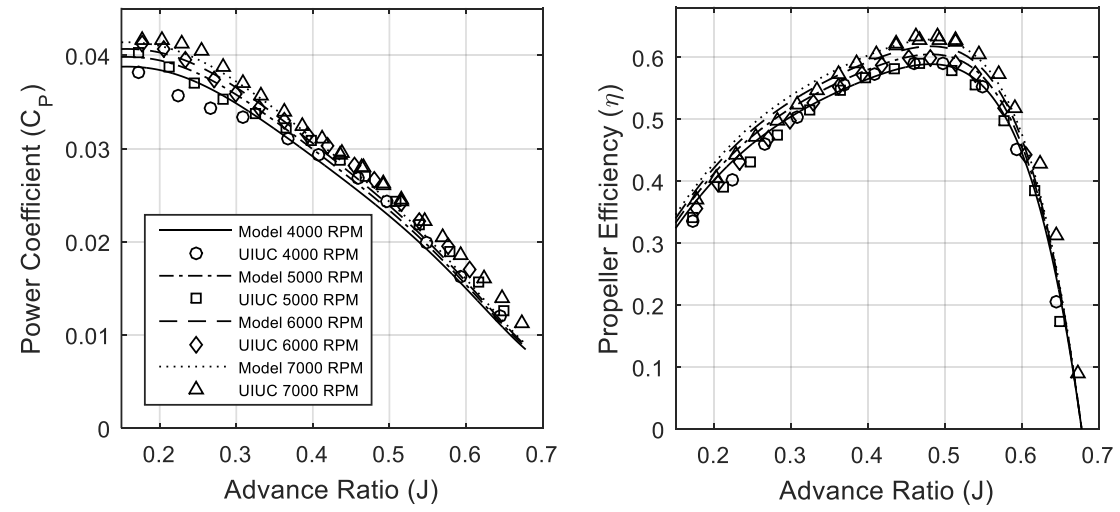

Figure 21 - Propeller Performance comparison with UIUC data for propeller 8x4.

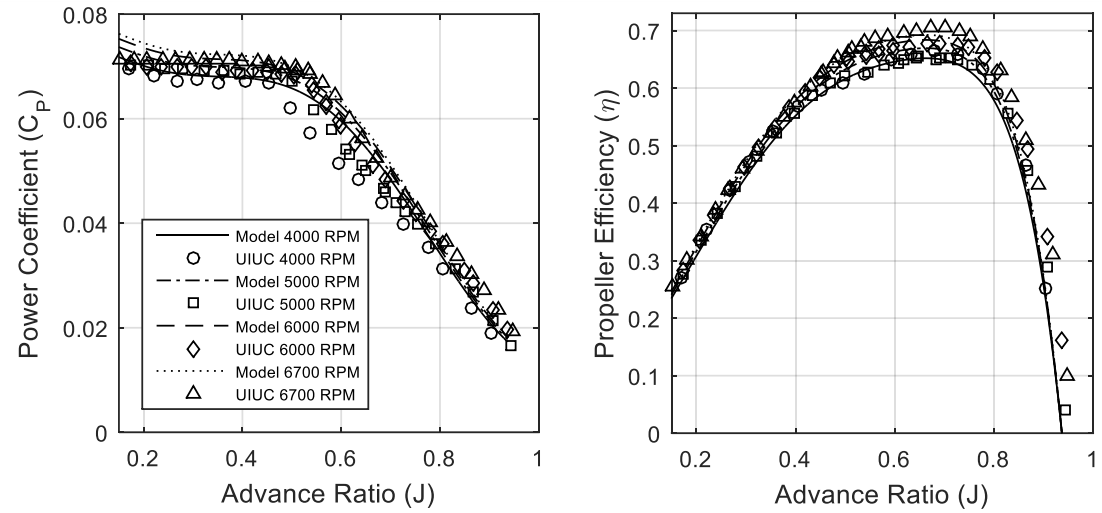

Figure 22 - Propeller Performance comparison with UIUC data for propeller 8x6.

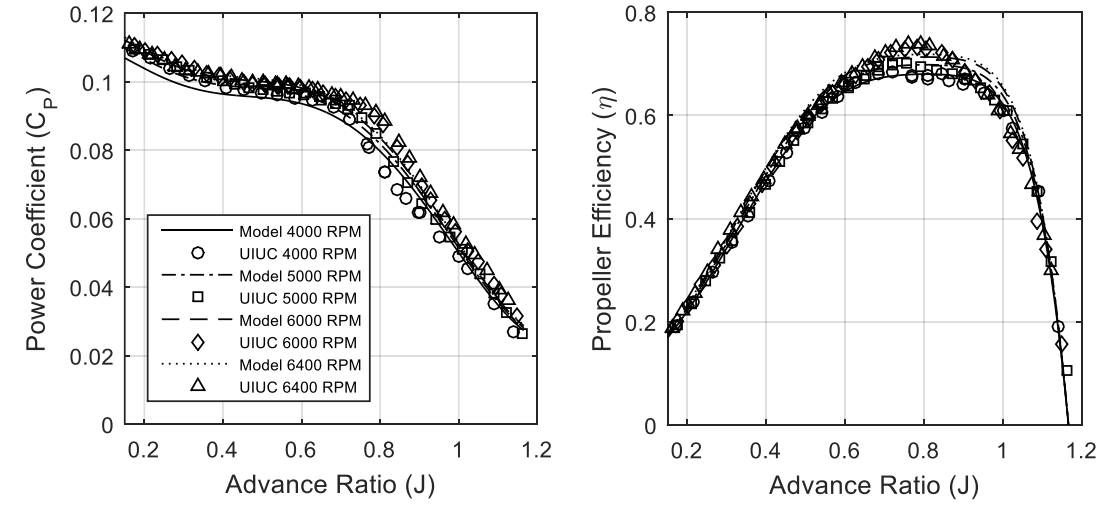

Figure 23 - Propeller Performance comparison with UIUC data for propeller 8x8.

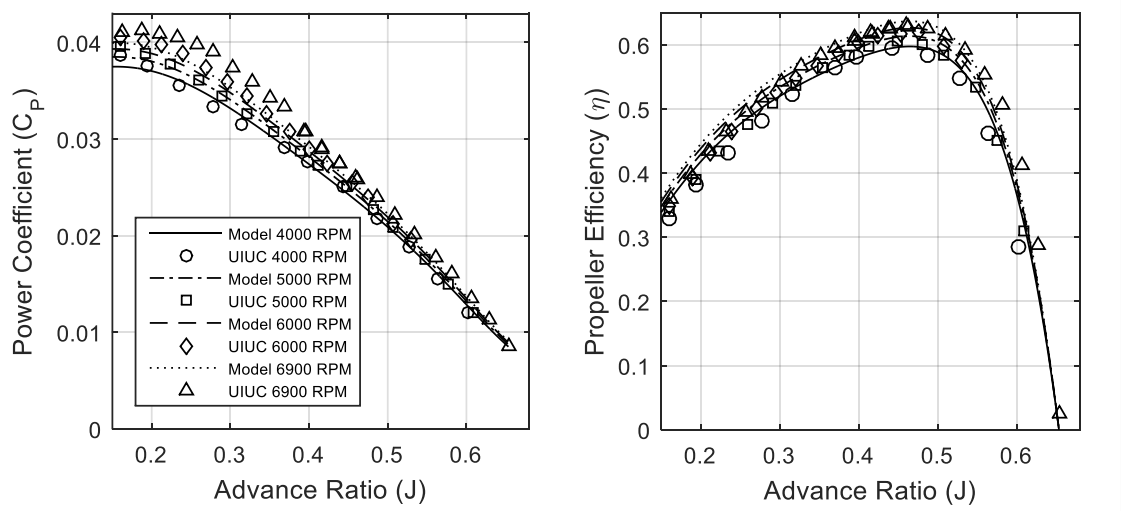

Figure 24 - Propeller Performance comparison with UIUC data for propeller 9x4.5.

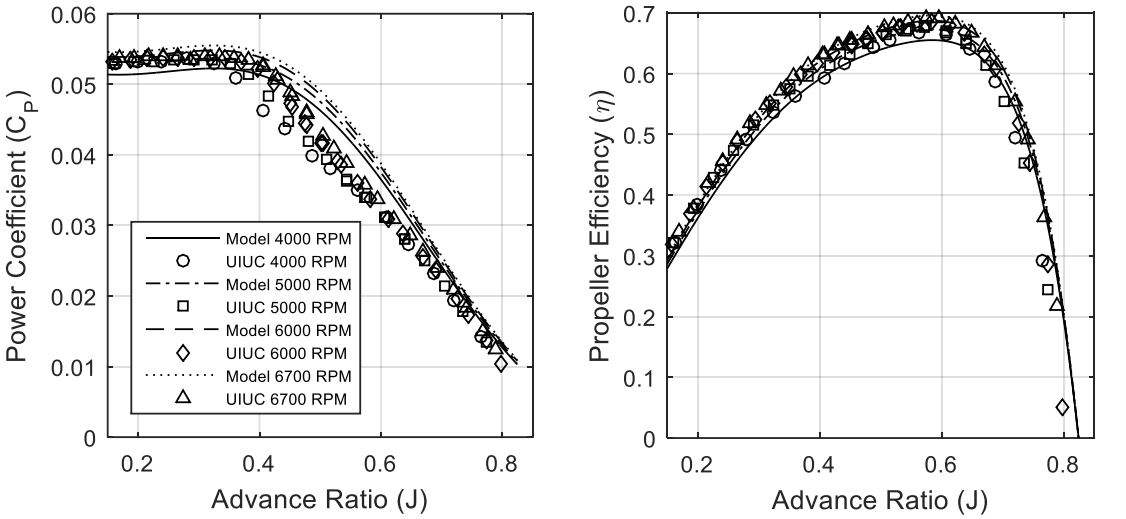

Figure 25 - Propeller Performance comparison with UIUC data for propeller 9x6.

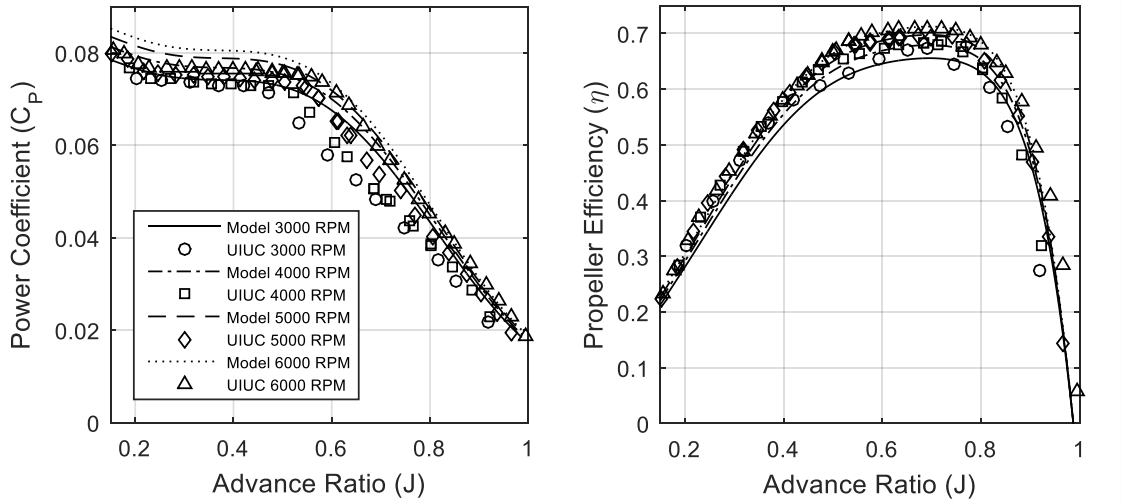

Figure 26 - Propeller Performance comparison with UIUC data for propeller 9x7.5.

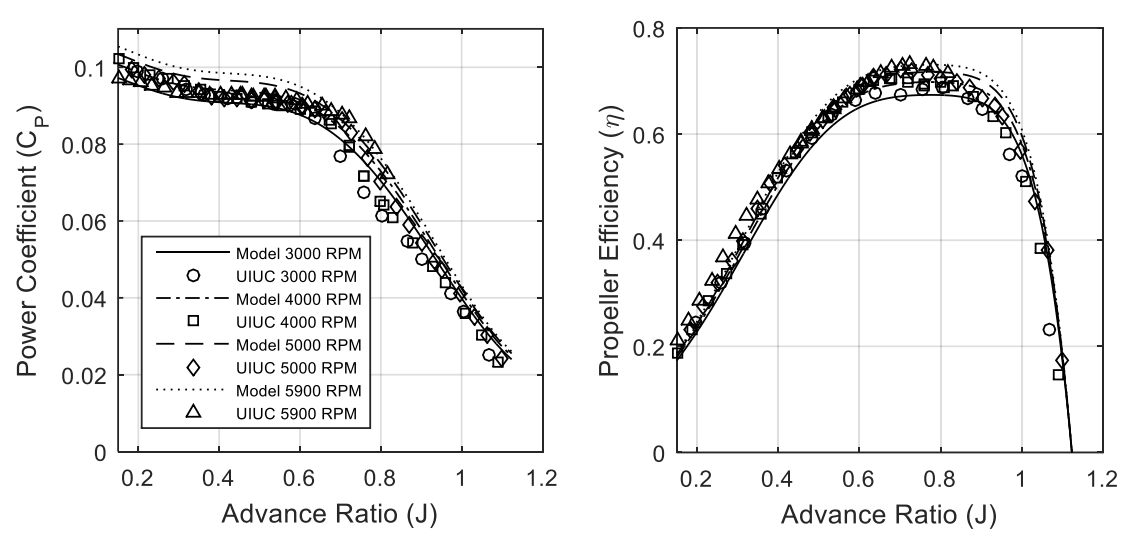

Figure 27 - Propeller Performance comparison with UIUC data for propeller 9x9.

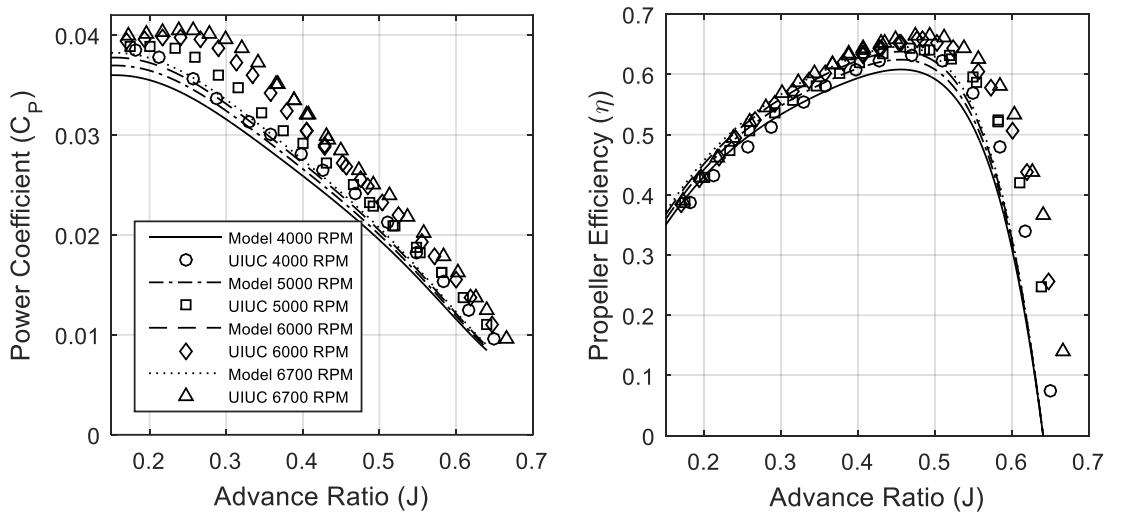

Figure 28 - Propeller Performance comparison with UIUC data for propeller 10x5.

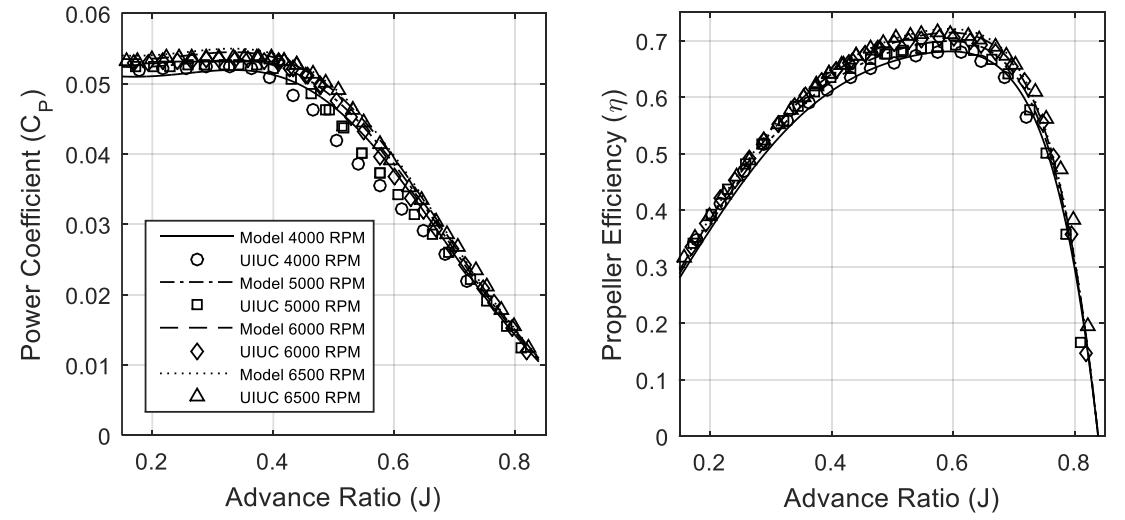

Figure 29 - Propeller Performance comparison with UIUC data for propeller 10x7.

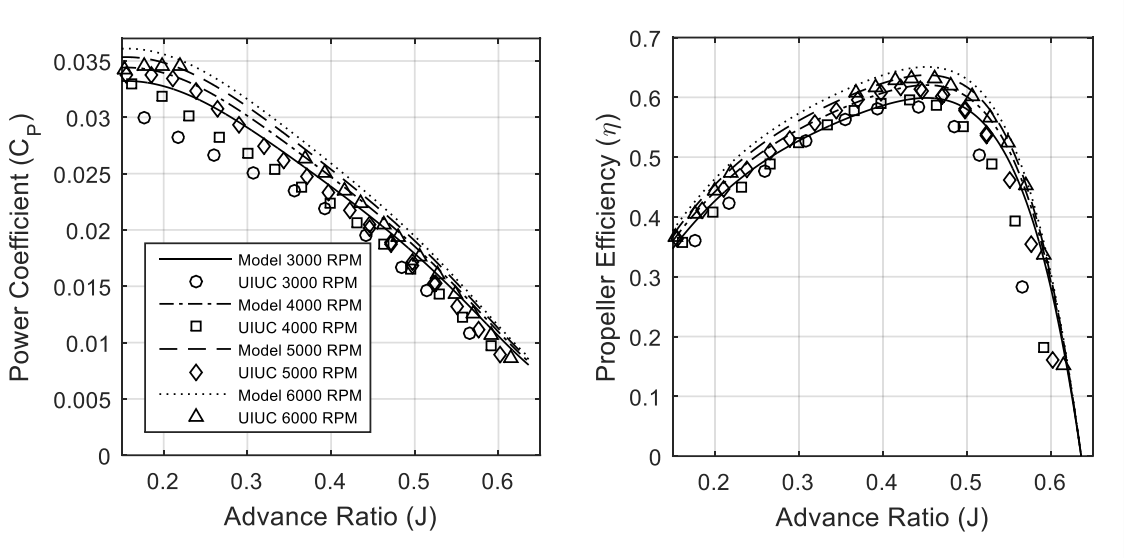

Figure 30 - Propeller Performance comparison with UIUC data for propeller 11x5.5.

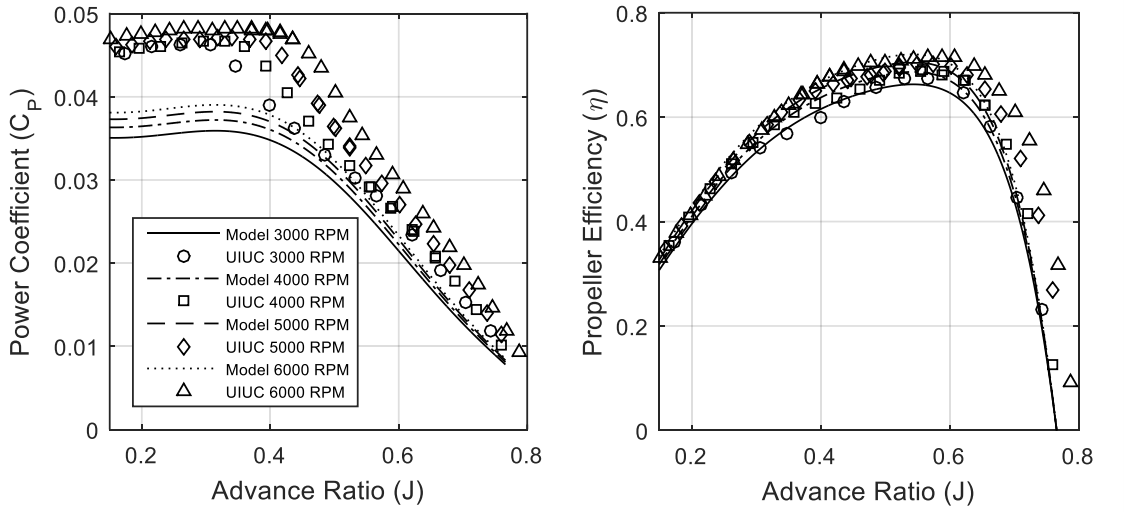

Figure 31 - Propeller Performance comparison with UIUC data for propeller 11x7.

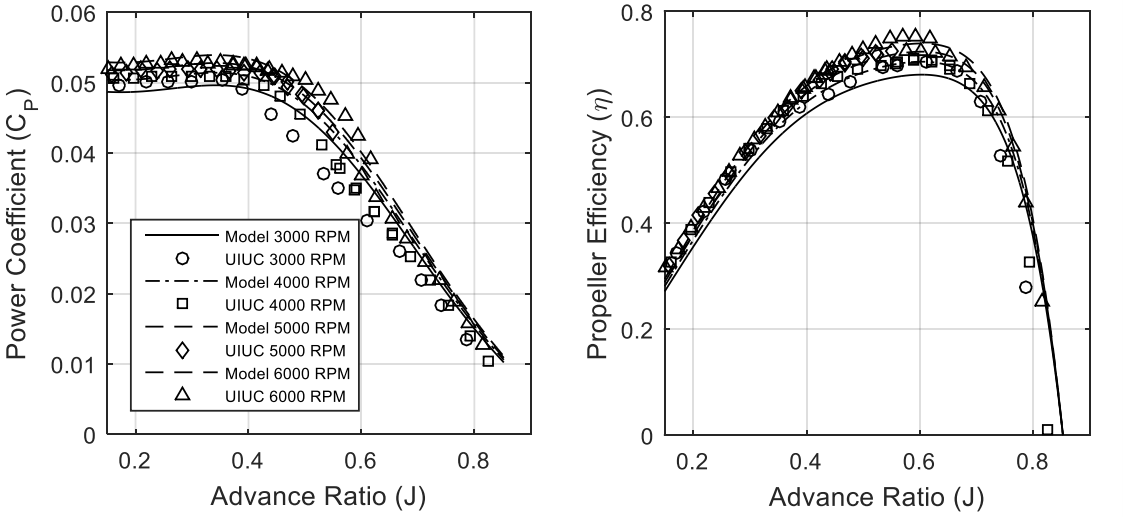

Figure 32 - Propeller Performance comparison with UIUC data for propeller 11x8.

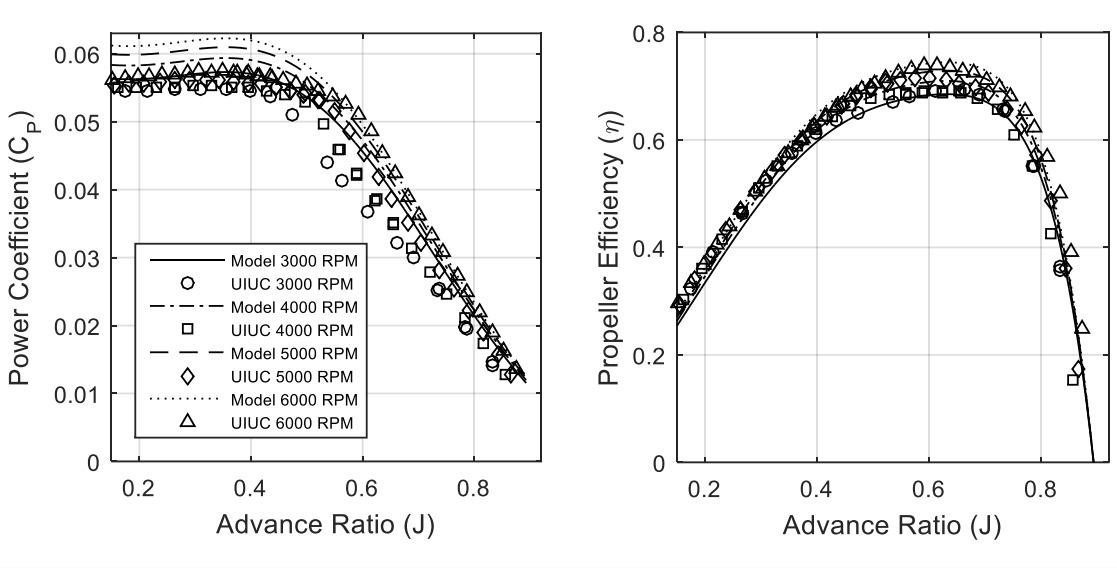

Figure 33 - Propeller Performance comparison with UIUC data for propeller 11x8.5.

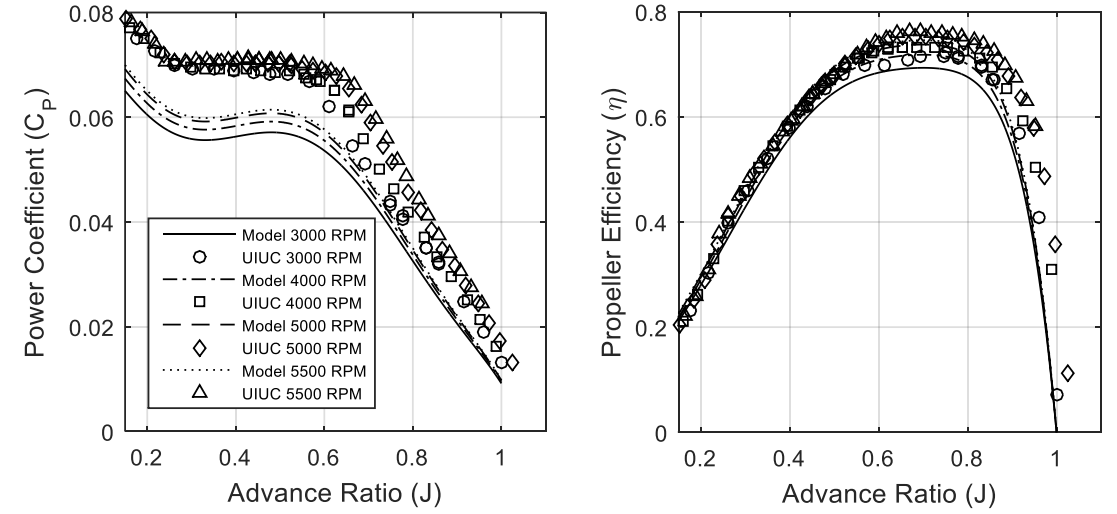

Figure 34 - Propeller Performance comparison with UIUC data for propeller 11x10.

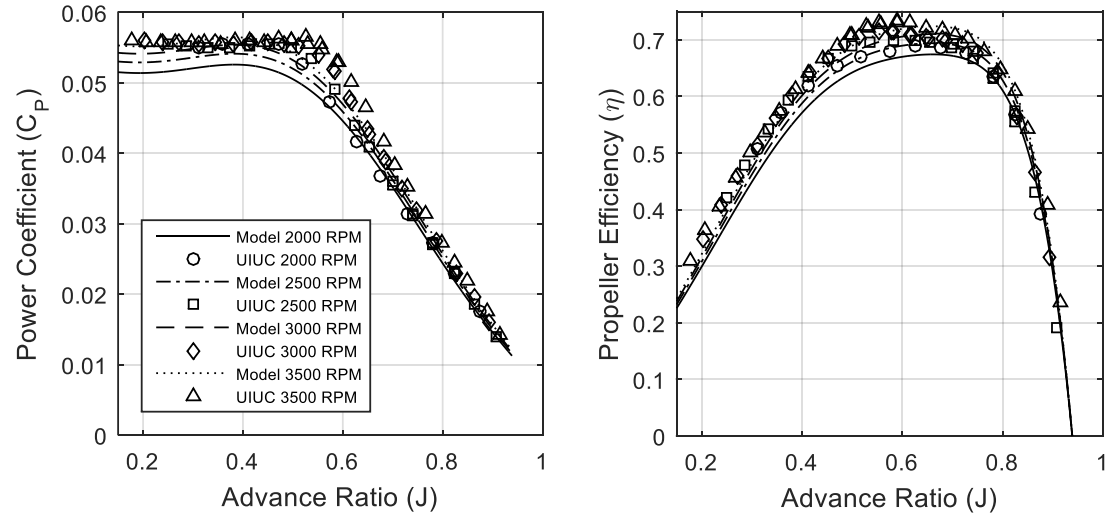

Figure 35 - Propeller Performance comparison with UIUC data for propeller 14x12.

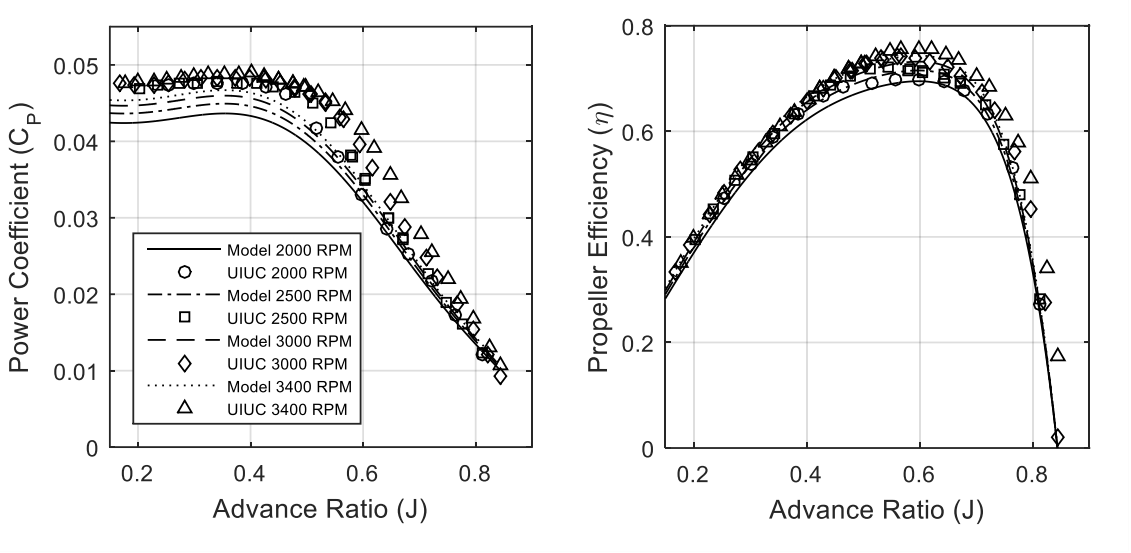

Figure 36 - Propeller Performance comparison with UIUC data for propeller 17x12.

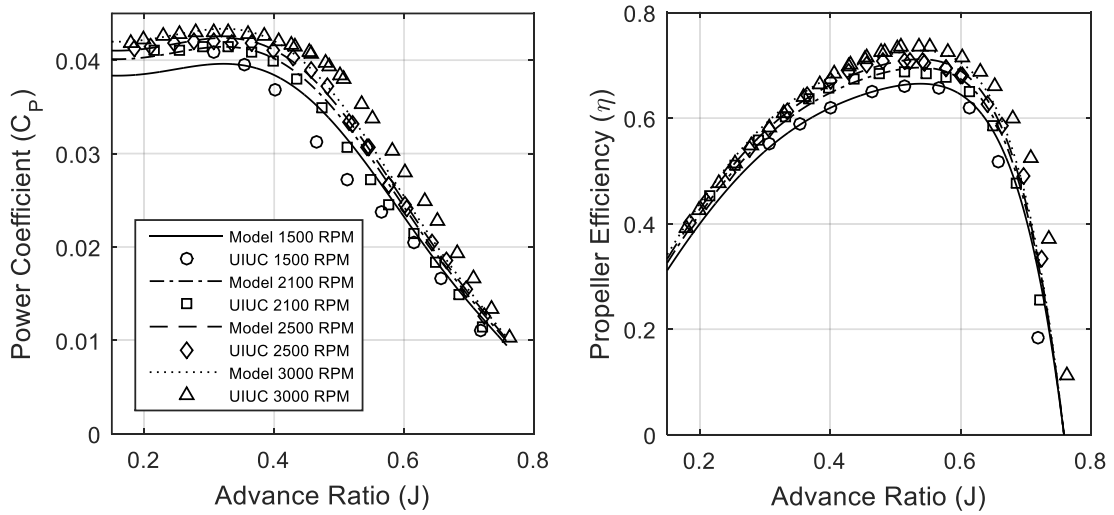

Figure 37 - Propeller Performance comparison with UIUC data for propeller 19x12.

In Figure 21 through Figure 37 the estimates made from the model are displayed, represented by line plots, along with the measurements made at UIUC, in order to examine how the analytical model can estimate the observed values of C_P and η. Comparing the different results, it is seen that:

1. The η estimates match the propeller performance data from measurements;
2. The C_P estimates match the propeller performance data from measurements for propellers 8x4, 8x6, 8x8, 9x4.5, 9x7.5, 9x9, 10x7, 11x8;
3. The C_P estimates for propellers 11x7 and 11x10 are the worst matches when compared with the propeller performance data from measurements for propellers;
4. It is possible to observe that both C_P and η, increase with the increase of the propeller rotational speed. This is a typical behavior for low Reynolds number conditions. Although this increase is more accurate for η estimates than the C_P ones, as observed in the data from 10x5, 10x7, 11x5.5, 11x7, 11x8, 11x5.5 and 19x12.

4.3.2 Application of the model to the data acquired at UBI

For this validation, some propellers were tested and compared to the results shown in the model. The propellers used were also from the APC Thin Electric family, 13x4, 13x10, 14x10, 15x6, 15x10, 16x10, 18x8, 20x8, 20x15.

Table 7 - Mean relative error (MRE), δ_{max} and standard deviation of the model's prediction of the propeller's tested at UBI.

Propeller	C_P			η		
	MRE [%]	δ_{max} [%]	σ	MRE [%]	δ_{max} [%]	σ
Propeller 7x4	20	42.75	0.0078	52.57	535.89	0.1913
Propeller 13x4	756.07	1061.2	0.0994	61.31	732.76	0.1459
Propeller 13x10	3.20	11.83	0.0015	28.31	404.06	0.1043
Propeller 14x10	8.93	13.32	0.0042	19.25	135.04	0.1149
Propeller 15x6	354.43	1080.6	0.0613	2869.3	159370	0.0958
Propeller 15x10	23.67	31.34	0.0101	23.09	403.54	0.1151
Propeller 16x10	30.23	42.62	0.0108	27.49	196.92	0.1445
Propeller 18x8	234.84	332.88	0.0457	16.25	97.38	0.0798
Propeller 20x8	734.89	971.73	0.1135	40.87	209.96	0.1754
Propeller 20x15	94.40	118.54	0.0353	17.21	67.86	0.0973

As observable in Table 7, the results are not positive for the majority of the propellers measured at UBI. The massive δ_{max} values calculated for propeller efficiency, are due to the sharp decline observed after peak efficiency is reached.

The results of this application are demonstrated in Figure 38 through Figure 47:

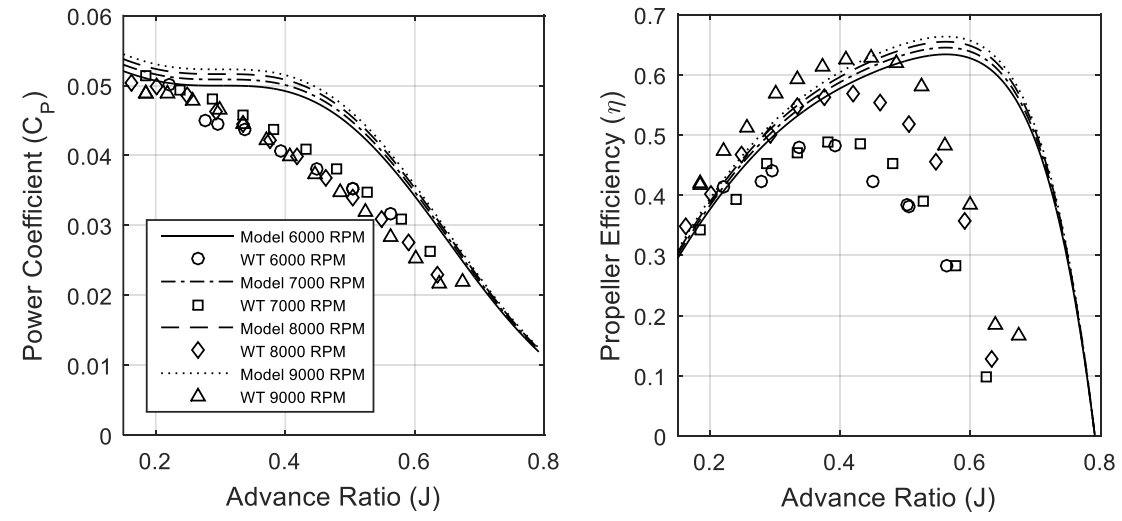

Figure 38 - Testing of the first model with data from propeller 7x4.

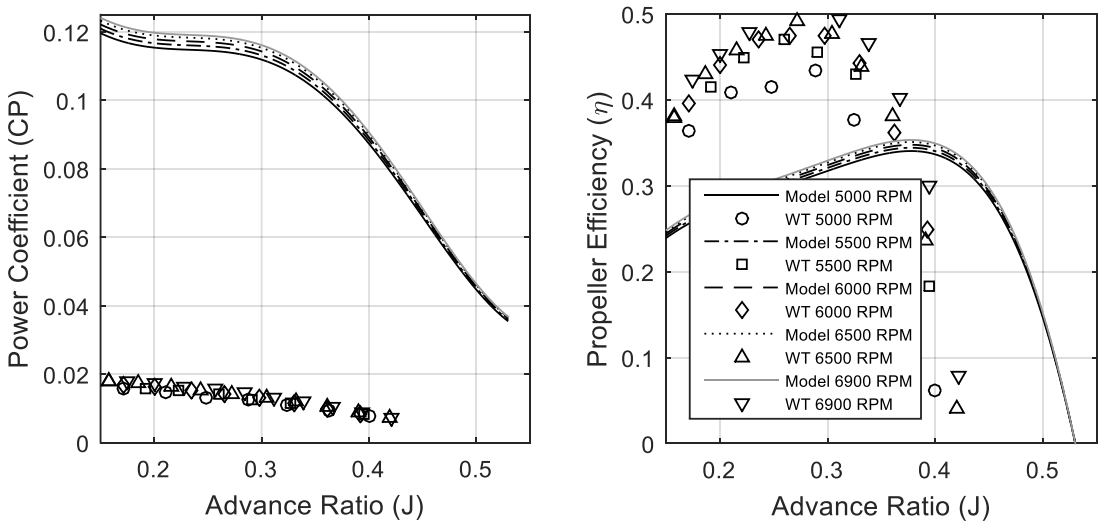

Figure 39 - Testing of the first model with data from propeller 13x4.

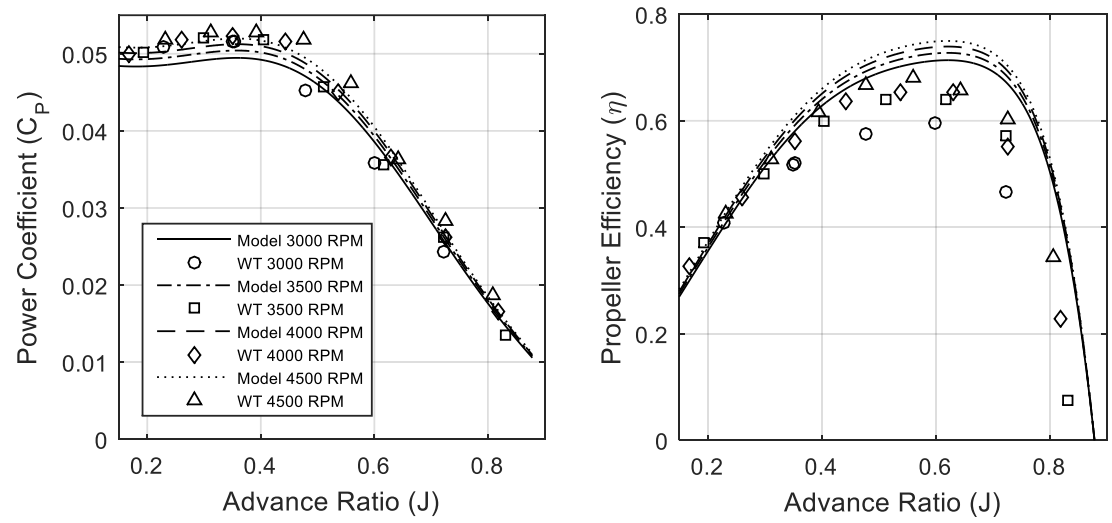

Figure 40 - Testing of the first model with data from propeller 13x10.

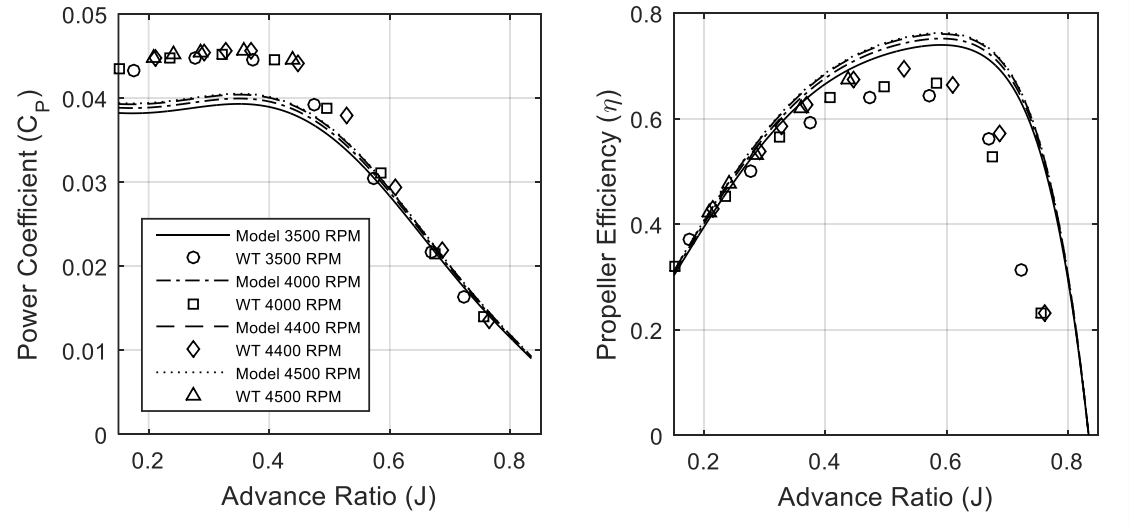

Figure 41 - Testing of the first model with data from propeller 14x10.

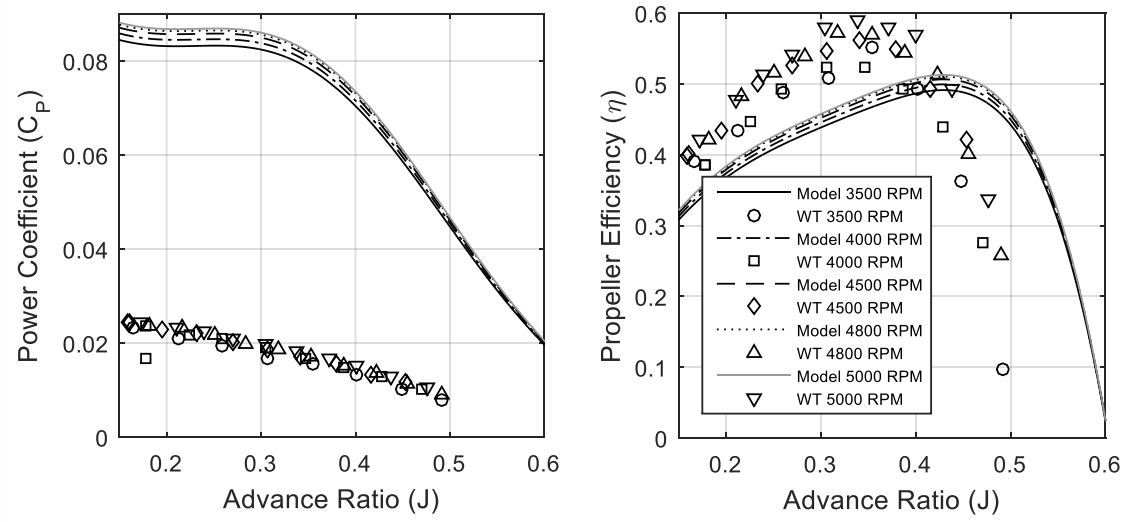

Figure 42 - Testing of the first model with data from propeller 15x6.

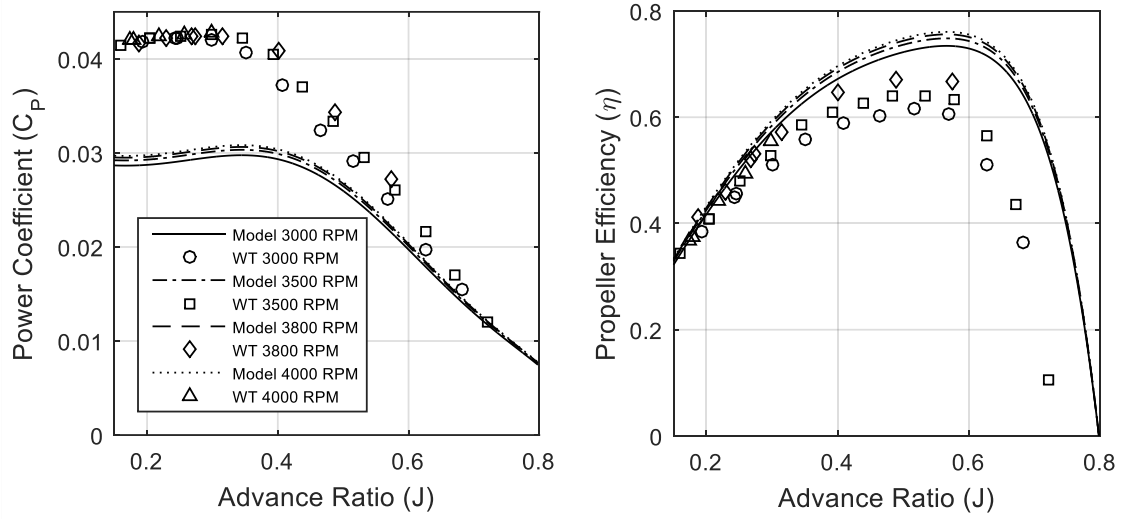

Figure 43 - Testing of the first model with data from propeller 15x10.

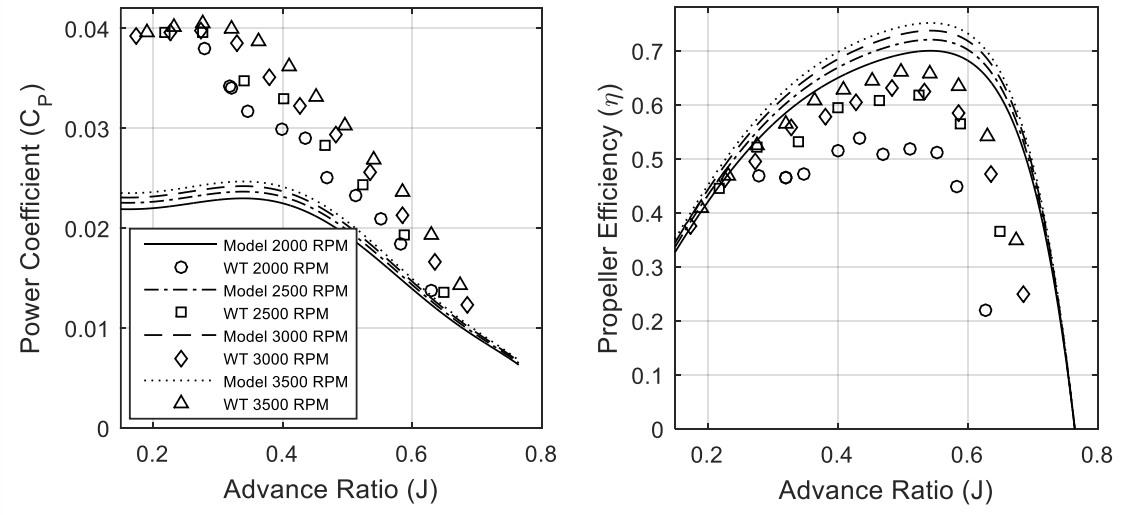

Figure 44 - Testing of the first model with data from propeller 16x10.

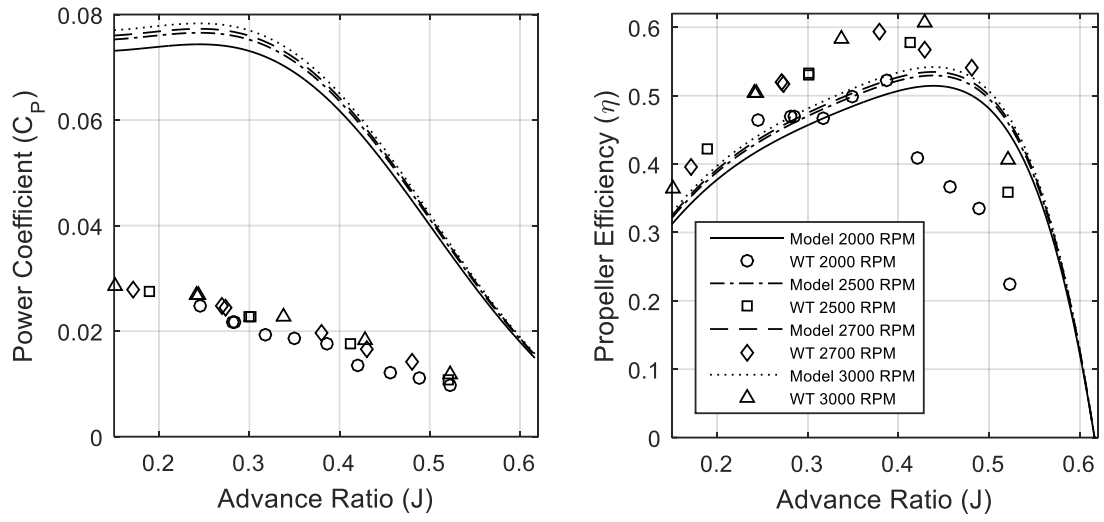

Figure 45 - Testing of the first model with data from propeller 18x8.

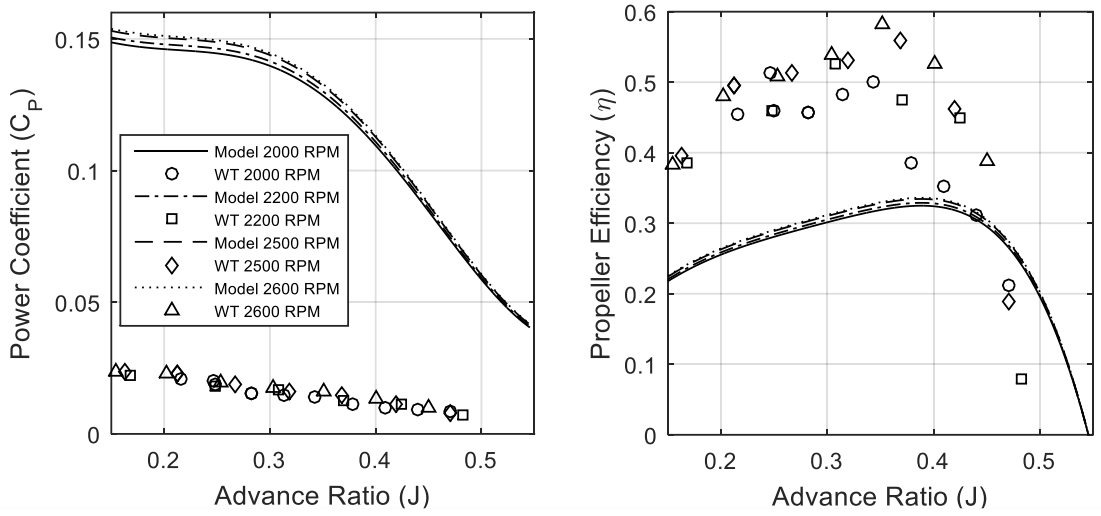

Figure 46 - Testing of the first model with data from propeller 20x8.

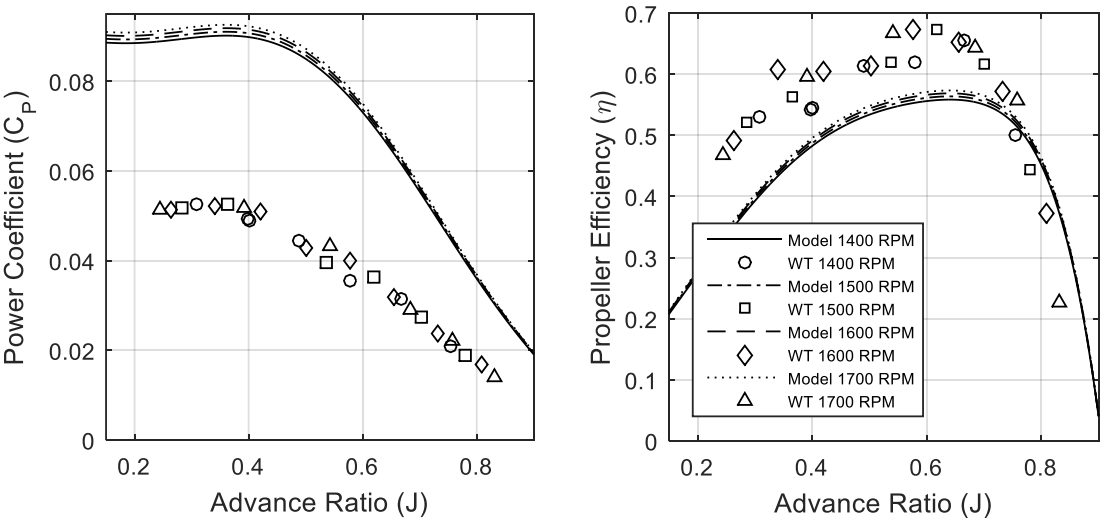

Figure 47 - Testing of the first model with data from propeller 20x15.

As observable, in Figures 39 through 47 the analytical model does not make accurate predictions of the performance of the tested propellers. This inaccuracy can be justified by analyzing Figure 48:

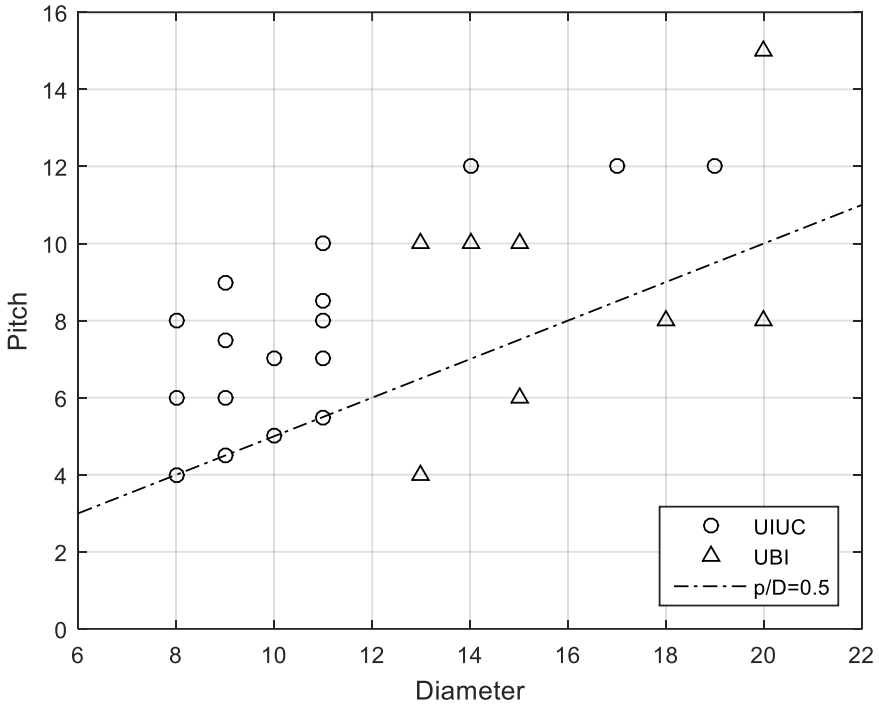

Figure 48 - Representation of the propellers used to create (data acquired from UIUC, circles) and validate (data acquired at UBI, triangles) the analytical model.

For some propellers, the prediction is more accurate than others, for example: propellers 13x10 and 14x10, shown in Figure 40 and Figure 41, respectively, are very accurate. This is due to two reasons:

- The most obvious one, is that the propellers' diameters are closer to the ones used to create the analytical model, therefore, the performance for propellers with greater diameter are inaccurate;
- The second, is that the analytical model was created using propellers with a $\frac{p}{D}$ ratio of no less than 0.5, and because the behavior of propellers with that ratio lower than 0.5 is unknown, the prediction is way off.

4.4 New Analytical Model

The data obtained at UBI has been used to further develop the analytical model, expanding the range of propellers that may be tested with it. This subsection shows the same procedure used to construct the first version of this analytical model, but with both data retrieved from UIUC Propeller Database [2] and the data acquired at UBI during the experimental procedure.

4.4.1 Power Coefficient

The data plots for power coefficient are shown in Figure 49, Figure 50 and Figure 51:

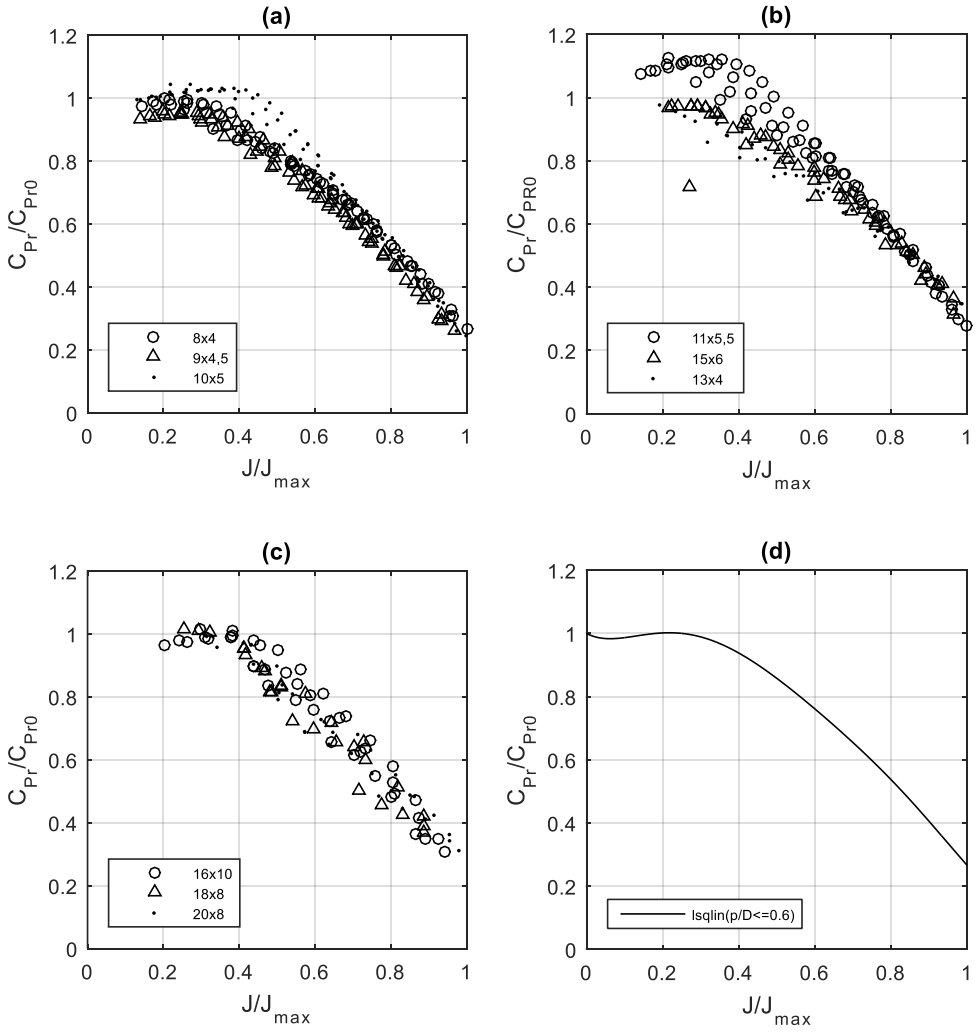

Figure 49 - Dispersion for propellers with $\frac{p}{D}$ ratio lower than 0.6 (a, b and c) and the results of *lsqlin* function in MATLAB® (d).

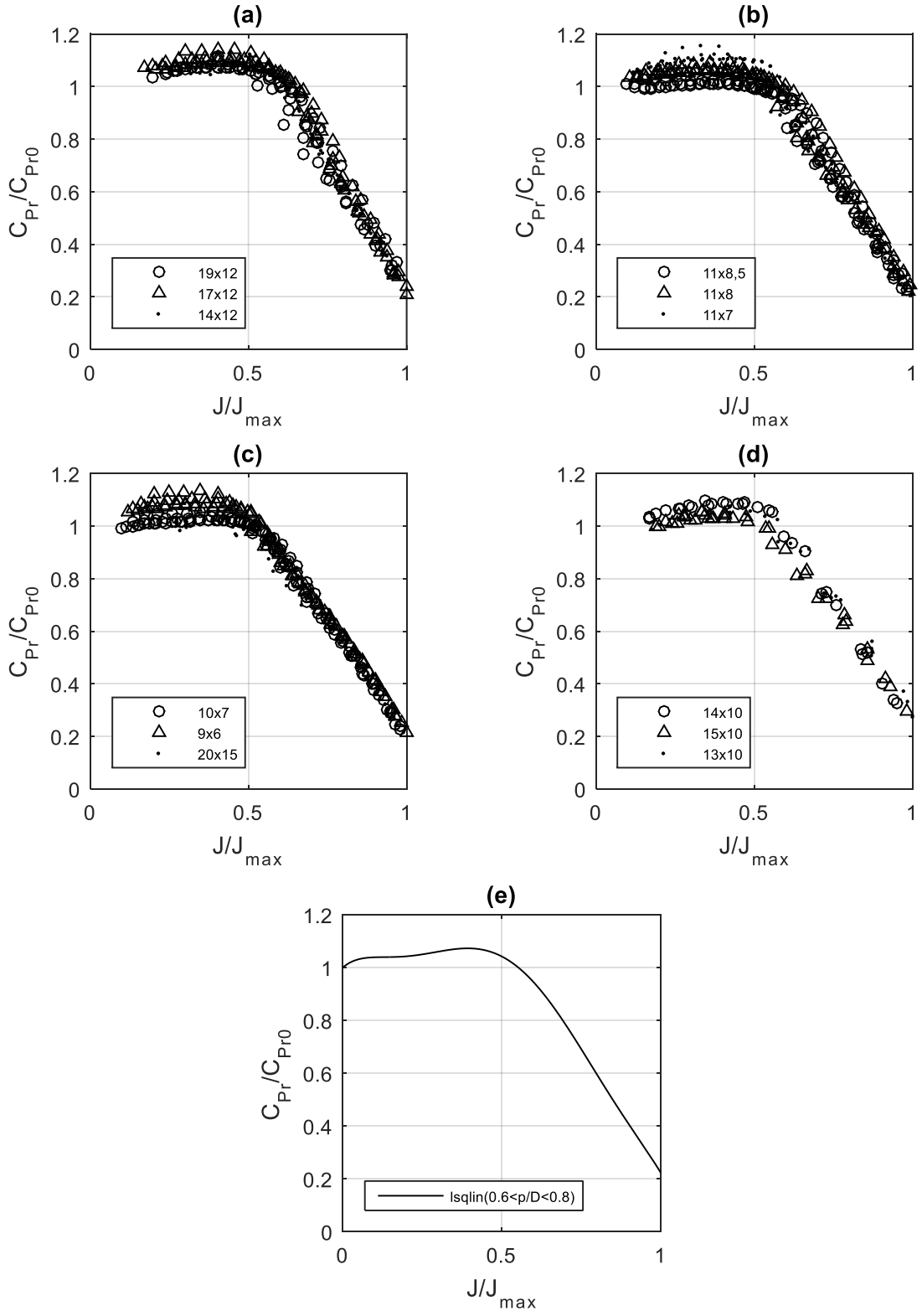

Figure 50 - Dispersion for propellers with $\frac{p}{D}$ ratio between 0.6 and 0.8 (a, b, c and d) and the results of *lsqlin* function in MATLAB® (e).

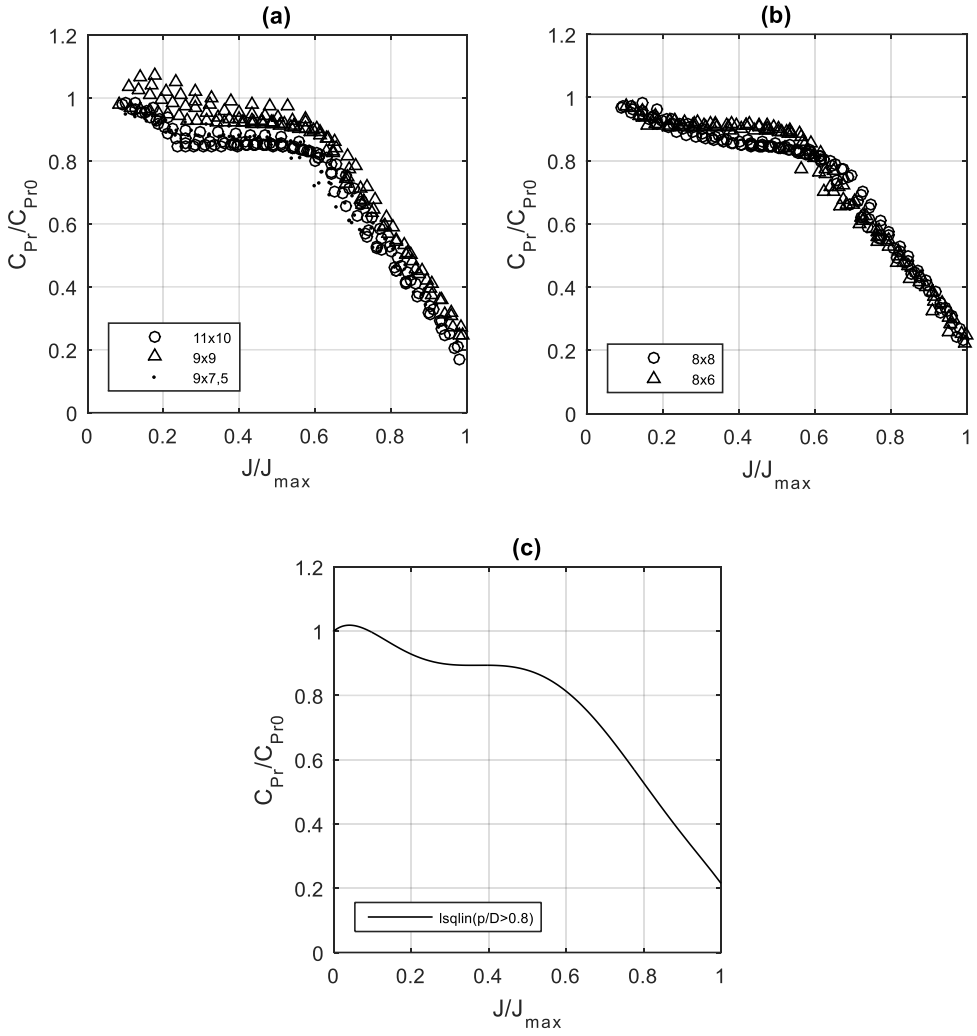

Figure 51 - Dispersion for propellers with $\frac{p}{D}$ ratio higher than 0.8 (a, b) and the results of *lsqlin* function in MATLAB® (c).

$$lsqlin\left(\frac{p}{D} < 0.6\right) = 10.4028\left(\frac{J}{J_{max}}\right)^6 - 35.9386\left(\frac{J}{J_{max}}\right)^5 + 47.8134\left(\frac{J}{J_{max}}\right)^4 - 29.9302\left(\frac{J}{J_{max}}\right)^3 + 7.5524\left(\frac{J}{J_{max}}\right)^2 - 0.6341\left(\frac{J}{J_{max}}\right) + 1 \quad (4.21)$$

$$lsqlin(0.6 < \frac{p}{D} < 0.8) = -24.5428\left(\frac{J}{J_{max}}\right)^6 + 78.5108\left(\frac{J}{J_{max}}\right)^5 - 91.1124\left(\frac{J}{J_{max}}\right)^4 + 45.4624\left(\frac{J}{J_{max}}\right)^3 - 10.1256\left(\frac{J}{J_{max}}\right)^2 + 1.0304\left(\frac{J}{J_{max}}\right) + 1 \quad (4.22)$$

$$lsqlin\left(\frac{p}{D} > 0.8\right) = -28.4845\left(\frac{J}{J_{max}}\right)^6 + 96.0444\left(\frac{J}{J_{max}}\right)^5 - 119.9588\left(\frac{J}{J_{max}}\right)^4 + 66.6777\left(\frac{J}{J_{max}}\right)^3 - 16.0662\left(\frac{J}{J_{max}}\right)^2 + 1.0026\left(\frac{J}{J_{max}}\right) + 1 \quad (4.23)$$

Again, after analyzing the data points, three categories were established for these plots, and the parameter that describes the difference is the $\frac{p}{D}$ ratio:

- $\frac{p}{D} < 0.6$, the data plots showed that the maximum value of $\frac{C_{Pr}}{C_{Pr0}}$ is attained between $\frac{J}{J_{max}}$ values of 0.3 and 0.4 (Figure 49);
- $0.6 < \frac{p}{D} < 0.8$, it was observed that the maximum value of $\frac{C_{Pr}}{C_{Pr0}}$ is attained at $\frac{J}{J_{max}}$ values of 0.4, and the value of $\frac{C_{Pr}}{C_{Pr0}}$ starts descending from somewhere between $\frac{J}{J_{max}}$ values of 0.5 and 0.6 (Figure 50);
- $\frac{p}{D} > 0.8$, the value of $\frac{C_{Pr}}{C_{Pr0}}$ reaches its maximum between 0.1 and 0.2 $\frac{J}{J_{max}}$ and stabilizes until around $\frac{J}{J_{max}} = 0.55$ (Figure 51).

Note that propellers such as APC Thin Electric 16x10 has a $\frac{p}{D} = 0.625$ but it is set with the plots of the propellers with a $\frac{p}{D} < 0.6$ because it behaved similarly, the APC Thin Electric 14x12 has a $\frac{p}{D} \cong 0.86$ and fits with the propellers with $0.6 < \frac{p}{D} < 0.8$ for the same reason, also, APC Thin Electric 8x6 has $\frac{p}{D} = 0.75$ and fits with the propellers with a $\frac{p}{D} > 0.8$. It was chosen to ignore these cases and proceed with the curve fitting because in the final equation it would show irrelevant, as shown in Table 9.

By utilizing a least square approach to the three lines shown, with the help of MATLAB® application “Curve Fitting Tool”, the following plot is obtained:

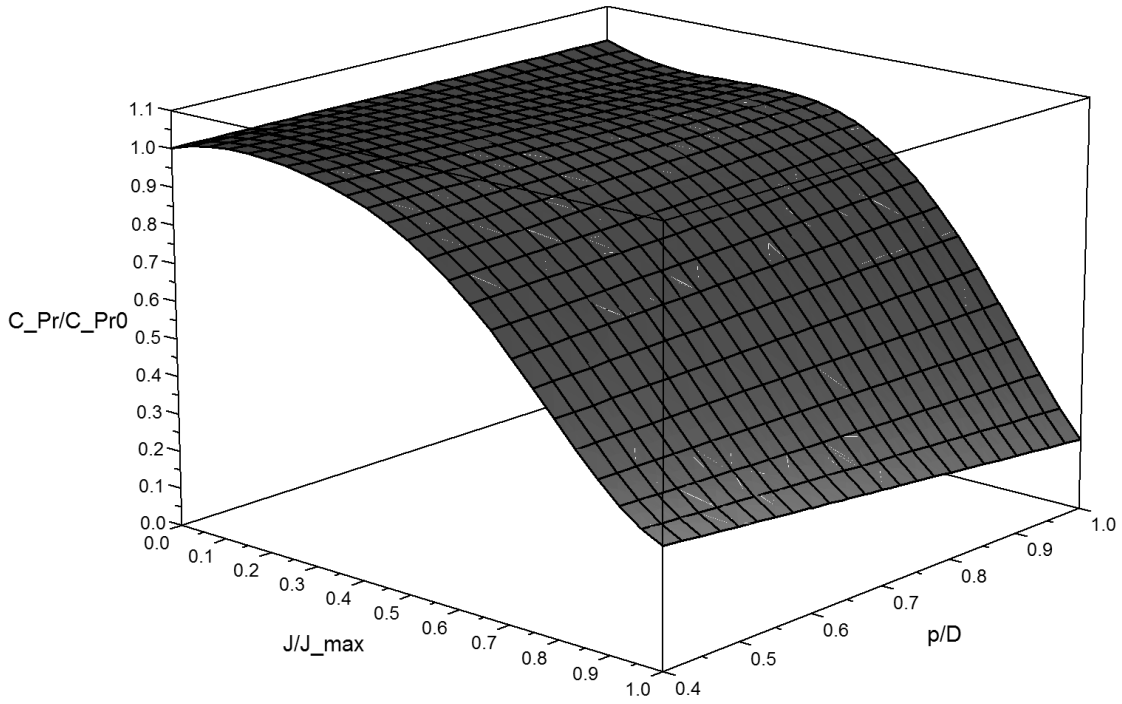

Figure 52 - 3D plot of $\frac{C_{Pr}}{C_{Pr0}}(\frac{J}{J_{max}},\frac{p}{D})$.

$$
\begin{aligned}
C_P = \frac{C_{Pr}}{C_{Pr0}}\left(\frac{J}{J_{max}},\frac{p}{D}\right) \\
= 1 + 1.177\left(\frac{J}{J_{max}}\right) + 0.004779\left(\frac{p}{D}\right) - 5.287\left(\frac{J}{J_{max}}\right)^2 \\
- 1.654\left(\frac{J}{J_{max}}\right)\left(\frac{p}{D}\right) + 8.743\left(\frac{J}{J_{max}}\right)^3 + 6.371 * \left(\frac{J}{J_{max}}\right)^2\left(\frac{p}{D}\right) \\
- 9.728\left(\frac{J}{J_{max}}\right)^4 - 6.741\left(\frac{J}{J_{max}}\right)^3\left(\frac{p}{D}\right) + 4.49\left(\frac{J}{J_{max}}\right)^5 \\
+ 1.812\left(\frac{J}{J_{max}}\right)^4\left(\frac{p}{D}\right)
\end{aligned}
\tag{4.24}
$$

4.4.2 Propeller Efficiency

To obtain a new model for propeller efficiency, the data obtained at UIUC and at UBI must be organized into separate plots, as done in subsection 4.2.2.

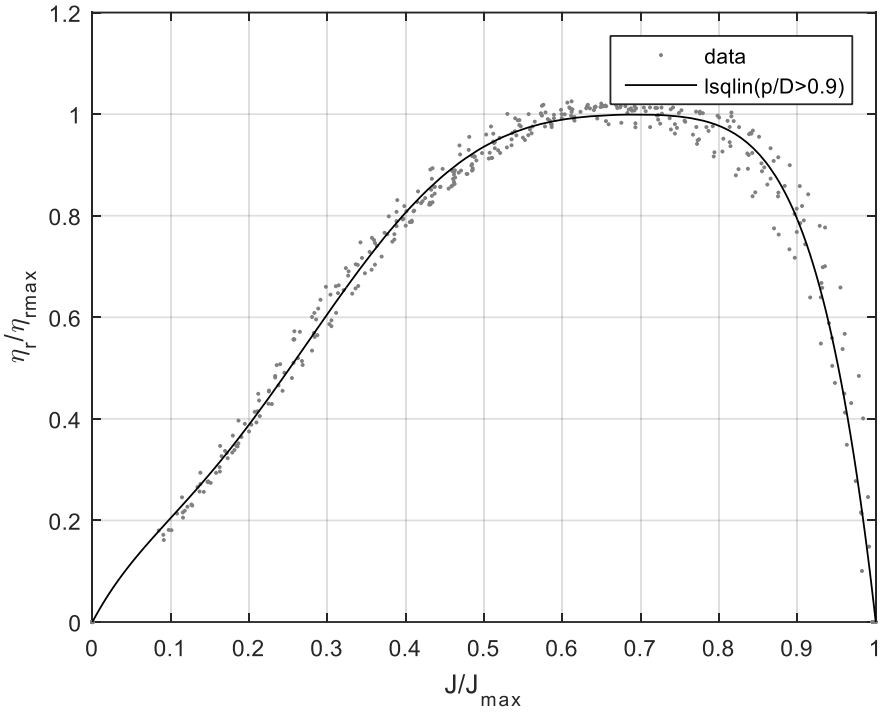

Figure 53 - 1 of 3 behaviors of propeller efficiency for $\frac{p}{D} > 0.9$.

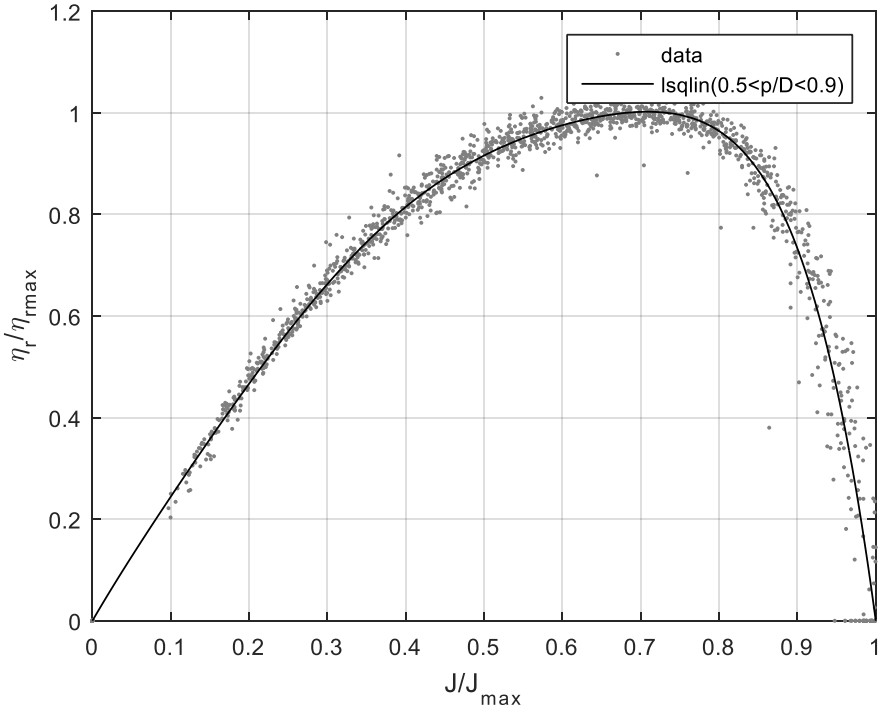

Figure 54 - 2 of 3 behaviors of propeller efficiency for $0.5 < \frac{p}{D} < 0.9$.

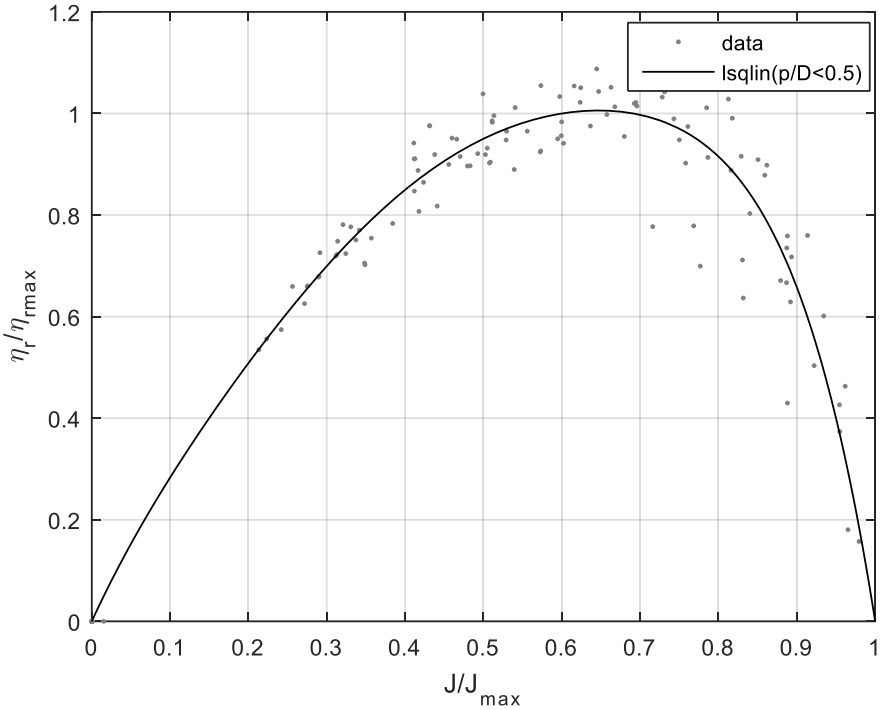

Figure 55 - 3 of 3 behaviors of propeller efficiency for $\frac{p}{D} < 0.5$.

According to the plots:

- $\frac{p}{D} > 0.9$, the curve is concave upwards between $0.1 < \frac{J}{J_{max}} < 0.3$;
- $0.5 < \frac{p}{D} < 0.9$, the curve is concave downward between $0.1 < \frac{J}{J_{max}} < 0.5$, and the maxima are hit at around $0.7 < \frac{J}{J_{max}} < 0.8$;
- $\frac{p}{D} < 0.5$, the curve is concave downward between $0.1 < \frac{J}{J_{max}} < 0.5$, and the maxima are hit at around $0.6 < \frac{J}{J_{max}} < 0.7$.

$$lsqlin\left(\frac{p}{D} > 0.9\right) = -77.1935\left(\frac{J}{J_{max}}\right)^6 + 202.5785\left(\frac{J}{J_{max}}\right)^5 - 196.5373\left(\frac{J}{J_{max}}\right)^4 + 83.3452\left(\frac{J}{J_{max}}\right)^3 - 15.0943\left(\frac{J}{J_{max}}\right)^2 + 2.9014\left(\frac{J}{J_{max}}\right) \quad (4.25)$$

$$lsqlin\left(0.5 < \frac{p}{D} < 0.9\right) = -29.4085\left(\frac{J}{J_{max}}\right)^6 + 65.2815\left(\frac{J}{J_{max}}\right)^5 - 51.8950\left(\frac{J}{J_{max}}\right)^4 + 16.7248\left(\frac{J}{J_{max}}\right)^3 - 3.3596\left(\frac{J}{J_{max}}\right)^2 + 2.6568\left(\frac{J}{J_{max}}\right) \quad (4.26)$$

$$lsqlin\left(\frac{p}{D} < 0.9\right) = -24.4753\left(\frac{J}{J_{max}}\right)^6 + 59.6017\left(\frac{J}{J_{max}}\right)^5 - 56.1026\left(\frac{J}{J_{max}}\right)^4 + 24.8533\left(\frac{J}{J_{max}}\right)^3 - 7.2335\left(\frac{J}{J_{max}}\right)^2 + 3.3564\left(\frac{J}{J_{max}}\right) \quad (4.27)$$

By applying the definition of a parabola, the following plot can be acquired:

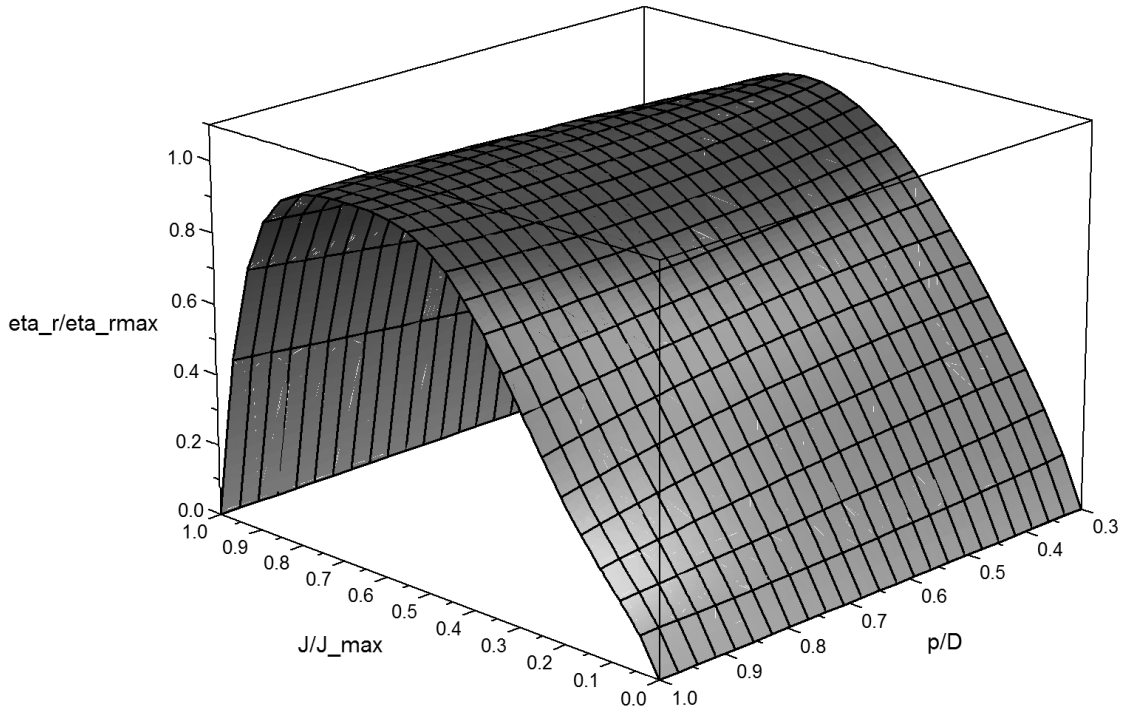

Figure 56 - 3D plot of $\frac{\eta_r}{\eta_{rmax}}(\frac{J}{J_{max}}, \frac{p}{D})$.

$$
\begin{aligned}
\eta = \frac{\eta_r}{\eta_{rmax}}\left(\frac{J}{J_{max}}, \frac{p}{D}\right) &= \left(\frac{p}{D}\right)^2 \\
&* \left(-275.0284158\left(\frac{J}{J_{max}}\right)^6 + 837.3278541\left(\frac{J}{J_{max}}\right)^5 \right. \\
&- 938.6448505\left(\frac{J}{J_{max}}\right)^4 + 466.6603959\left(\frac{J}{J_{max}}\right)^3 \\
&\left. - 95.74279874\left(\frac{J}{J_{max}}\right)^2 + 5.427814965\left(\frac{J}{J_{max}}\right)\right) - \left(\frac{p}{D}\right) \\
&* \left(-282.7805492\left(\frac{J}{J_{max}}\right)^6 + 891.0573894\left(\frac{J}{J_{max}}\right)^5 \right. \\
&- 1032.988581\left(\frac{J}{J_{max}}\right)^4 + 533.0383366\left(\frac{J}{J_{max}}\right)^3 \\
&\left. - 116.4783213\left(\frac{J}{J_{max}}\right)^2 + 8.151725438\left(\frac{J}{J_{max}}\right)\right) \\
&+ 5.702262681\left(\frac{J}{J_{max}}\right) - 38.01485015\left(\frac{J}{J_{max}}\right)^2 \\
&+ 161.4243788\left(\frac{J}{J_{max}}\right)^3 - 315.6039562\left(\frac{J}{J_{max}}\right)^4 \\
&+ 279.2845206\left(\frac{J}{J_{max}}\right)^5 - 92.79235578\left(\frac{J}{J_{max}}\right)^6
\end{aligned}
\tag{4.28}
$$

4.4.3 Additional Parameters

Again, with the same methodology, the additional parameters of J_{max}, C_{Pr0} and η_{rmax} must be determined to calculate the real values of C_P and η.

Table 8 - Values of D, p, J_{max}, C_{Pr0} and η_{rmax} for each propeller.

D [in]	p [in]	J_{max}	C_{Pr0}	η_{rmax}
7	4	0.692	0.0055	0.061
8	4	0.674	0.0048	0.071
8	6	0.951	0.0089	0.078
8	8	1.170	0.0134	0.083
9	4.5	0.650	0.0049	0.071
9	6	0.801	0.0057	0.078
9	7.5	0.992	0.0100	0.083
9	9	1.110	0.0116	0.083
10	5	0.668	0.0044	0.075
10	7	0.839	0.0060	0.081
11	5.5	0.616	0.0036	0.073
11	7	0.791	0.0050	0.084
11	8	0.837	0.0057	0.086
11	8.5	0.885	0.0065	0.084
11	10	1.020	0.0097	0.087
13	4	0.427	0.0023	0.055
13	10	0.831	0.0060	0.077
14	10	0.801	0.0050	0.082
14	12	0.935	0.0065	0.089
15	6	0.510	0.0030	0.066
15	10	0.732	0.0050	0.079
16	10	0.727	0.0052	0.076
17	12	0.846	0.0055	0.091
18	8	0.588	0.0035	0.069
19	12	0.759	0.0050	0.091
20	8	0.493	0.0030	0.065
20	15	0.867	0.0070	0.090

By working with the parameters presented in Table 8 and utilizing MATLAB® application "Curve Fitting Tool" the following plots have been obtained:

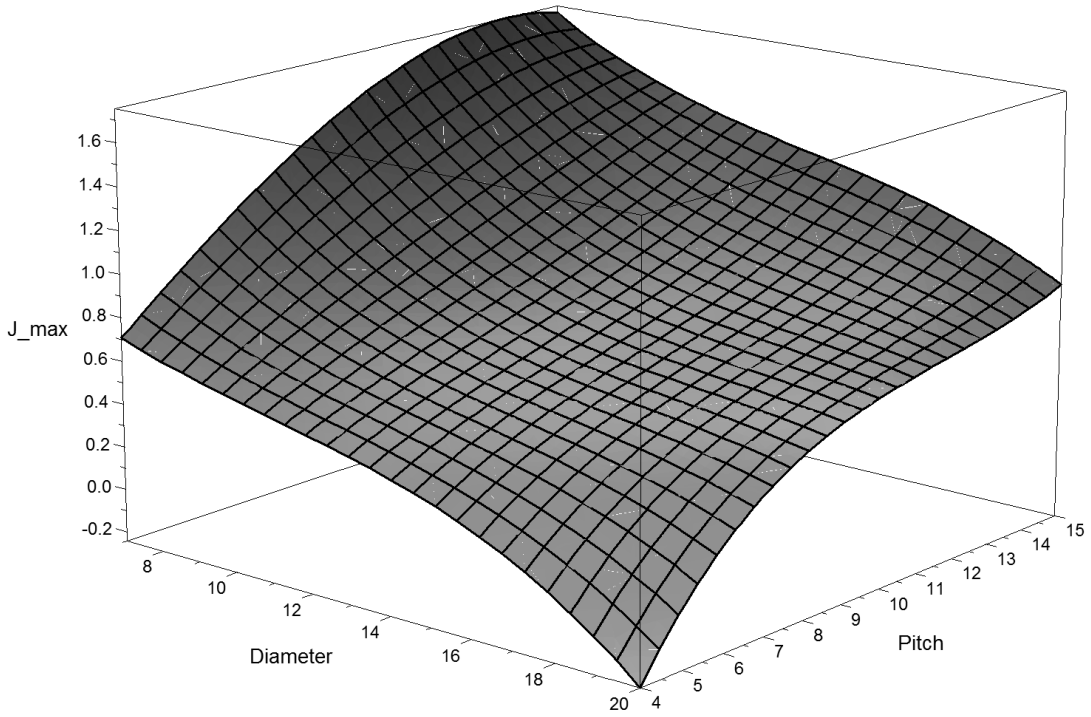

Figure 57 - 3D plot of $J_{max}(D,p)$.

$$J_{max}(D,p) = -1.099 + 0.1789D + 0.7614p - 0.001555D^2 - 0.1169Dp - 0.01523p^2 - 0.0005051D^3 + 0.005775D^2p + 0.003119Dp^2 - 0.0007585p^3 - 0.000004304D^3p - 0.000273D^2p^2 + 0.0001492Dp^3 - 0.00001965p^4 \quad (4.29)$$

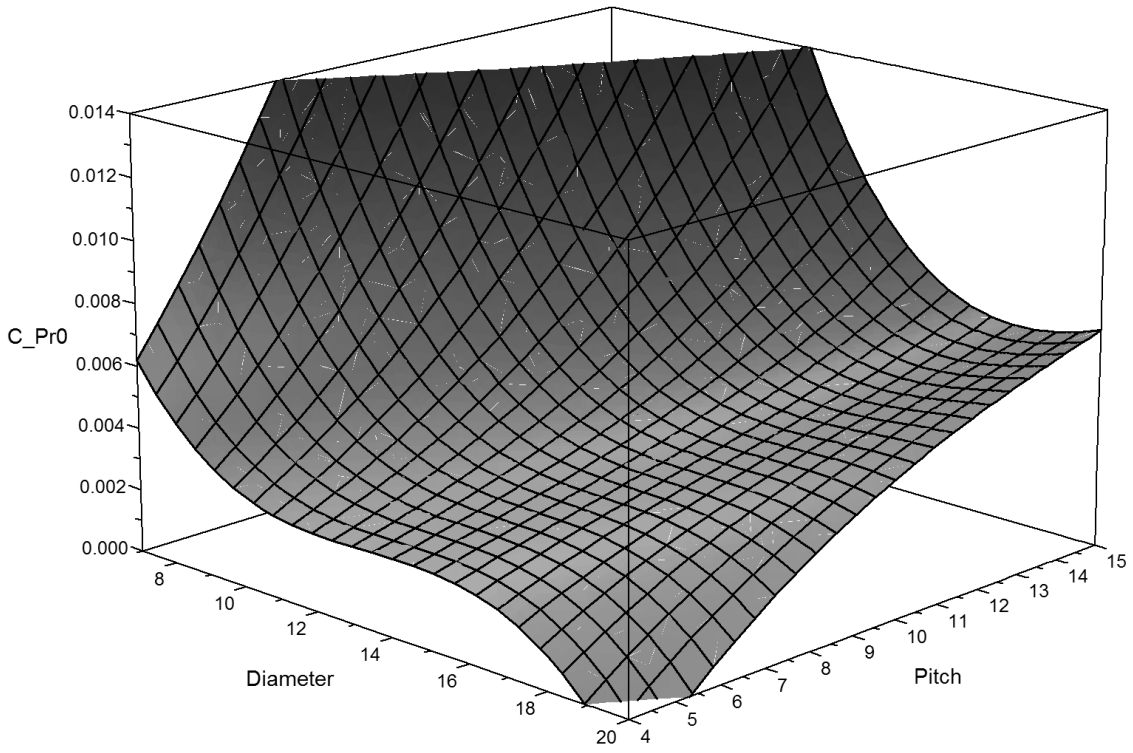

Figure 58 - 3D plot of $C_{Pr0}(D,p)$.

$$C_{Pr0}(D,p) = -0.3875 + 0.1077D + 0.05883p - 0.01285D^2 + 0.002117Dp - 0.01179p^2 + 0.0006309D^3 - 0.0001054D^2p - 0.00006636Dp^2 + 0.0009324p^3 - 0.00001161D^4 + 0.000005865D^3p - 0.00001089D^2p^2 + 0.0000178Dp^3 - 0.00003423p^4 \quad (4.30)$$

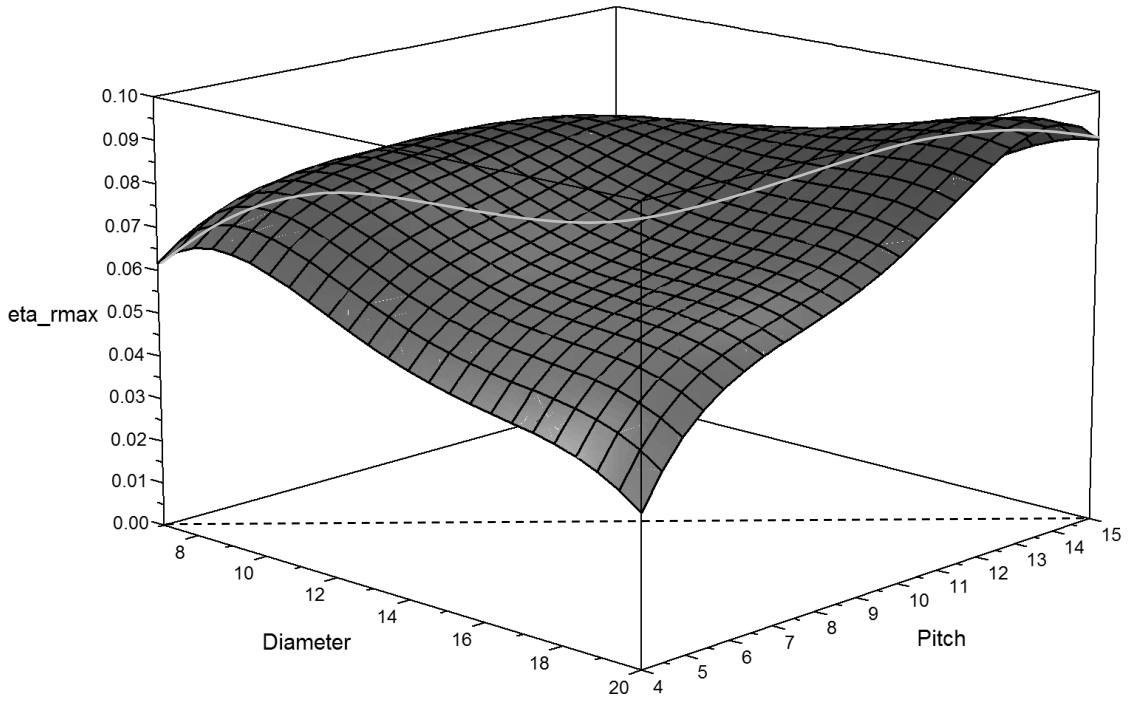

Figure 59 - 3D plot of $\eta_{rmax}(D,p)$.

$$\eta_{rmax}(D,p) = 0.0136 - 0.00469D + 0.005591p + 0.0004904D^2 - 0.0008541Dp + 0.0001986p^2 - 0.00001569D^3 + 0.00003468D^2p - 0.00001612Dp^2 + 0.000002577p^3 \quad (4.31)$$

Note that the lines represented in Figure 59 represent the constant $\frac{p}{D} = 0.75$ plane and its intersection with the η_{rmax} surface plot, which shows an increase in the η_{rmax} value with the increase of propeller diameter. This is due to the propeller diameter and propeller RPM being related to the Reynolds number calculation which will affect the propeller efficiency.

4.5 Verification of the new model

As done previously in subsection 4.3 the new analytical model shall be compared to all the data used to construct it. Table 9 demonstrates the results of the calculation of the mean relative error. The observed data of C_P and η is plotted against *J*, the same *J* values are used to calculate the estimates from the analytical model. The relative error is then calculated for every point measured for each propeller and averaged to acquire a mean relative error (MRE). Table 9 also exhibits the maximum error value and standard deviation for each propeller.

Table 9 - Mean relative error, Max relative error and standard deviation of the model's prediction of all the propellers and total R^2 value.

Propeller	C_P			η		
	MRE [%]	δ_{max} [%]	σ	MRE [%]	δ_{max} [%]	σ
Propeller 7x4	12.09	20.41	0.0056	29.57	327.39	0.1071
Propeller 8x4	5.53	18.36	0.0016	17.90	430.70	0.0879
Propeller 8x6	4.82	21.97	0.0026	14.51	509.16	0.0641
Propeller 8x8	5.79	22.04	0.0054	2.56	32.17	0.0180
Propeller 9x4.5	4.34	27.52	0.0019	6.41	54.52	0.0283
Propeller 9x6	10.54	56.49	0.0037	7.71	366.58	0.0342
Propeller 9x7.5	3.95	14.67	0.0026	5.94	250.44	0.0290
Propeller 9x9	6.48	16.14	0.0058	4.93	86.09	0.0281
Propeller 10x5	13.42	22.71	0.0043	10.34	210.61	0.0625
Propeller 10x7	4.38	25.99	0.0018	1.94	34.90	0.0130
Propeller 11x5.5	6.72	22.18	0.0015	8.79	99.85	0.0453
Propeller 11x7	9.58	19.49	0.0041	14.48	462.19	0.0896
Propeller 11x8	4.71	29.63	0.0020	16.57	1007.6	0.0512
Propeller 11x8.5	4.32	15.88	0.0021	6.20	106.26	0.0479
Propeller 11x10	5.14	18.88	0.0032	15.81	529.31	0.1059
Propeller 13x4	12.70	28.27	0.0023	11.81	225.34	0.0350
Propeller 13x10	10.69	23.80	0.0045	5.39	23.47	0.0342
Propeller 14x10	7.79	13.99	0.0033	6.14	39.82	0.0338
Propeller 14x12	8.18	15.22	0.0044	4.66	25.13	0.0297
Propeller 15x6	10.02	48.01	0.0024	5.14	46.25	0.0311
Propeller 15x10	9.36	14.74	0.0038	8.03	144.15	0.0363
Propeller 16x10	7.54	15.80	0.0028	9	123.83	0.0566
Propeller 17x12	21.27	31.51	0.0086	28.65	1597.4	0.1014
Propeller 18x8	9.39	28.51	0.0021	9.66	28.83	0.0533
Propeller 19x12	6.3	15.54	0.0026	7.38	228.85	0.0511
Propeller 20x8	6.82	18.22	0.0012	9.04	45.18	0.0416
Propeller 20x15	3.01	7.5950	0.0017	4.86	14.95	0.0310
Average MRE	7.9585			10.1267		
R^2 (total)	0.9717			0.8595		

As observed, the maximum value for the mean relative error for C_P is 21.2697% and for η is 29.5730%. The values of standard deviation show that the measured data points are close to the model's predictions. As for the lowest value of the mean relative error for C_P is 3.0110% and for η is 1.9375%. The result for R^2 calculation is also shown, being 0.9717 for C_P and 0.8595 for η.

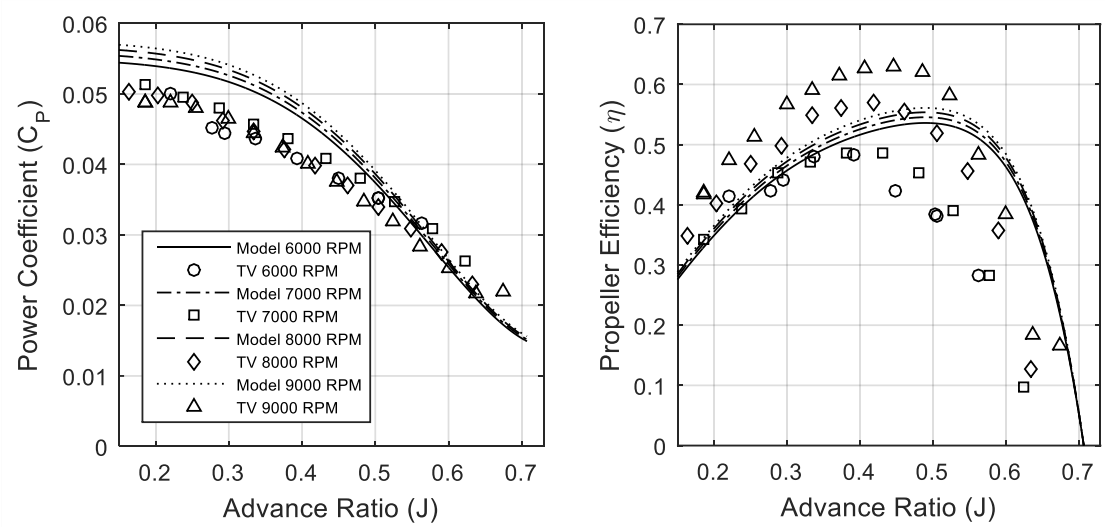

Figure 60 - Propeller Performance comparison with UBI data for propeller 7x4.

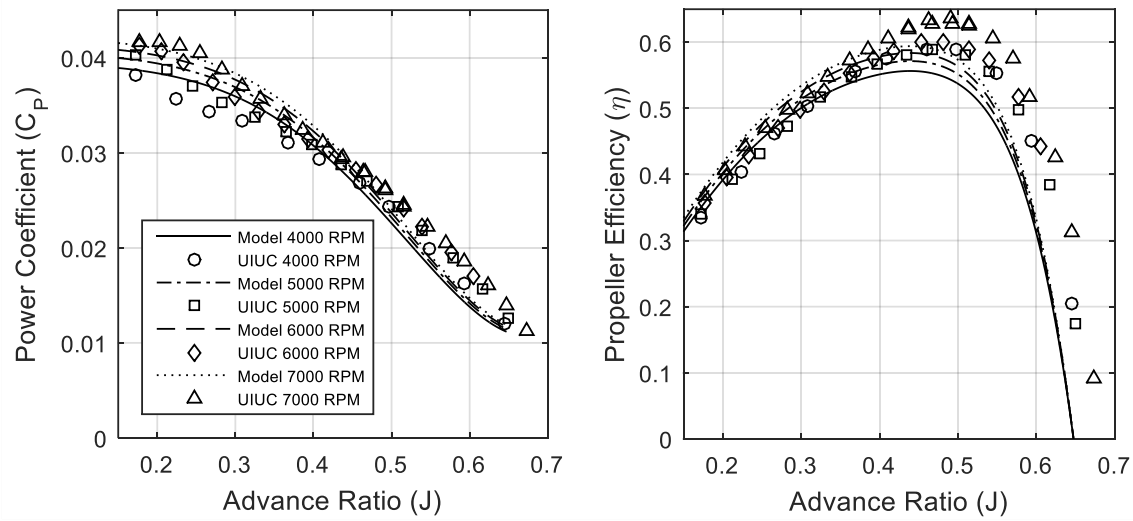

Figure 61 - Propeller Performance comparison with UIUC data for propeller 8x4.

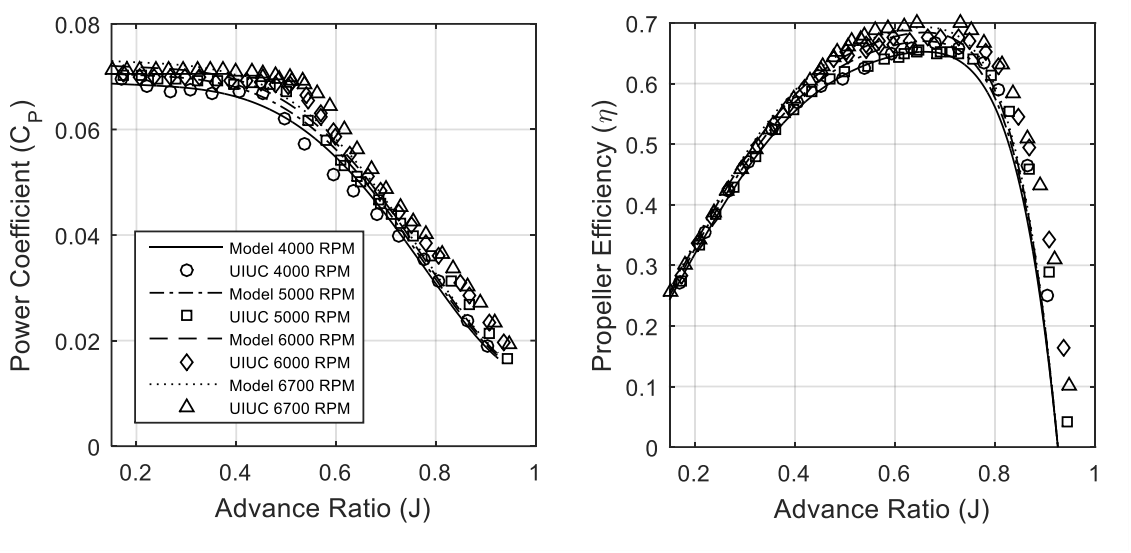

Figure 62 - Propeller Performance comparison with UIUC data for propeller 8x6.

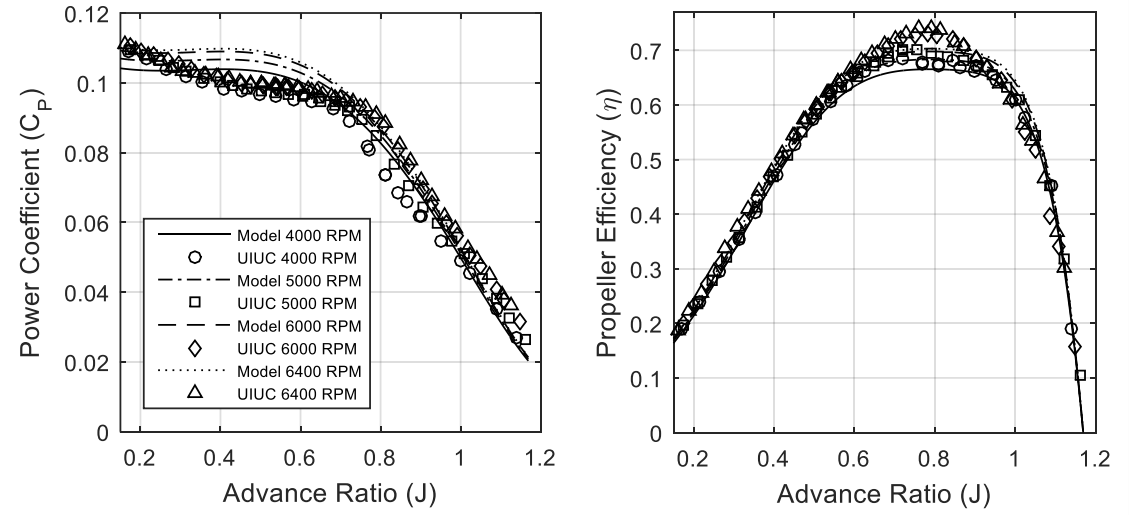

Figure 63 - Propeller Performance comparison with UIUC data for propeller 8x8.

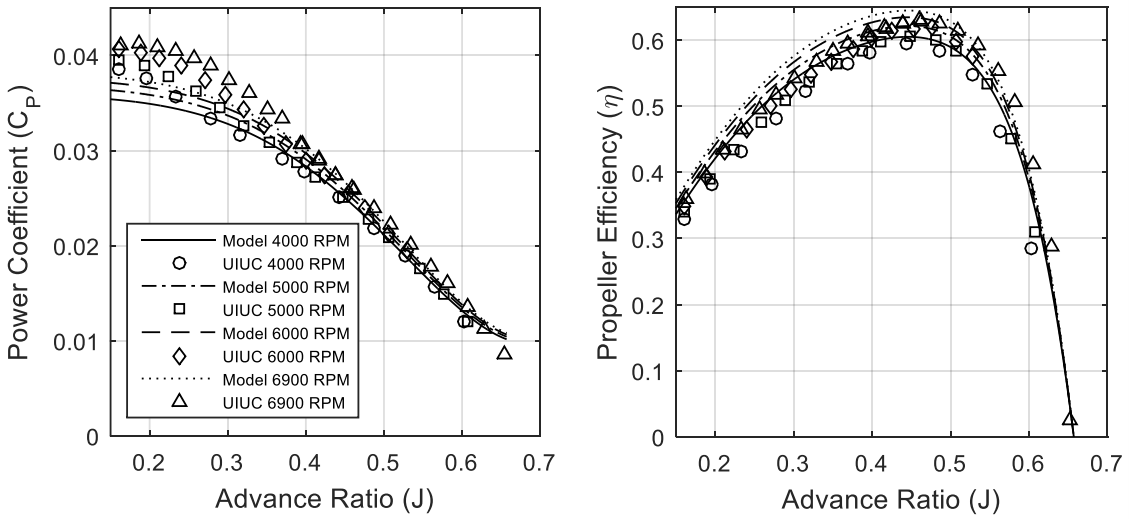

Figure 64 - Propeller Performance comparison with UIUC data for propeller 9x4.5.

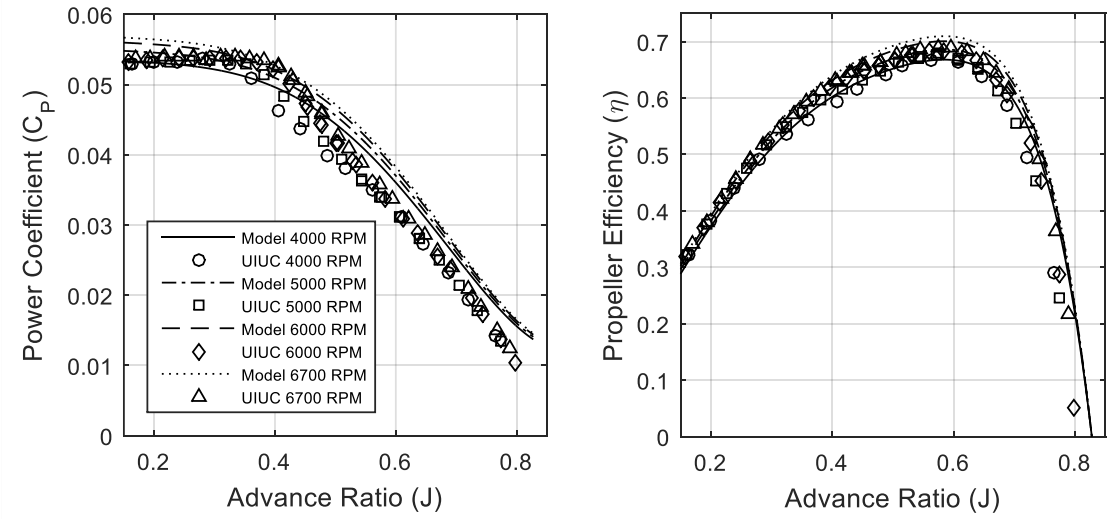

Figure 65 - Propeller Performance comparison with UIUC data for propeller 9x6.

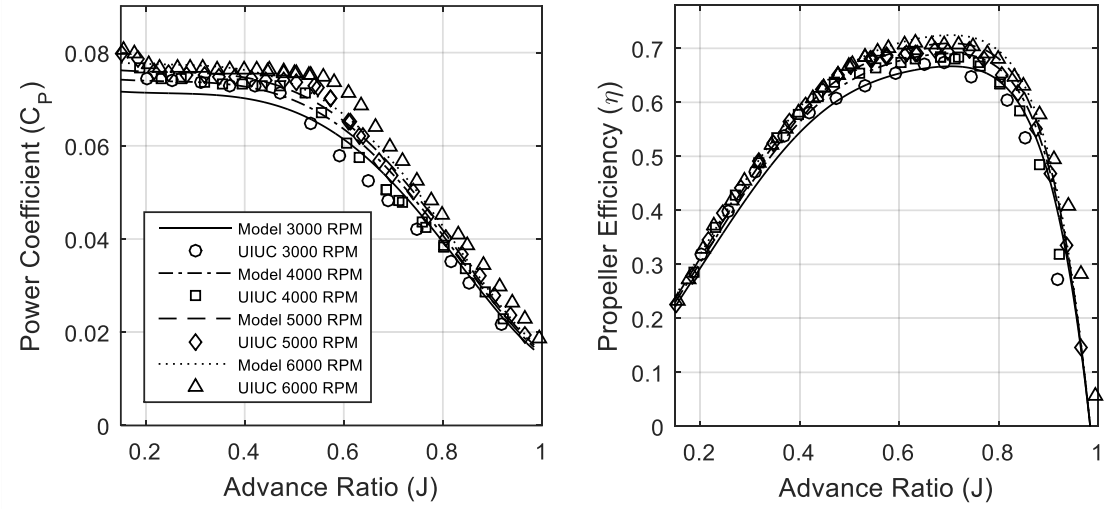

Figure 66 - Propeller Performance comparison with UIUC data for propeller 9x7.5.

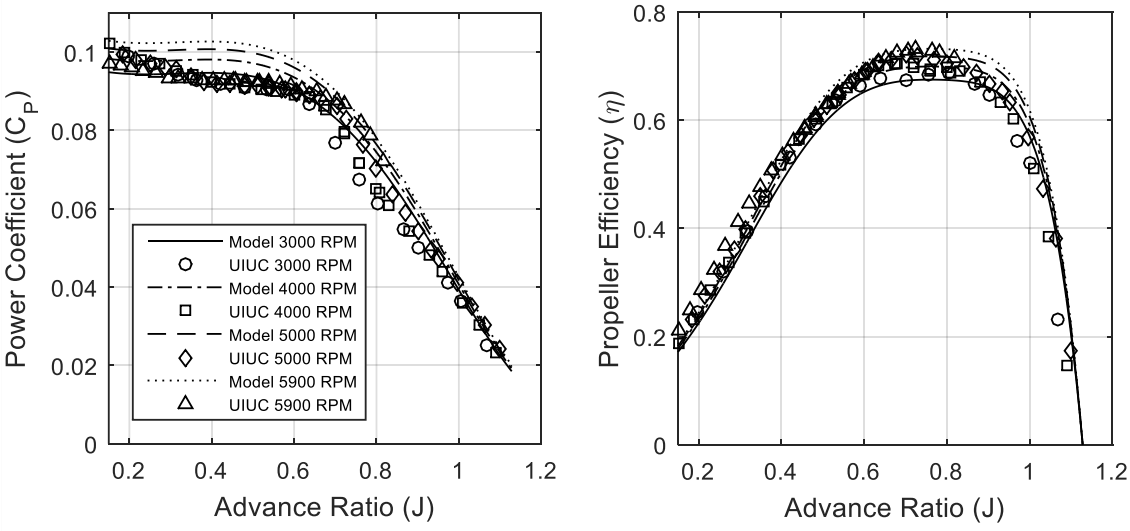

Figure 67 - Propeller Performance comparison with UIUC data for propeller 9x9.

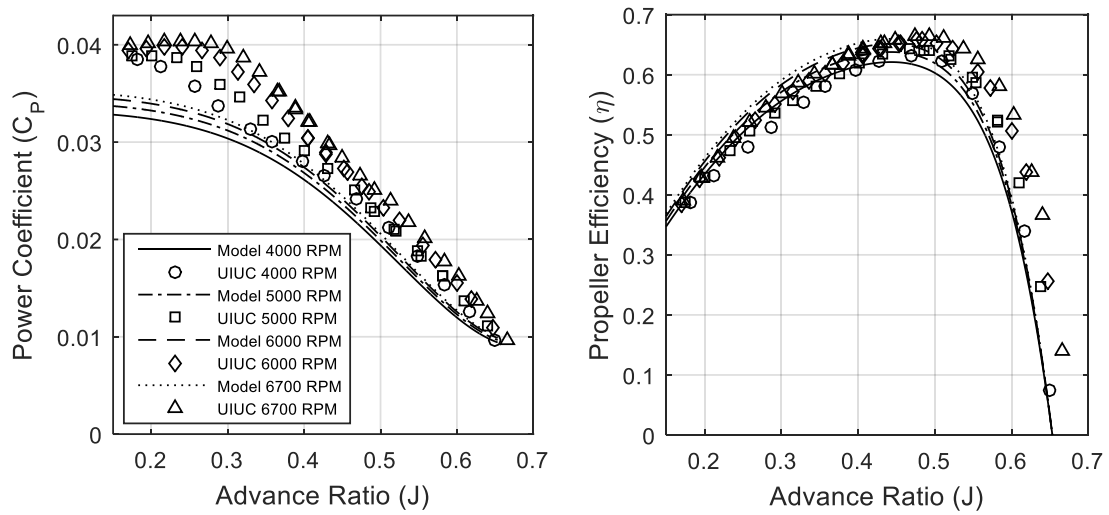

Figure 68 - Propeller Performance comparison with UIUC data for propeller 10x5.

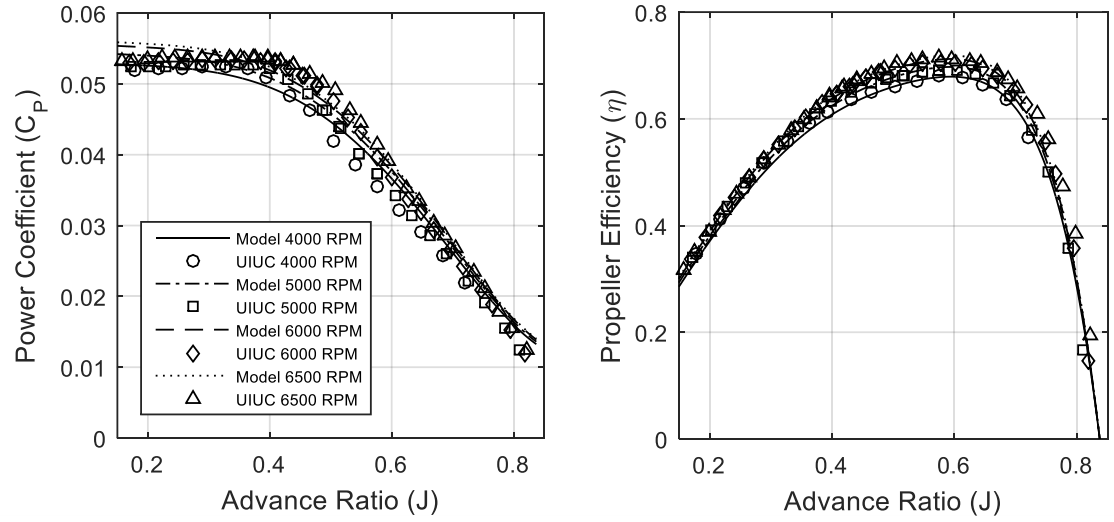

Figure 69 - Propeller Performance comparison with UIUC data for propeller 10x7.

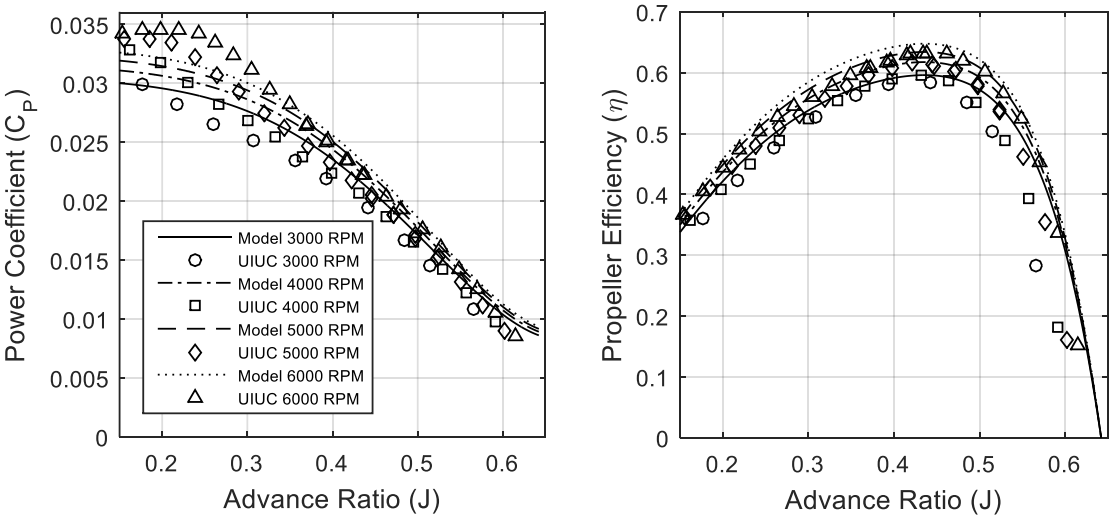

Figure 70 - Propeller Performance comparison with UIUC data for propeller 11x5.5.

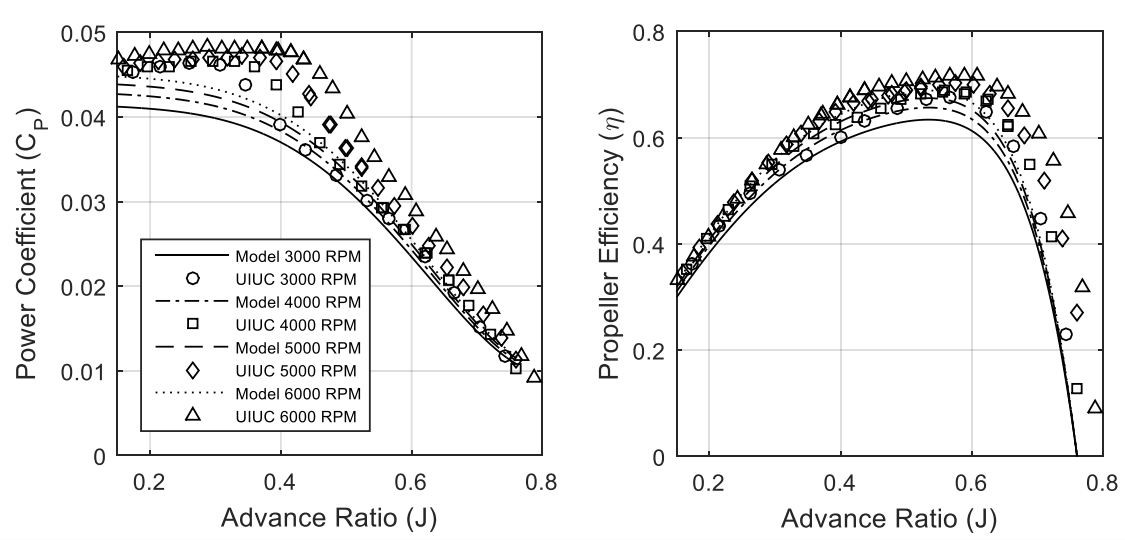

Figure 71 - Propeller Performance comparison with UIUC data for propeller 11x7.

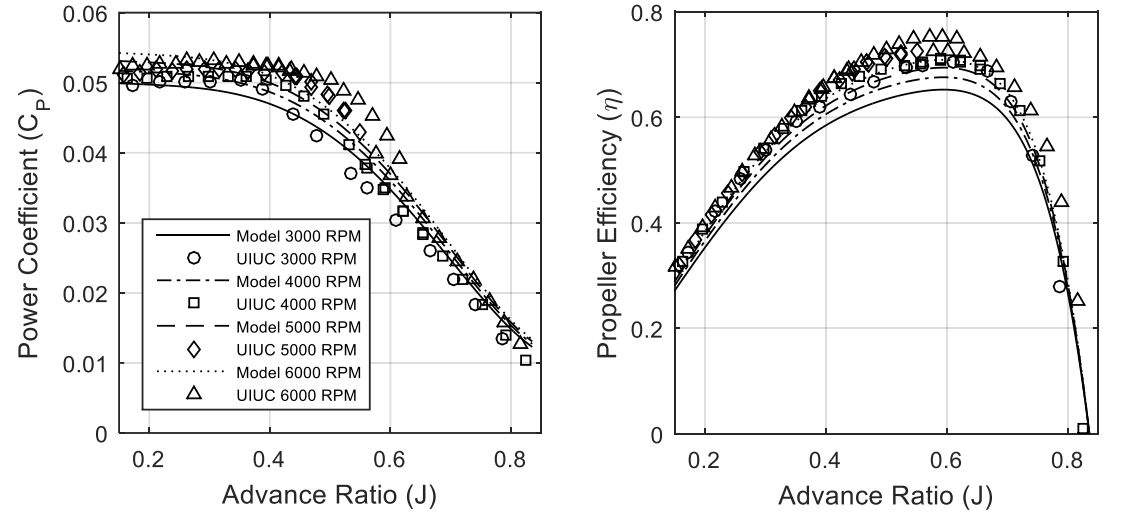

Figure 72 - Propeller Performance comparison with UIUC data for propeller 11x8.

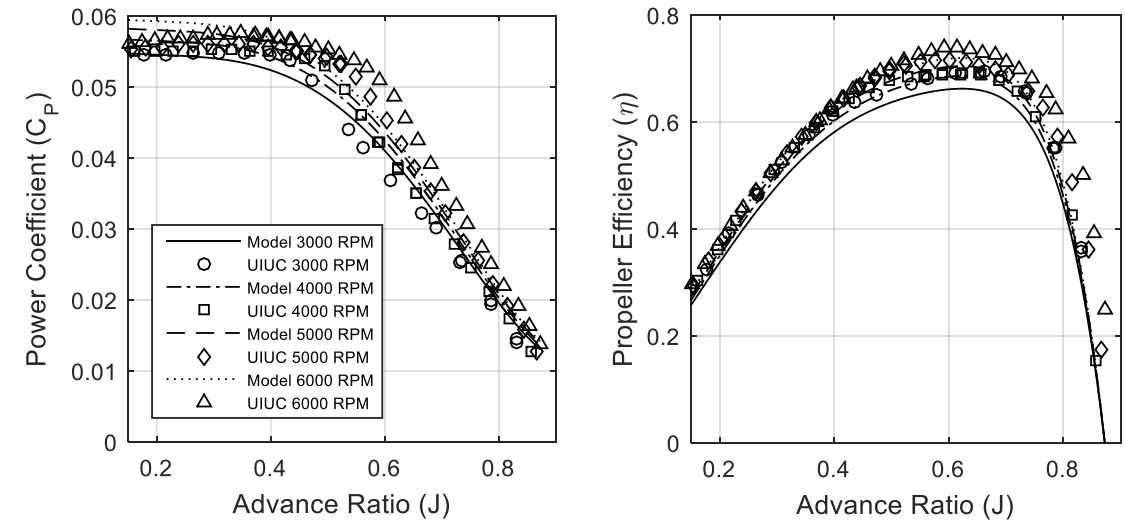

Figure 73 - Propeller Performance comparison with UIUC data for propeller 11x8.5.

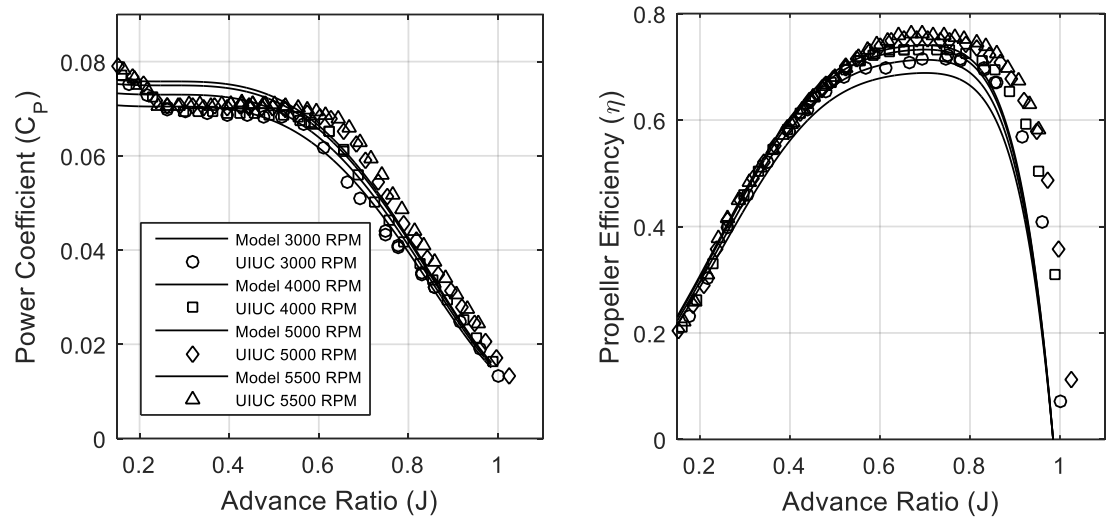

Figure 74 - Propeller Performance comparison with UIUC data for propeller 11x10.

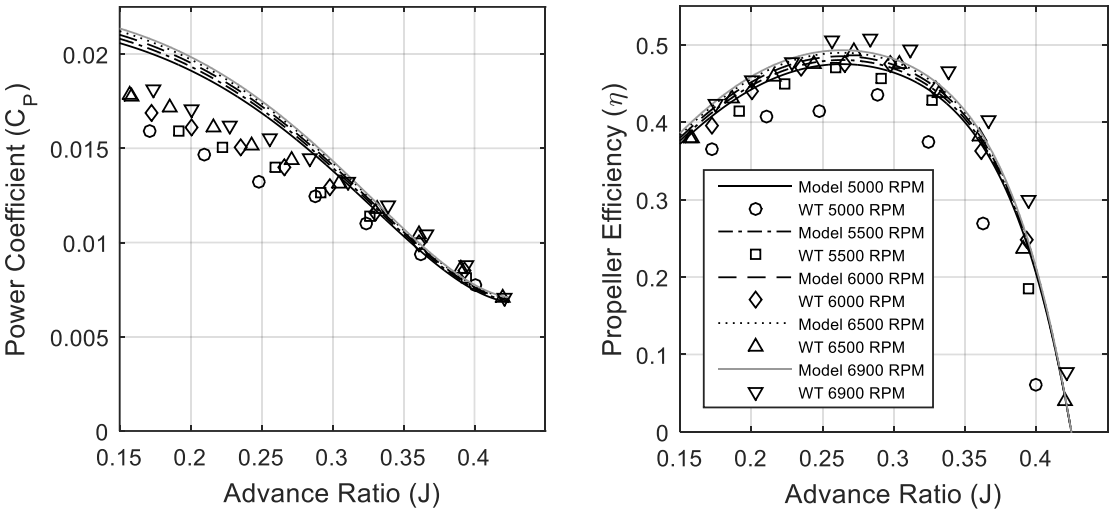

Figure 75 - Propeller Performance comparison with UBI data for propeller 13x4.

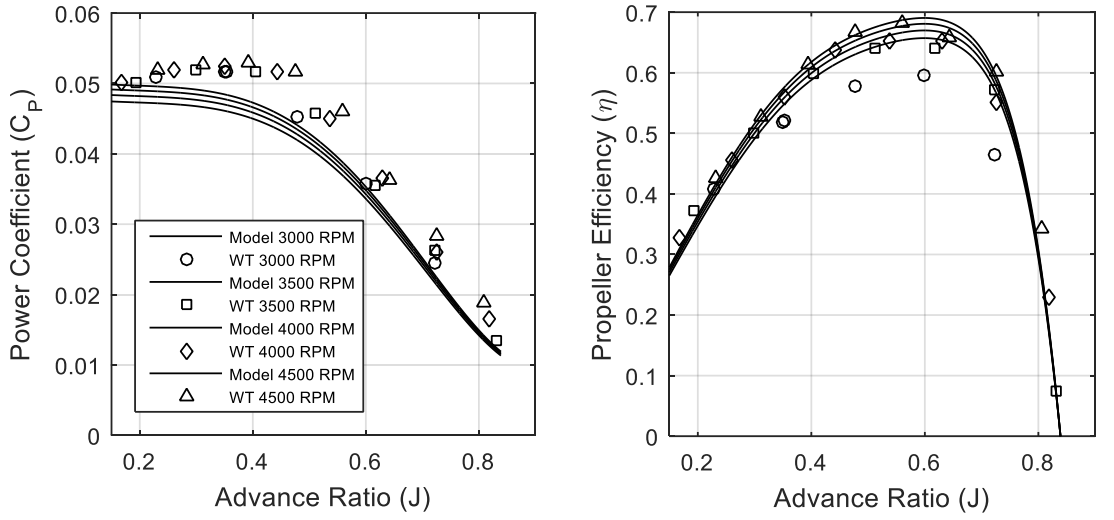

Figure 76 - Propeller Performance comparison with UBI data for propeller 13x10.

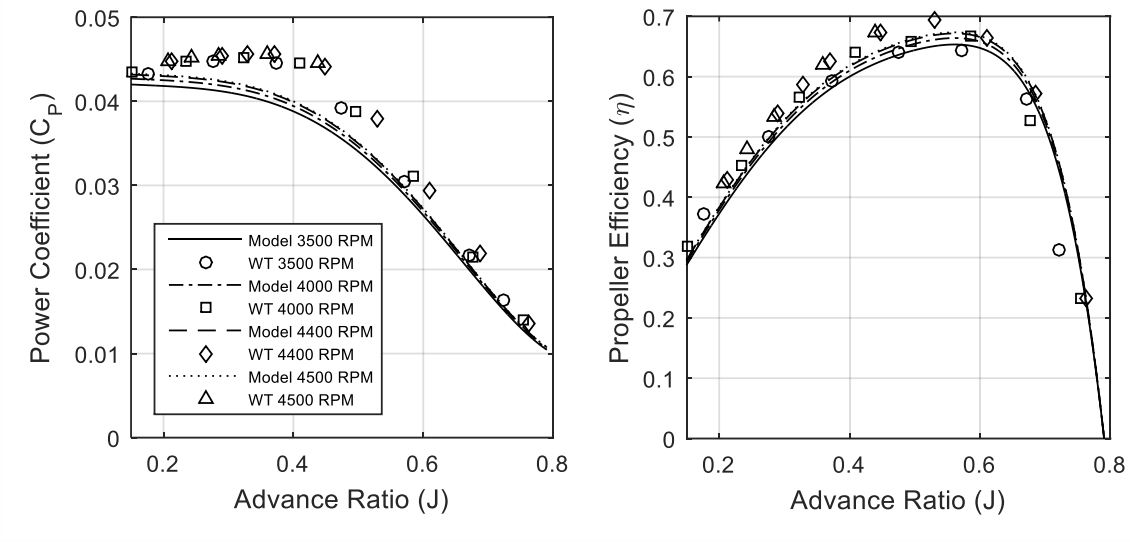

Figure 77 - Propeller Performance comparison with UBI data for propeller 14x10.

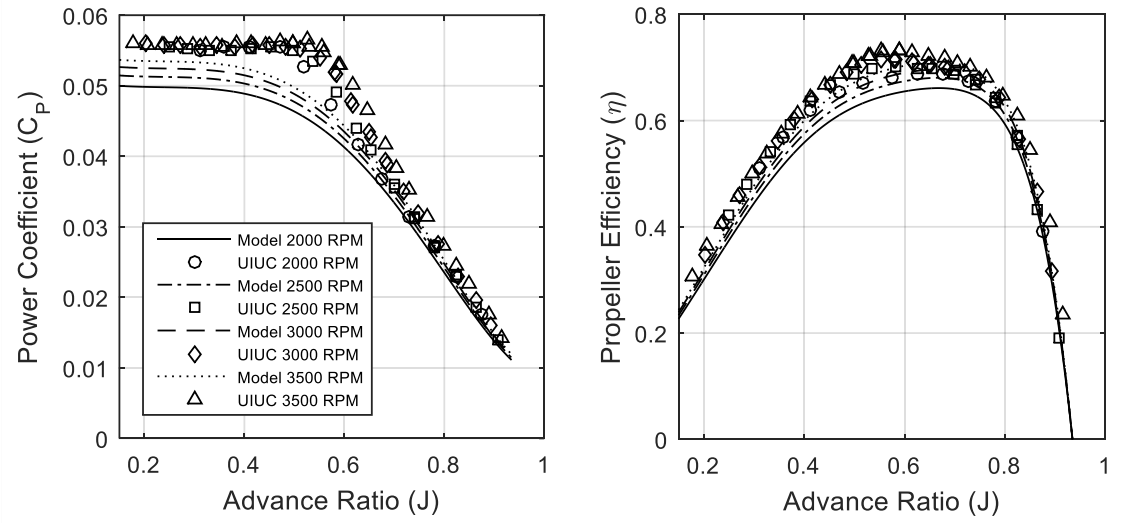

Figure 78 - Propeller Performance comparison with UIUC data for propeller 14x12.

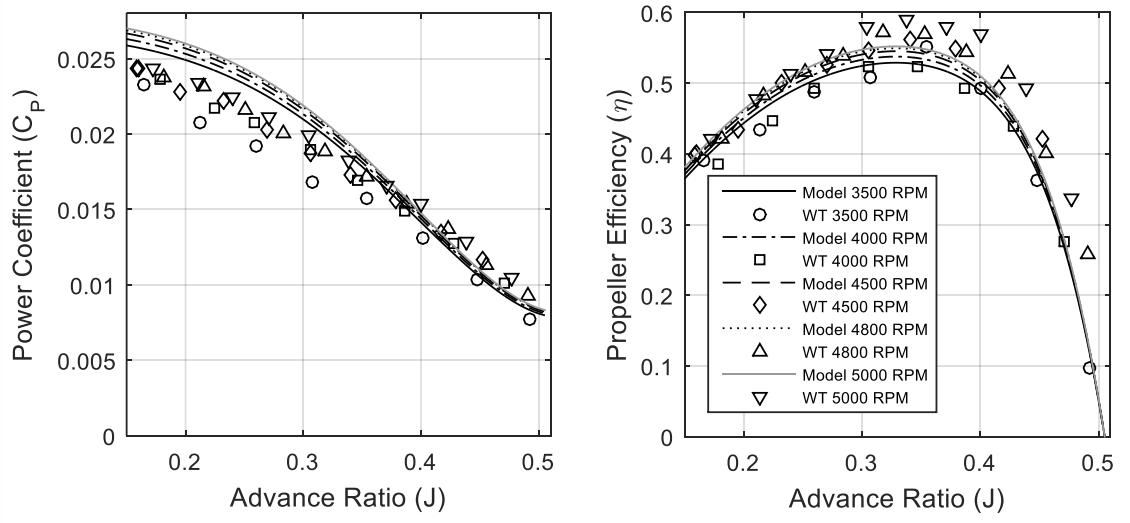

Figure 79 - Propeller Performance comparison with UBI data for propeller 15x6.

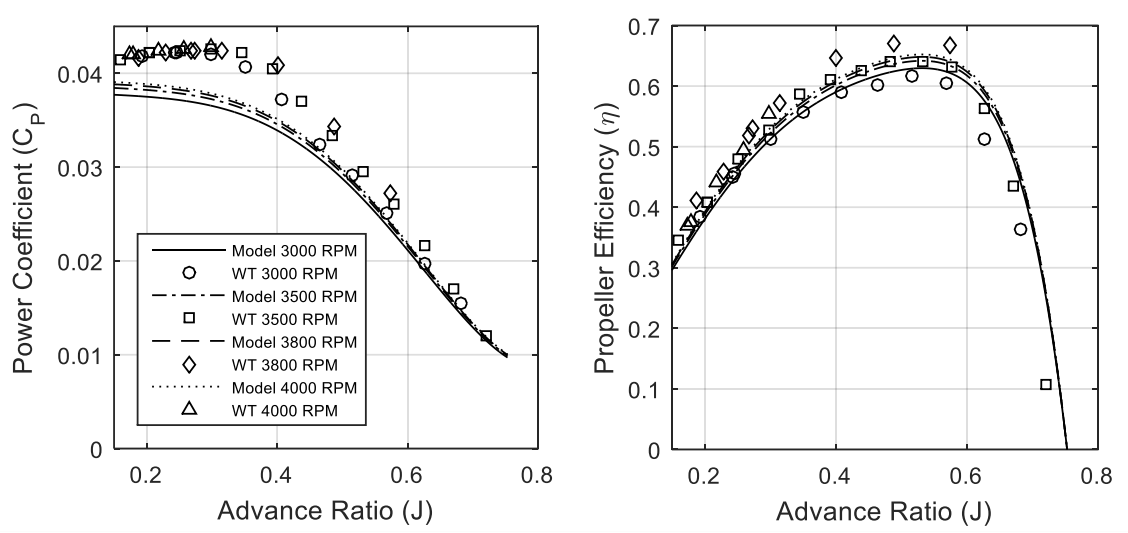

Figure 80 - Propeller Performance comparison with UBI data for propeller 15x10.

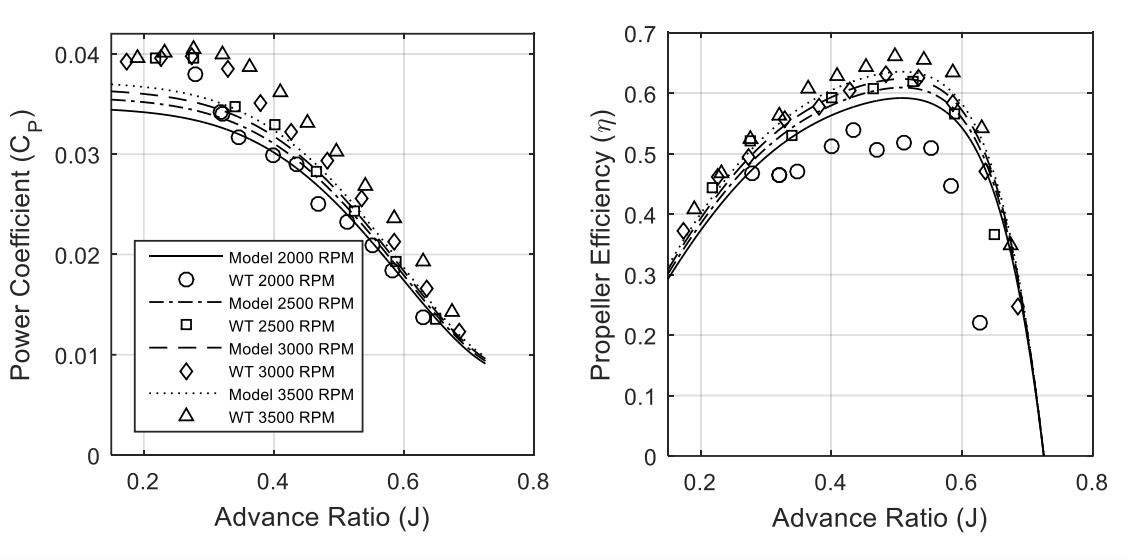

Figure 81 - Propeller Performance comparison with UBI data for propeller 16x10.

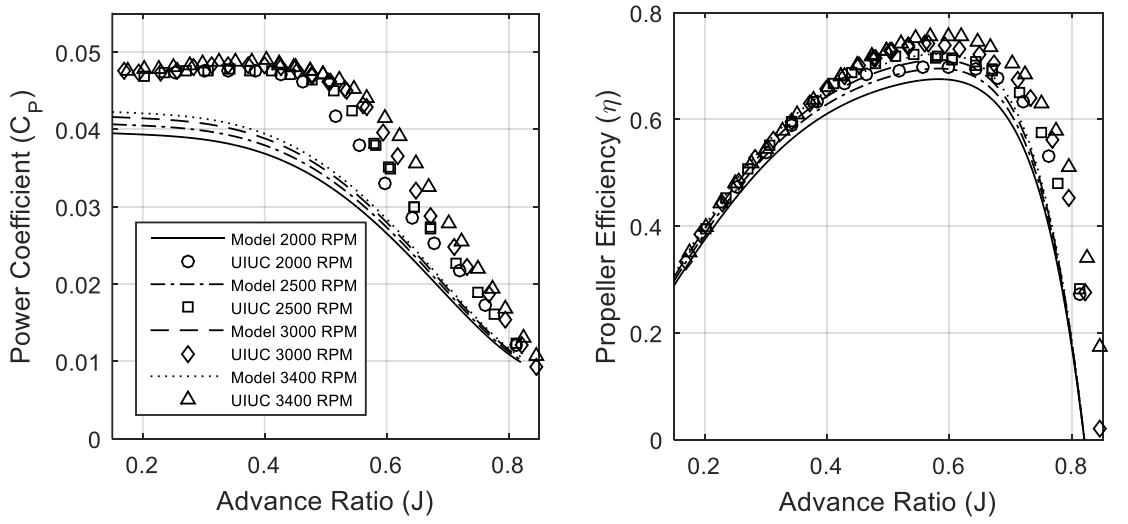

Figure 82 - Propeller Performance comparison with UIUC data for propeller 17x12.

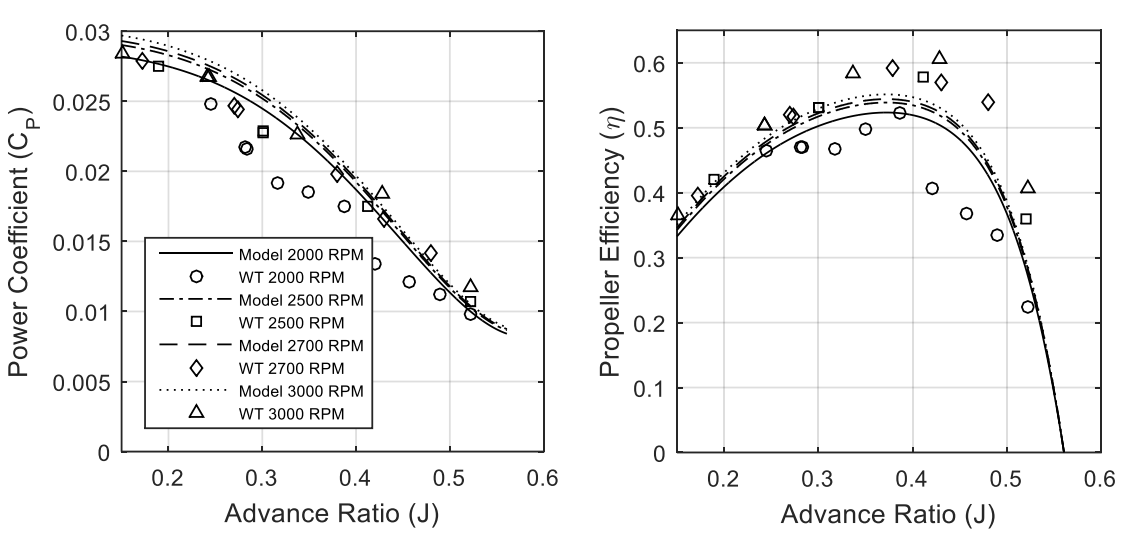

Figure 83 - Propeller Performance comparison with UBI data for propeller 18x8.

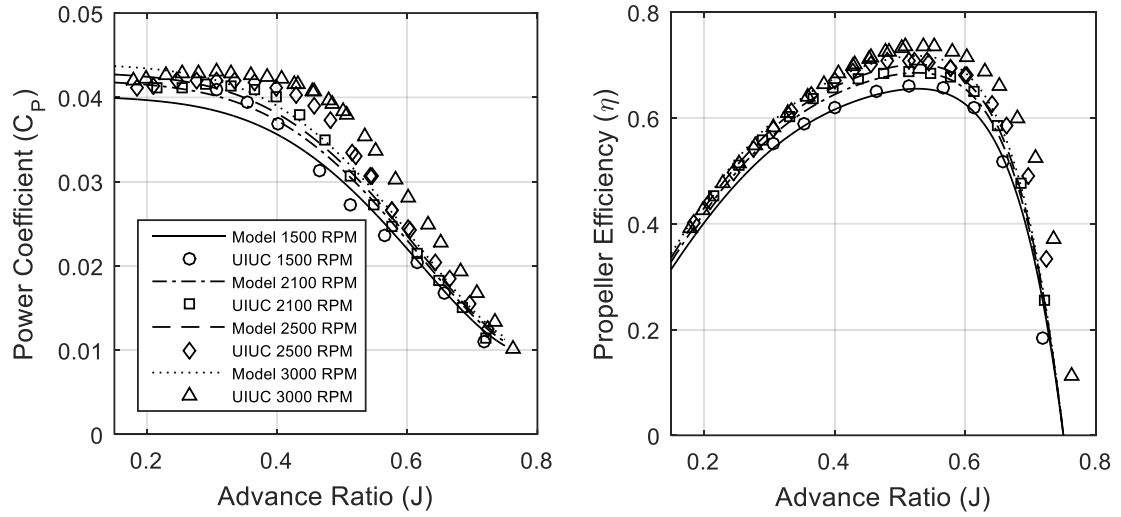

Figure 84 - Propeller Performance comparison with UIUC data for propeller 19x12.

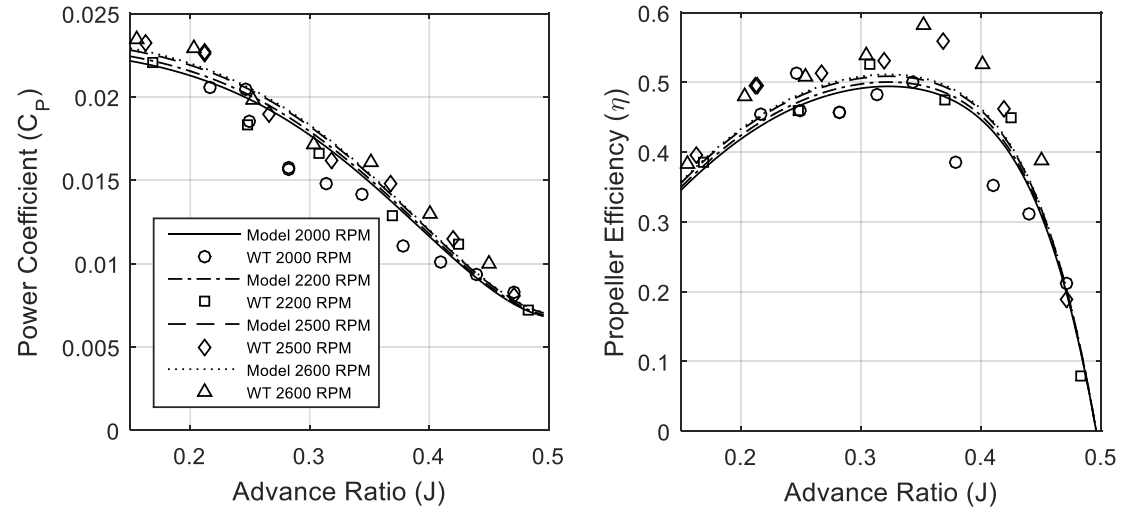

Figure 85 - Propeller Performance comparison with UBI data for propeller 20x8.

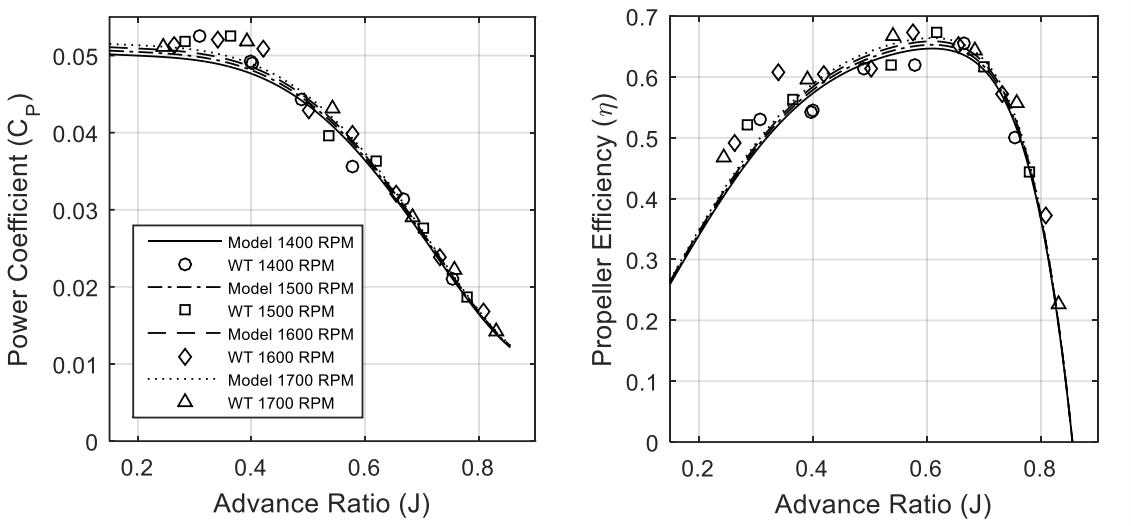

Figure 86 - Propeller Performance comparison with UBI data for propeller 20x15.

Graphs presented in Figure 60 through Figure 86 represent the propeller performance estimates for C_P and η plotted alongside the measurements taken at UIUC for propellers 8x4, 8x6, 8x8, 9x4.5, 9x6, 9x7.5, 9x9, 10x5, 10x7, 11x5.5, 11x7, 11x8, 11x8.5, 11x10, 14x12, 17x12 and 19x12, and the measurements taken at UBI, namely the 7x4, 13x4, 13x10, 14x10, 15x6, 15x10, 16x10, 18x8, 20x8, 20x15 propellers.

Through analyzing the differences between the estimates and the observed values, it is possible to observe that:

1. Regarding the η, the estimates have an average MRE of 10.1267% with the measurements of the propeller performance data;
2. As for the C_P, the values are not matched so well because the behavior of the curves for the power coefficient varies a lot;
3. As observable mainly in APC 17x12 Thin Electric Propeller performance data, regarding the C_P, the estimate made from the model indicates values lower than the data from measurements. This is due to the C_{Pr0} calculation, which defines the height of the curve, as the curvature itself closely resembles the curvature from the measured values;
4. This is also applicable to η. The values of *J* where η reaches 0, differ from where the measured data reaches the same value, this is due to the prediction of the J_{max} value from the model;
5. The C_P curve types for propellers 8x8, 9x9, 11x7 and 11x10, do not resemble the curvature of the measured values, this happens since the model was created from an LSQ approximation, and not an interpolation, the curvature may not be very accurate.

Chapter 5

Conclusion

This work has presented the development and validation of an analytical model for the APC Thin Electric Propeller family, achieving every goal cited in the objectives section of this study:

- Creation of an analytical model to estimate the power coefficient with a $R^2 = 0.9717$;
- Creation of an analytical model to estimate the propeller efficiency with a $R^2 = 0.8595$;
- Various tests of propellers belonging to this family were ran at UBI's wind tunnel.

The analytical model created can estimate the propeller's performance parameters for propellers with a diameter and pitch close to the ones used in the construction of the model, also with a $\frac{p}{D}$ ratio inside the whole range of values of this ratio used in this study. As shown in subsection 4.2.2, the model will not estimate accurately when using propellers with parameters outside of the ones used during the project.

When using the model, it is advised to use propellers with a diameter range between [7,20], a pitch range between [4,15] and a $\frac{p}{D}$ ratio between [0.4;1] for more accurate results, if the tested propeller does not meet one of these three conditions, the results may not be accurate. With the conducted experiments in DCA more data regarding propellers tested at LRN conditions has been acquired, therefore increasing the database.

5.1 Future Work

After creating the analytical model for one family of propellers, there is still work to be done. A recommendation that can further improve the research on propellers tested at LRN conditions are:

- Conduct the same study, but using a different propeller family available at UIUC such as: Aeronaut Carbon Electric, APC Carbon Fiber, APC Slow Flyer, APC Sport, Graupner CAM Prop, Graupner CAM Slim, Graupner Super Nylon, GWS Direct-Drive, GWS Slow Flyer, Kavon FK, Kyosho, Master Airscrew, Master Airscrew Electric, Master Airscrew G/F, Master Airscrew Scimitar;
- Create one analytical model able to estimate the performance parameters of all the propeller families mentioned above;

- Conduct more experimental studies at UBI to “feed” the already existing analytical model with more information, to widen the range of propellers that can be accurately estimated by this model.

References

[1] M. S. Selig and J. B. Brandt, "Propeller Performance Data at Low Reynolds Numbers," in *49th AIAA Aerospace Sciences Meeting*, Orlando, FL, 2011.

[2] J. Brandt, R. Deters, G. Ananda and M. Selig, "UIUC Propeller Database," [Online]. Available: https://m-selig.ae.illinois.edu/props/propDB.html. [Accessed 18 March 2018].

[3] M. Drela, "DC Motor / Propeller Matching," 3 March 2005. [Online]. Available: http://web.mit.edu/drela/Public/web/qprop/motorprop.pdf. [Accessed 21 September 2018].

[4] B. R. Gyles, "Prop Selector," [Online]. Available: http://www.hoppenbrouwer-home.nl/ikarus/software/propselector.htm. [Accessed 2 September 2018].

[5] E. P. Lesley, "Propeller tests to determine the effect of number of blades at two typical solidities," Washington D.C., 1939.

[6] D. Marten and J. Wendler, QBlade Guidelines, v0.6 ed., 2013.

[7] J. Morgado, JBLADE v17 Tutorial, Covilhã, 2013.

[8] M. Drela, "QPROP Propeller/Windmill Analysis and Design," 23 12 3007. [Online]. Available: http://web.mit.edu/drela/Public/web/qprop/. [Accessed 5 September 2018].

[9] M. Drela, "QPROP Formulation," MIT, 2006.

[10] E. E. Larrabee and S. E. French, "Minimum induced loss windmills and propellers," *Journal of Wind Engineering and Industrial Aerodynamics,* pp. 15:317-327, 1983.

[11] M. Drela, "QPROP User Guide," 6 July 2007. [Online]. Available: http://web.mit.edu/drela/Public/web/qprop/qprop_doc.txt. [Accessed 28 September 2018].

[12] M. Drela, "XROTOR Download Page," 24 3 2011. [Online]. Available: http://web.mit.edu/drela/Public/web/xrotor/. [Accessed 12 September 2018].

[13] M. Drela and H. Youngren, "XROTOR User Guide," 13 November 2003. [Online]. Available: http://web.mit.edu/drela/Public/web/xrotor/xrotor_doc.txt. [Accessed 28 September 2018].

[14] R. W. Deters, G. K. Ananda and M. S. Selig, "Reynolds Number Effects on the Performance of Small-Scale Propellers," in *AIAA Aviation*, Atlanta, GA, 2014.

[15] P. M. C. Carrola, Manual do utilizador da balança de testes de hélices de baixo Reynolds e túnel de vento subsónico existentes no Departamento de Ciências Aeroespaciais da UBI, Covilhã, 2016.

[16] P. Alves, "Low Reynolds Number Propeller Performance Measurement in Wind Tunnel Test Rig, Master's thesis," Covilhã, 2014.

[17] R. J. S. d. Sousa, Sistema de Hélice de Passo Variável para UAVs Elétricos, Covilhã, 2012.

[18] M. Â. R. Silvestre, P. Alves, P. Santos, P. Gamboa and J. C. Páscoa, "Propeller Performance Measurementes at Low Reynolds Numbers," *International Journal of Mechanics,* vol. 9, 2015.

[19] J. Duque, Sebenta de Matemática Computacional, Covilhã, 2012.

[20] R. L. Burden and J. D. Faires, Numerical Analysis, Youngstown State University: Cengage Learning, 2010.

[21] H. Abdi, "The Method of Least Squares," in *Encyclopedia of Measurement and Statistics*, Dallas, Neil Salkind, 2007.

[22] H. P. Gavin, "Constrained Linear Least Squares," 2015.

[23] P. Carrola, "In-Flight Thrust Measuring System Using Onboard Force Transducer, Master's thesis," Covilhã, 2017.

[24] J. O. Rawlings, S. G. Pantula and D. A. Dickey, Applied Regression Analysis: A Research Tool, Second Edition, North Carolina State University: Springer, 1998.